Master thesis : Characterization of silica biomaterials and its interaction with cells

Auteur : Oliver Cervello, Lluis
Promoteur(s) : 1749; Geris, Liesbet
Faculté : Faculté des Sciences appliquées
Diplôme : Master en ingénieur civil biomédical, à finalité spécialisée
Année académique : 2016-2017
URI/URL : http://hdl.handle.net/2268.2/3363

Improvement of the biological performance of CaPs coatings by using the PILP-mineralized collagen method

Lluís Oliver Cervelló

Supervisor in Liège: Liesbet Geris
Supervisor in Maastricht: Pamela Habibovic
PhD supervisor in Maastricht: Daniel de Melo Pereira

Master thesis submitted for the degree of
MSc in Biomedical Engineering

University of Liège
Applied Sciences Faculty

Academic Year 2016-2017

Acknowledgments

First of all I want to acknowledge to my daily supervisor Daniel. Without him, this work would not have been possible. I have no words to express my gratitude as most of the things I have learned here are from him. Thank you also for the unconditional support, for the hours spent together in the lab and for allowing me to discover how interesting this world of bone regeneration is.

To my supervisor in Maastricht, Pamela Habibovic, for accepting me in her research group and for always giving me the opportunity to discuss ideas without any limitation. Of course, thank you to the rest of the group: David, Víctor, Sabine, Ziryan, JiaPing, Denis, Roger and Virginia, for always being available to help.

To my supervisor in Liège, Liesbet Geris, who made contact between me and the group in Maastricht, allowing me to discover how interesting is the research world. Thank you also for accepting me in the Master and being available during it to discuss any doubt.

To Ana Vallés and Guillermo Vilariño, who actually were the first persons introducing me in the research world. I feel like this work is also part of them.

To my flatmates, for our international dinners and the hours spent in the kitchen together; and especially to Mike, who was always there for me.

I cannot forget Sara, who became my half during my stay in Maastricht, and Pablo, who although back in Spain, was always supportive. You both know that I could not have done this work without you.

To my parents and my sister, always relying on me.

Abstract

Mineralization of collagen via a polymer-induced liquid-precursor (PILP) method was used to mimic the intrafibrillar mineralization of collagen. This method was optimized and adapted to achieve a coating of PILP-mineralized collagen in microplates for cell culture experiments.

Prior to mineralization, optimization experiments were performed, to find the best conditions to obtain a homogeneous coating of collagen fibres. The first optimization step was tuning buffer conditions (pH, ionic strength, col-I concentration) that allow collagen fibril self-assembly, showing the characteristic D-spacing, from an acid-dissolved stock solution. It was found that the best conditions to obtain this kind of collagen fibrils were 100 μg/mL of collagen in FFB with 200 mM NaCl, 100 μg/mL of collagen in FFB with 400 mM NaCl and 500 μg/mL of collagen in FFB with 400 mM NaCl. The second optimization step was regarding the coverage of the tissue culture plastic substrate by fibrils, and two methods were tested. In the first method, quite homogeneous coatings were attempted by deposition of sequential layers of fibril suspensions. The second was a two-step method: first a thin, non-fibrillar layer of collagen was deposited, followed by fibril formation in the second step. The later method proved to be most effective, as observed by immunostaining and SEM. Observation of collagen banding pattern and confirmation of intrafibrillar mineralization of collagen was done by TEM. Furthermore, the effectiveness of the PILP solution was tested by mineralizing bovine type-I commercial MatrixMEM collagen membranes. Quantification of mineral content was done by TGA.

The PILP-mineralized collagen coating is hypothesized to have better biological performance than current biomimetic calcium phosphate coatings. To study so, five different substrates (TCPS, hydroxyapatite, collagen, PILP-mineralized collagen and collagen-coated hydroxyapatite coatings) were prepared for a resorption experiment with osteoclasts. Surface morphology of the samples was analysed by SEM, and calcium phosphate phases were identified by XRD.

Osteoclast cells were obtained by differentiating murine RAW 264.7 macrophages under the influence of RANKL. Cell density and RANKL concentration optimization experiments were also performed. A seeding density of 4000 cells/cm^2 and 100 ng/mL of RANKL were found as optimal conditions.

Osteoclast formation on the different substrates was assessed by TRAP staining, and quantification of TRAP activity and DNA amount. The morphology and the number of osteoclasts present in each substrates were analysed by SEM, as well as the resorption of the different calcium phosphate coatings. Results from TRAP staining and SEM indicated that PILP-mineralized collagen coatings performed the best, showing a greater amount of osteoclast-like cells than the rest of the coatings. Although resorption was not observed in any of the coatings, some degradation of collagen was found, which could indicate the beginning of the resorption process, but no clear conclusions could be done.

Following the resorption study, collagen micropatterning was attempted and it was also suc-

cessful by using μCP with PVA. However, its mineralization by PILP method was not possible due to the limitation of time.

Overall, PILP-mineralized collagen coatings showed promising clues to improve the biological performance of the biomimetic coatings used nowadays in the clinic.

Contents

Chapter 1: Introduction

1.1 Current trends and shortcomings in bone disease treatments

Bone tissue has a high capacity of regeneration, which allows fractures to heal without the need of surgical intervention. This is because of its inherent ability to resorb and deposit mineral depending on external factors. Nevertheless, when a defect reaches a certain critical size (generally 2.5 times the radius of the bone), the ability of bone to regenerate on its own is compromised [1]. Furthermore, owing to an increase in life expectancy, age related bone disorders have trended and they are expected to double by 2020 [2]. In particular, osteoporosis or osteoarthrosis have a high incidence, especially among women (osteoporosis affects 200 million women worldwide – approximately one-fifth of women aged 70 [3]. These disorders lead to a weakening of the bone tissue, which becomes more brittle, increasing its failure probability [4].

Autologous bone grafting (the transplant of bone from one site to another, within the same organism) is still the prevailing method of filling in bone defects, yielding the fastest osseointegration and avoiding immunological reaction. However, the use of autografts introduces some drawbacks, such as limited availability and the need for a second surgery, which increases risks of infection and donor morbidity [5]. Those problems can be partially solved by using allogeneic bone grafts (bone transplants obtained from donor banks) or xenografts (transplant of material obtained from a different species) [2] [6] but in both cases, biomaterials have to be denatured in order to avoid an immunological response, which includes risk of contamination or infection due to an incomplete denaturation. This fact together with the decrease of biological performance (due to the different processing techniques), shows the importance of finding alternatives to these approaches [7].

1.2 Bone tissue engineering

Tissue engineering or regeneration strategies normally employ a combination of a support structure, named a scaffold or matrix, with added biological components such as regeneration inducing factors, cell types native to that tissue, or both. Of these three elements, in the case of bone tissue engineering, the scaffold plays the most important role as it acts as a template for new tissue formation while maintaining the structural integrity of the damaged area [8]. A successful tissue engineered strategy, e.g. involving a scaffold only, should perform at least as well as autologous grafts in terms of tissue ingrowth and recovery time.

Nowadays, a great variety of synthetic grafts have been developed to substitute autologous bone grafts. The biomaterials used in synthetic grafts for bone tissue regeneration have to fulfil specific requirements. Generally, for a biomaterial aiming at regeneration of a critically sized defect, the ideal solution would be a construct that fits the gap and maintains the mechanical

stability, while gradually allowing its substitution by native tissue.

Such material should have the ability of promoting differentiation of pluripotent cells into the osteogenic lineage – a property known as osteoinduction. It should also be osteoconductive – supporting the proliferation and migration of cells into the construct, allowing for vascularisation and deposition of native extracellular matrix. Porosity is a critical parameter for osteocondution and vascularisation, with ideal pore size in the range of 100 to 400 μm, and micro pores of 2 to 50 μm to favour protein adsorption and osteoblast adhesion [9] [10]. Obviously, both the material and its products of degradation have to be biocompatible. Moreover, the degradation rate should tuned to allow sufficient time for tissue ingrowth and maturation. Mechanical proprieties are essential as well; for instance, the modulus of elasticity of cortical bone is about 18 GPa, hence, scaffolds designed to support loadings should have mechanical properties in the same range [11] [12] [13].

Most of the material properties here outlined depend on each other, which makes finding the best suitable material always a compromise, and never easy. An example is the interplay between porosity, mechanical strength and degradation of a material. Porosity is critical for tissue ingrowth and neovascularization, but decreases the mechanical strength of a construct. Increasing the mechanical strength can be done by considering other materials, but the biodegradability usually decreases. Nevertheless, fine tuning a material's physico-chemical properties can be achieved to a certain degree, by e.g. applying certain treatments on the surface, to render it with properties different than those of the bulk material. This allows for a balance of mechanical properties (supported by the bulk) and surface chemistry and topography that is more amenable to the physiological environment [53].

Traditionally, bioinert materials (materials that do not degrade in vivo [15]) like alumina, zirconia, titanium alloys or ultra high molecular weight polyethylene (UHMWPE), have been used to repair bone defects [16]. For instance, Titanium and its alloys (mostly Ti_6Al_4V) are interesting because their mechanical strength and fatigue resistance are higher than the characteristic values for bone. As a consequence, they can be used for load bearing applications like hip or knee replacement. However, due to the mismatch of mechanical properties, the implant sustains the larger part of the load. Lack of external mechanical stimulus leads to the loss of bone mass in the area surrounding the implant (an effect called stress-shielding), causing it to shift loose. This is a major cause of revision surgery for hip arthroplasty (30 % of the patients needing revision after 7 years [17]). Bioinert materials are tipically surrounded by a layer of fibrous tissue, which does not allow a proper biointegration of the material. Besides of the aforementioned disadvantages, bioinert materials do not bind directly with bone and in some metals like Ti, a thin oxide layer is normally formed in the surface, which can generate the release of some metal ions resulting in an immune and inflammatory response [53] [54]. Therefore, bone tissue engineering requires scaffolds that better meet the requirements listed above, and the design of biomaterials is generally moving towards having an active part in directing cell behaviour and tissue integration in vivo, as opposed to the passive state of bioinert materials. These biomaterials are known as bioactive materials and their main goal it is not only to avoid rejection of the implant but also to stimulate new bone formation with its specialized function. A common rationale to develop such cell-instructing materials is looking to the native tissue and trying to mimic its structure or function. To develop these biomimetic materials, as they are named, insight is needed on the intricacies of bone tissue. Bone composition and structure will be reviewed in the following section.

1.3 Composition of bone

Bone can be seen as a heterogeneous composite material, characterized by being a mineralized connective tissue. Throughout the body, a large variety of shapes and sizes of bones can be distinguished, depending on the functions and structures that it has to support. Being a connective tissue, it has cells embedded in extra-cellular matrix (ECM), which provides the perfect environment for bone cells to perform their function [19] [20].

1.3.1 Bone cells

Bone is a dynamic tissue that undergoes continuous remodelling during life. Bone remodelling is necessary to regulate calcium and phosphate homeostasis, renew damaged bone as well as to adjust the bone architecture to changes in the environment [19]. This physiological process involves three principal cell types: osteoblasts, which are responsible for deposition of new bone, osteoclasts, that remove mineralized bone, and osteocytes, which orchestrate the formation/resorption of bone.

Osteoblasts are derived from multipotent mesenchymal stem cells and their main function is the production of bone matrix [21]. They are normally found on the layer of bone matrix that is being actively produced . Nevertheless, some of them remain on inactive bone surfaces, transforming into bone lining cells [22].

Osteoclasts originate from hematopoietic cells of the monocyte-macrophage lineage. They are specialised in bone resorption, that generally involves the dissolution of the HA crystals and decomposition of the organic matrix. This is achieved by acidification of an extracellular pocket, and secretion of proteases [21]. In healthy adult bone, the formation and resorption phenomena occur at the same rate, which ensures the maintenance of a constant bone mass [23]. Any disruption of this balance can generate bone pathologies, like osteoporosis.

Osteocytes are the most abundant cells in bone, representing over 90% of adult bone cells [24]. They are matured osteoblasts that now reside in a lacuna surrounded by the bony matrix. Osteocytes are interconnected by long cellular protrusions through narrow channels in the osteoid. These protrusions improve the formation and activation of osteoclast precursors, the stimulation of bone resorption and the regulation of mesenchymal stem cell differentiation [25] [26]. It is hypothesized that osteocytes act as strain "sensors" [27], however, it is still not clear how do they respond to mechanical stimulus.

1.3.2 Extracellular matrix

Although the ECM is very complex, it is possible to differentiate between an organic phase (mainly composed of collagen fibrils and non collagenous proteins) and an inorganic phase (mineral nanocrystals):

(a) The organic phase constitutes about 25% of the total weight of the bone. This phase is mainly composed of proteins and proteoglycans, with type I collagen being the most abundant, accounting for 90% of the overall weight (type III and IV are also present [28]) [19] [20]. The rest is accounted by non collagenous proteins (NCPs), such as osteocalcin, osteonectin or osteopontin, which play an important role in cell signaling, metabolism and attachment, as well as matrix organization and mineralization [23].

(b) The inorganic phase represents about 65% in weight of the bone. Bone mineral is constituted by nanometer scale, crystalline platelets of highly substituted hydroxyapatite (HA), $Ca_10(PO_4)_6(OH)_2$ that contains some impurities, such as carbonate (4-6 %) [29], and other ionic substitutes, e.g. sodium (0.9%), magnesium (0.5%) [20] and potassium. The size of these crystals is about 40-50 nm in length, 20-30 nm in width and 2-10 nm in thickness. The crystals are formed within the collagen fibres and they are oriented parallel between them and to the long-axis of the collagen fibrils [20] [29] [30].

(c) Water represents the remaining 10% of the bone's weight. Although the amount of water is much less compared to the rest of the components, it should not be ignored as it acts as a plasticizer, contributing greatly to the mechanical properties of bone [20].

1.3.3 Structure of bone

Bone is a hierarchically structured composite material that can be arranged in many different ways depending on the local mechanical and biological demands. It should be kept in mind that bone structure (and composition) varies from one species to another and some differences can be found even within a single organism. However, bone tissue is generally divided in different hierarchical levels. At the nanoscopic level, tiny hydroxyapatite platelets are embedded along the long-axis direction of the collagen fibrils. These fibrils are then arranged in a parallel array, forming the lamellae or lamellar bone. In particular, lamellar bone is constituted of large concentric rings of lamellae with thickness of about 5-10 μm. The lamellae are arranged in concentric rings around a central Harvesian canal that allows the irrigation of bone tissue. This structure forms the osteon (osteonal bone), which has a diameter of about 100-200 μm and a length of 1-3 mm. Finally, at the macroscopic level and depending on the packed density of the osteons, it is possible to distinguish between cortical and trabecular bone (see Figure 1.1) [20].

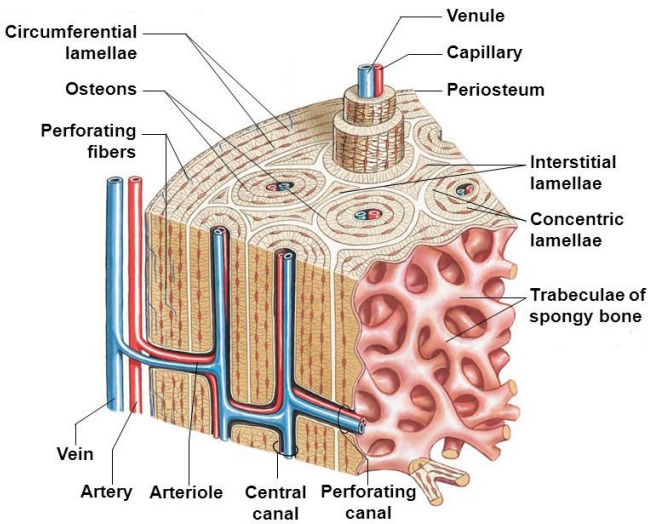

Figure 1.1: Structure of bone.

Cortical bone is dense and compact and it comprises 80% of the skeleton [27].]. It is present in the outer parts of the bones and its main function is to provide mechanical strength, as well as to protect organs such as the brain or the uterus.

Trabecular bone is less dense and has higher porosity than cortical bone. Its architecture and density vary depending on the location in the skeleton, as well as with aging. Moreover, it has more biological activity than the cortical bone, as it harbours the bone marrow, a highly vascularized tissue, which is responsible of hematopoiesis. It also plays an important role in

the immune response [31]. The main function of trabecular bone is to act as a shock absorber [32].

With this general overview on the biology, cells and structure of bone tissue, we can actually focus more in depth on bioactive materials for bone regeneration.

1.4 Calcium phosphate ceramics

Among bioactive materials for bone regeneration, calcium phosphate (CaP) bioceramics have a lot of potential, owing to their high biocompatibility and osteoconductive properties as well as their ability to form direct bonds with bone tissue [33] [34]. The use of CaP ceramics has also backed up by their physicochemical similarity to bone mineral, and their ability to undergo resorption, both in vitro [33] and in vivo [35].

Different calcium phosphate ceramics can be distinguished, with varying composition and crystal structure, granting them distinct physicochemical properties. It is important to remark that while most CaPs are osteoconductive, not all of them are osteoinductive. Furthermore, solubility, crystallinity, Ca/P ratio, surface roughness and surface energy of calcium phosphates may affect protein adsorption, cell adhesion and cell differentiation [36]. Table 1.1 summarizes composition and some physicochemical properties of the most widely used calcium phosphate ceramics, while some of them are described in more detail below:

(a) **Hydroxyapatite**: HA is the CaP that most resembles bone apatite, and is very stable above pH 4.3. It is characterized by its hexagonal crystal structure and its Ca/P ratio of 1.67 (stoichiometric synthetic HA). Furthermore, HA is highly biocompatible, it has good osteoconductivity and slow resorption (5%-15% per year), which makes HA an ideal material for dentistry and orthopaedic applications. However, as the mechanical strength of HA is low (38-300 MPa depending on the measurement technique and porosity [37]) its use is restricted to low load-bearing applications, such as cements or coatings [38] [39]. In some cases, slow resorption is not desired and some work has focused in tuning the resorption rate. Fleming et al. created a composite made of calcium carbonate with a thin coating of HA, achieving a biomaterial that initially behaved as pure HA but after the resorption of this coating (few months), the calcium phosphate was absorbed much more rapidly [40]. The main application of HA is in dentistry and orthopaedics [41].

(b) **Tricalcium phosphates**: TCPs are considered to be fast resorbing ceramics as they have greater solubility than HA [40]. Two dominant phases can be distinguished in TCP: α-TCP and β-TCP. The α-TCP has a monoclinic crystal structure while the β-TCP is characterized by a pure hexagonal (rhombohedral) structure. Despite both TCPs having the same Ca/P ratio, their different crystal structure provides different physicochemical properties. For instance, α-TCP is more soluble than β-TCP [45]. It is also important to remark the importance of the porous dimensions and its interconnectivity, which also influences bone regeneration and the degradation of the ceramic. In this way, not only macroporosity should be taken into account but also microporosity. For instance, H. Yokozeki et *al.* shown that micropores of β-TCP of about 0.2-0.5 μm affected bone resorption [42]. Because of its good bioactivity, biodegradability, osteoconductivity and osteoinductivity, β-TCP has been more used in the clinics than α-TCP [36] [43].

(c) **Biphasic calcium phosphates**: BCPs are calcium phosphates composed of two different phases, allowing the possibility to obtain materials with properties that are between the two CaPs separately. One of the most widely used BCPs is made of a mixture of HA

and β-TCP, leading to a ceramic with low solubility (from the HA), osteoconductivity and osteoinductivity (from the TCP) [10] [36]. The resulting CaP has a Ca/P ratio that varies between the one of the HA and the one of the TCP, depending on the percentage of each phase, which also influences the bioactivity of the ceramic [44]. BCPs are mainly used as bone fillers [45].

(d) **Octacalium phosphate**: OCP occurs as an intermediate phase of the thermodynamically more stable HA and it has a triclinic crystal structure. OCP is also biocompatible and osteoconductive [45] [48]. It has been reported that when OCP was implanted in subperiosteal region of mouse calvaria, it was able to form a very similar structure to the one observed at the first phases of the mineralization in intramembranous bone formation, which may be related with the chemical nature of the OCP [49]. Although OCP has been used as a filling material in bone defects of animal models [50], it has not been translated into the clinics yet [45].

Phase	Chemical formula	Ca/P ratio	Density (g/cm^3)
Dicalcium phosphate anhydrate (DCPA)	$CaHPO_4$	1/1	2.89
Dicalcium phosphate dihydrate (DCPD)	$CaHPO_4{\cdot}2H_2O$	1/1	2.32
Octacalcium phosphate (OCP)	$Ca_8(PO_4)_4(HPO_4)_2{\cdot}5H_2O$	8/6	2.61
α-Tricalcium phosphate (α-TCP)	$Ca_3(PO_4)_2$	3/2	2.86
β-Tricalcium phosphate (β-TCP)	$Ca_3(PO_4)_2$	3/2	3.07
Hydroxyapatite (HA)	$Ca_{10}(PO_4)_6(OH)_2$	10/6	3.16
Tetracalcium phosphate (TTCP)	$Ca_4P_2O_9$	2/1	3.05

Table 1.1: Physicochemical properties of the most widely used calcium phosphate ceramics [46] [47] [45].

1.4.1 Calcium phosphate coatings

Due to their brittleness and low mechanical properties, bulk CaPs cannot be used in load-bearing applications. However, their high biocompatibility and osteoconductivity have led to their use as coatings of metallic implants, especially in orthopaedics and dentistry, allowing to combine the mechanical strength of metallic materials with the biological response of calcium phosphates. In this way, calcium phosphate coatings enhance the fixation of the implant, by allowing a direct connection with the bone tissue [51]

Plasma sprayed coatings

Several techniques are used to achieve CaPs coatings, and plasma spraying is one of the most relevant, as it is applied to implants currently used in the clinic [52]. This technique deposits a thin layer of calcium phosphate (normally HA) onto the surface of a metal. Briefly, a direct current of high energy is applied between a cathode and an anode, generating an electric arc. The electric discharge ionizes an inert gas, forming a high temperature (20.000K) plasma. CaP powders introduced in the hot plasma (with a carrier gas) melt and are deposited on the surface of the substrate [53] (see Figure 1.2). With this technique, a coating of about 50 μm can be obtained [54].

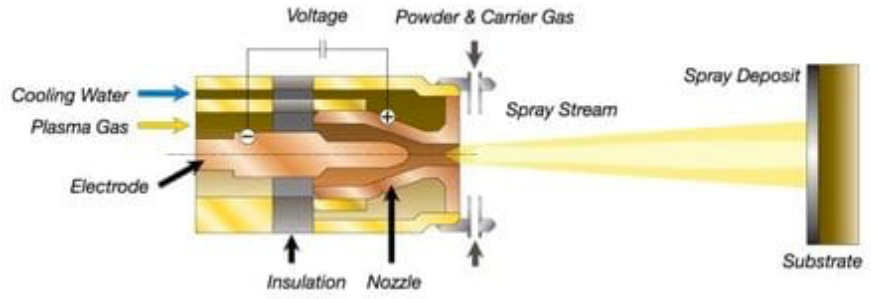

Figure 1.2: Plasma-sprayed technique [55].

A drawback of this technique is the modification of the properties of the initial powders (in terms of phase composition and structure) due to the thermal instability of the CaPs, as they reach high temperatures within the plasma. Theoretically, when the CaPs powders are injected into the plasma, only the surface of the particles melt, allowing adhesion among the particles, and also between the particles and the substrate. This melt part of the particle generates an amorphous phase that surrounds the crystal phase of the original powder, creating a final coating that actually does not have the same phase composition of the initial powder [56]. However, by controlling the initial dimensions of the powders, the spraying distance, the gas and the cooling process of the coating, it is possible to control the CaP phase deposited [53]. Plasma spraying is the preferred method for coating hip prosthesis.

Despite the great success of plasma sprayed coatings in the clinic, they still have some significant drawbacks. One of the major concerns is the possible dissolution and degradation of HA due to instability and/or disintegration of HA coating, leading to a loss of contact between the implant and the native tissue, poor fixation and short-term failure of the implant, in the worst case scenario [57]. Furthermore, plasma spraying can only be applied with stable CaPs (HA or TCP) [58]. In addition, implants with complex geometries can not be coated by using this method, due to the line-of-sight coating process [59]. There are a number of possible alternative methods for applying a CaP coating on a substrate, such as high-velocity oxy-fuel spraying (HVOF) [60], electrophoretic deposition [53], sol-gel deposition [61] or pulsed laser deposition [62], among others. However, biomimetic deposition seems to offer the best alternative to the rest of techniques [58].

Biomimetic coatings

These coatings are obtained by immersing the materials in Simulated Body Fluids (SBF), a type of solution that mimics some aspect of the physiological environment, e.g. the ion concentration, pH and temperature of human blood plasma [63]. The first formulation of SBF was developed by T. Kokubo in 1991, where a method was described to evaluate the potential bioactivity, specifically bone-binding ability, of a target material. The formation of

a layer of apatite upon immersion in SBF was generally regarded as an indication of good integration with bone tissue [64]. Many modifications of the initial composition of SBF have been reported, by T. Kokubo [65] and others. For instance, P. Habibovic et *al.* used a two-step biomimetic coating to obtain a coating of hydroxyapatite on Ti_6Al_4V implants. In the first step, implants were immersed in 5x concentrated SBF, obtaining an amorphous calcium phosphate coating. Afterwards, the implants were soaked in a second solution, where the composition was very similar to the first one but with less content of magnesium (Mg^{2+}) and carbonate ions (HCO_3^-), which are known as crystal growth inhibitors. Consequently, a crystalline CaP coating was achieved [66].

These biomimetic coatings have also been applied in hydrogels. For example, Madhumath et al., created a composite of chitosan/HA introducing a chitosan membrane in a solution of $CaCl_2$ and Na_2HPO_4 at pH 7.4. HA deposition occurred on the surface of the membrane [67]. The main advantage of these biomimetic methods compared to spray techniques is that structures with complex geometries can be easily coated. Besides, this process takes place at low temperature, which increases the range of materials that can be coated, as well as incorporation of organic molecules. Finally, bone-like apatite coatings are achieved with this technique, leading to biomaterials that have better interaction with native bone tissue.

Despite the clinical success and the advantages of biomimetic methods [68], they succeed only in replicating the inorganic phase of bone. To obtain coatings that more closely resemble the native tissue, other aspects can be considered, for instance, incorporating the organic phase, or replicating the structure of bone, could be some aspects to take into account. These questions have also been considered by some research groups, trying to improve biomaterials for bone regeneration, considering the structure and main components of the native bone. To reach this goal, a lot of investigations have focused on the comprehension of the mineralization of bone.

1.5 Bone mineralization process

Despite bone composition and structure being known to a very fine detail, the same cannot be said of the mineralization process and this is a very active field of research. Biomineralization of bone is the process whereby hydroxyapatite crystals are deposited in an ordered way in the organic ECM of bone. In this ECM, collagen plays a crucial role. A collagen molecule consists of a highly repetitive amino acid sequence, normally Glycine-X-Y, with X often being Proline and Y Hydroxyproline. Three of these polypeptide chains fold into a triple-helical structure, consisting of two identical chains ($\alpha 1$) and a different one ($\alpha 2$) and forming tropocollagen molecules [69]. The tropocollagen undergoes a self-assembly process to create a quarter staggered arrangement of parallel units and form microfibrils, which aggregate to form collagen fibrils. This quarter-staggered array generates a periodic banding pattern within the fibrils, forming a 67 nm repeat model (40 nm hole zone and 27 nm overlap zone). This 40 nm hole is thought to act as a template for mineral deposition and affect the final size, orientation and shape of the crystals as well as their distribution [20].

While collagen serves the role of structural matrix to become mineralized, non collagenous proteins (NCPs) are also essential to proper matrix mineralization, as they act as modulators, inhibiting or promoting mineral formation. Without them mineralization cannot occur, as they act as signalling molecules, orchestrating all the mineralization process. Generally, NCPs are made of long flexible chains, containing a great number of acid residues. They also have a lack of three-dimensional structure and they are depleted in hydrophobic residues [73] [74].

NCPs are able to bind to calcium and also have high affinity for collagen. It has been shown that when NCPs are in solution, they inhibit HA nucleation, while they induce intrafibrillar

mineralization when they are attached to a substrate [20]. Consequently, the binding of NCPs to collagen fibrils may promote intrafibrillar nucleation [70]. The prenucleation clusters of these charged amino acids form nucleating sites and control the conversion of the ACP into parallel organized fashion of hydroxyapatite crystals [71] [72]. As these clusters are negatively charged, they are attracted towards positively charged regions within collagen. Due to this fact, the amorphous precursor fills the spaces between collagen fibrils, probably by capillarity, although a lot of questions still remain. The ACP is then solidified and transformed into oriented nanoscopic crystals of HA, directed by the collagen fibrils. Figure 1.3 shows this process.

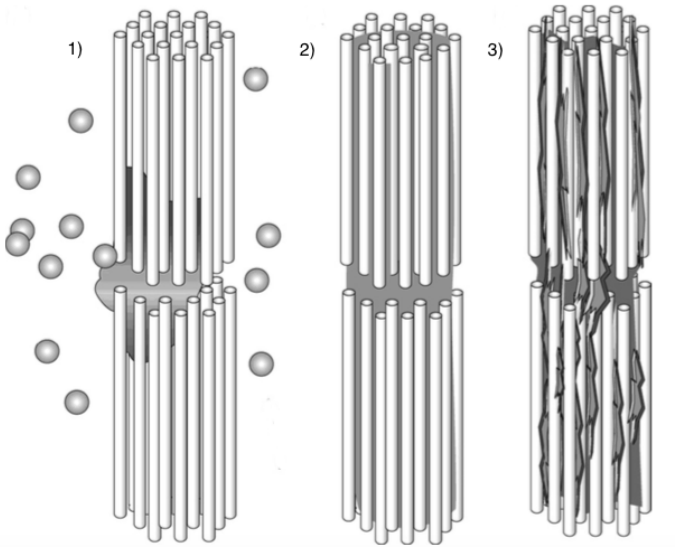

Figure 1.3: Collagen template-mediated mineralization theory [20].

Among NCPs, the small integrin-binding ligand N-linked grycoprotein (SIBLING) family has paid a lot of attention. This family consist of osteopontin (OPN), bone sialoprotein (BSP), dentin matrix protein 1 (DMP1), dentin sialophosphoprotein (DSPP) and matrix extracellular phosphoglycoprotein (MEPE).

These proteins are well characterized because all of them are located in the same chromosome region, display the Arg-Gly-Asp (RGD) sequence (known as the cell-binding motif because it allows the binding of cells to the ECM) and are secreted into the ECM of bone during osteoid formation and bone mineralization [75].

OPN is expressed in bone by osteoblastic and osteoclastic precursor cells and it is essential in the metabolic regulation of bone. It has been shown to play an inhibitory role in HA formation and growth in the ECM mineralisation. BSP is thought to act as a crystal nucleator but also to cryptic cell adhesion site and to regulate bone resorption of osteoclasts, indicating that BSP is one of the most potent proteins to act as a nucleator of HA [77] [78]. This was shown by Curtain et *al.*, who demonstrated that dephosphoryled bone BSP inhibited the differentiation of osteoclasts [79]. BSP is present exclusively in mineralized tissues and Gordon et *al.* demonstrated that osteoblasts overexpressing BSP enhance mineralization [80]. Moreover, MEPE is also important in bone mineralization and phosphate homeostasis. This was confirmed by David and colleagues, who observed that mice treated with recombinant MEPE had less number and activity of osteoclasts [75].

1.6 Biomineralization-inspired materials

Due to the extreme complexity of studying biomineralization processes in vivo, in vitro models have been developed to examine collagen mineralization [81]. These in vitro models

have the advantage of reducing variables, allowing the control over the reaction environment, which makes it easier to study independent parameters. Although these models are not able to prove what exactly occurs in vivo, they provide insightful clues, while at the same time driving the research in biomaterials that aim to mimic collagen mineralization. The defining characteristic of in-vivo mineralized collagen is the intimate contact between nanoplatelets of HA within collagen fibrils – so called intrafibrillar mineralization – which makes bone essentially a nanocomposite. It is this composition and arrangement at the nanoscale, coupled with higher levels of organization at larger scale, that ultimately give bone its outstanding mechanical properties [82].

First approaches to mimic bone formation were developed by introducing type I collagen substrates into simulated body fluid (SBF), on the premise that biological HA is in constant contact with the extracellular fluid, and thereby mineralization of collagen would occur as part of the interaction with body fluid [83]. Nevertheless, mimicking the natural bone formation was not possible by this method, as mineralization did not occur within the collagen fibrils but only on their surface and thereby, it was believed that other factors may play a role in mineralization, such as NCPs, as explained above.

Based on the hypothesis that NCPs are essential in intrafibrillar mineralization of collagen, a polymer-induced liquid-precursor (PILP) process has been successful in mimicking the collagen template-mediated mineralization process by using polyaspartic acid as a process-directing agent, replacing the role of NCPs in vivo. Polyaspartic acid shares some characteristics common to all NCPs, namely the disordered structure and high abundance of acidic side groups. Much like some NCPs, pAsp is able to prevent CaP nucleation by sequestering ions, forming an ion-polymer complex. This pAsp-stabilized ACP precursor somehow infiltrates the collagen fibrils, and the amorphous mineral matures into HA crystals over time [20] [84] [85].

It is interesting to note that in the PILP process, at the early stages of mineralization, collagen fibrils still appear smooth when observed by SEM, owing to the fact that most of the mineral is located inside the fibrils. After longer mineralization times, the fibril surface become rougher because of extrafibrillar deposition [20]. The PILP approach shed light on the hypothesized role of NCPs in bone mineralization, while allowing biomaterials scientists the opportunity to go further in biomimetic materials. The use of pAsp as NCP analogue allowed intrafibrillar mineralization of collagen fibrils in-vitro, a big step in bringing artificial materials closer to the native composition and structure of bone tissue [86] [87] [88] [89] [90].

It is remarkable that the PILP process has not been limited to the mineralization of collagen, but has also been applied to possible synthetic replacements for the structural matrix. For example, Yuping Li et *al.* used thermoresponsive hydrogels composed of elastin-like recombinamers to simulate the collagen template. These hydrogels were mineralized by PILP process, obtaining a composite that contained a mineral density and microporous structure very similar to the natural bone [91].

Although the PILP process has been successful in mimicking the bone mineralization at fibril scale, the mechanism by which it happens is still under debate [85]. Furthermore, from the perspective of material's design for bone regeneration, there are still some points that can be improved. Using collagen as structural matrix has restrictions (obtained from an animal source) that could be overcome by replacement with a synthetic polymer. Another example is the penetration depth of the PILP phase, which could be a limiting factor in dense collagen scaffolds, as solidification of PILP could block the entry of further mineral precursor [74]. While obtaining the "building block" of bone is certainly a step in the right direction, the matter of its organization in levels similar to those found in-vivo poses another interesting challenge.

Moreover, there is also a lack of research in the interaction of these biomaterials with cells and the comparison with other polymer/CaPs. The following section focuses on cell-material interactions, particularly for the case of calcium phosphates. The link between osteoinduction and osteoclast resorption will be mentioned as well.

1.7 Cell-material interaction in CaPs

The interaction between a biomaterial and the surrounding tissue plays an important role in the success of a regenerative strategy. When a biomaterial is implanted, the homeostasis of the body is always disrupted and the implant is recognised as a foreign body by the immune system, leading to a cascade of effects (foreign body response). Control over the inflammatory response could play and important role in bone tissue engineering, due to the intimate relation between bone and the immune system [92]. This was studied by Liu X-H and colleagues, who demonstrated that the inflammatory cytokines Interleukin-6 (IL-6) and Prostaglandin (E_2) regulate osteoclast differentiation and resorption [93]. As a consequence, it may be possible to engineer biomaterials, in particular CaPs, to drive this immune response toward osteogenesis, obtaining osteoinductive CaPs.

Although many osteoconductive CaPs has been studied and used in the clinic [94], the same cannot be said of osteoinductive CaPs. Nonetheless, more and more investigations are done trying to make this property a characteristic of CaPs and several authors have noticed the ability of some CaPs to induce the novo bone formation. For example, different groups have shown the osteogenic ability of OCP coatings in vivo. In particular, F. Barrère el *al.*, demonstrated that the microporous structure on OCP induced bone formation [95]. P. Habibovic and colleagues also shown that Ti implants biomimetic coated with OCP were osteoinductive [58]. Furthermore, some research groups have shown that CaPs have to meet specific requirements regarding their macro- and microstrusture, as well as their chemical composition in order to be osteoinductive [5].

Trying to explain the relationships between CaPs characteristics and osteoinduction, diverse theories have been developed. Basically, these theories have been divided into two kinds: the ones that support that osteoinduction is related to physicochemical properties of materials and the ones that aim that osteoinduction is influenced by structural/topographical features. The discussion of these theories exceeds the purpose of this thesis and the reader is invited to consult [92] for a nice review of them. Interestingly, there is some support that microstructured CaPs stimulate osteoclast formation before new bone formation, proposing that osteoclasts may play an important role in osteoinduction [92]. Y. Shiwaku et al. studied if the chemical composition and the microstructure of BCPs had any influence in osteoclasts differentiation and de novo bone formation in vitro. They found that osteoclasts differentiation was affected by increasing the HA content of BCPs, while the presence of micropores did not affect it. Furthermore, the composition of the BCP not only influenced the differentiation of osteoclast, but also their ability to secrete clastokines that induced bone formation [96]. Similarly, but in vivo, N. Kondo and colleagues observed that purified β-TCP implanted in dog dorsal muscles was resorbed by osteoclasts and led to new bone formation [97]. Also in vivo, N. Akiyama and co-workers implanted porous calcium-deficient hydroxyapatite in the dorsal muscles of dogs and rats. After two weeks of implantation, they observed a great amount of TRAP-positive multinucleated cells and new bone formation after four days. However, in the rat samples only a few number of osteoclast were found and no bone formation was observed after 6 weeks, indicating that osteoclast formation could be one of the main factors to induce osteoinduction

[98]. This section will finish by examining the osteoclast resorption of calcium phosphates in more of detail.

1.7.1 Osteoclast resorption of calcium phosphates

Although a brief introduction to osteoclasts has been presented previously, it is considered important to study them in more in detail to understand how osteoclasts resorption of calcium phosphates is produced.

Osteoclasts are multinucleated giant cells that are formed by the fusion of mononuclear monocyte/macrophage precursors and the activation of tartrate-resistant acid phosphatase (TRAP) enzyme. However, for these precursors to differentiate into osteoclasts, they need the influence of macrophage colony stimulating factor (MCSF) and receptor activator NF-κB ligand (RANKL), which are supplied by osteoblasts (RANKL is expressed in osteoblast membrane). During this differentiation process, osteoblasts also secrete osteoprotegerin (OPG), a decoy receptor for RANKL to control the formation of osteoclasts [99].

As explained previously, osteoclasts are responsible for bone mineral degradation (bone resorption). It has been demonstrated in vitro that osteoclasts degrade CaPs in a very similar way to bone mineral. In brief, osteoclasts attached to the substrate start to secrete acidic substances and proteolytic enzymes, such as cathepsin K. While the acidic environment (pH = 4 or 5) is responsible for HA dissolution, protease action is needed to hydrolise the matrix proteins, such as collagen. [45] [92] [99].

However, in vivo, CaPs can be resorbed both by cells (osteoclasts and macrophages) and passively (dissolution, erosion or fragmentation). Cell resorption versus dissolution processes of CaPs depend on the chemical and physical composition of CaPs [92]. The influence of these properties was shown by Yamada et *al.*, who studied how the Ca/P ratio in HA/β-TCP influenced osteoclastic resorption. In a first approach, they concluded that solubility influences osteoclast behaviour: the higher the HA/β-TCP ratio, the lower the solubility as TCP is more soluble than HA. By comparing BCP with different HA/β-TCP ratios with pure β-TCP, they showed that that osteoclastic resorption in HA/β-TCP with 25/75 ratio was higher than HA/β-TCP with 75/25 ratio, demonstrating that resorption decreased with increasing HA fraction. They also compared HA/β-TCP with 25/75 ratio with pure β-TCP (that has higher solubility than HA/-beta-TCP). From the previous finding, they expected TCP to show higher resorption than BCP. However, they observed the contrary. This was explained by the fact that in the resorption cycle of osteoclast (resorption/migration), the shift between the resorption phase and the migration one occurred earlier on β-TCP than on BCP [100]. As a consequence, they finally concluded that the amount of calcium and phosphate ions in the environment may play a critical role in the osteclasts behaviour, showing that cellular resorption does not have to follow necessarily the same trend that physicochemical dissolution of CaPs [44].

Surface architecture of CaPs also plays a relevant role in osteoclast resorption. Noel et *al.* studied how osteoclast resorption of β-tricalcium phosphate could be controlled by modifying the surface architecture. In particular, they cultured human peripheral blood monocytes on the surface of two TCPs with submicron- or micron-scale and differentiated them to osteoclasts. It was found that the TCP with submicron-scale promoted resorption of osteoclasts, while the micron-scale surface did not allow either the survival or resorption of osteoclasts. [35] [101]. S. Patntirapong and colleagues also demonstrated that mammalian osteoclasts respond to Co^{2+} extracted from a CaP substrate, which stimulated osteoclast formation and activation [102].

1.8 Motivation of the project

Bone tissue has a high capacity of regeneration, which allows fractures to heal without the need of surgical intervention. However, it is only capable of doing so for defects under a critical size. One of the joints most commonly affected is the hip [4].

Although hip implants have a good performance in short term, they may fail due to loosening of the implant in long term. To avoid it, plasma-sprayed coatings of calcium phosphate have been developed, obtaining coatings with similar composition to the mineral phase of bone tissue. Nevertheless, due to the shortcomings previously described, a switch to techniques that provide coatings with better performance, such as biomimetic coatings, is needed. In an effort to better mimic the composition of bone, a thin collagen layer on top of these biomimetic CaP coatings can be added. Nonetheless, the native ECM bone structure is still missing.

The goal of this project is to evaluate the biological performance of a material that more closely mimics bone tissue, comparing it to current biomimetic coatings; namely, a biomaterial composed of the same "unit cell" than bone tissue is made of: a collagen fibril showing intrafibrillar mineralization. By improving the similarity with native tissue, the performance and interaction with the surrounding tissue are expected to increase. To assess this, the resorption potential of the material will be evaluated, the hypothesis being that a PILP-mineralized collagen should be more readily resorbed than conventional CaP coatings.

What is presented here is a collagen/CaP coating synthesized using the PILP process. In brief, it is possible to create a thin collagen coating and mineralize it in a PILP solution, obtaining coatings that are very close in composition and structure to native bone.

Following the resorption study, attempts were made to micropattern this collagen/CaP coating obtained previously. The rationale of this micropatterning is based on the fact that by having a particular pattern of collagen/CaPs, it is possible to control cell morphology, growth and even differentiation. As a consequence, a micropatterned collagen/CaP coating made, for instance, on a hip implant would allow to direct osteoclastic resorption and potentially guide osseointegration.

Chapter 2: Materials and methods

2.1 Sample preparation for osteoclast resorption of calcium phosphates

2.1.1 Calcium phosphate solutions

Two calcium phosphate coatings were prepared on standard tissue culture polystyrene microplates, one yielding mainly an HA phase, and another yielding mainly an OCP phase. The HA coating is obtained in a two-step incubation, with the first solution depositing a thin amorphous coating, and the second forming globular HA crystals. Both these solutions are modifications of a 5x concentrated SBF, with slight modification, and incubation with either of them was for 24 hours at 37°C in a incubator (100% humidity, 5% CO_2). The preparation of the solutions is described below:

(a) **5xSBF (A)**: This solution is a modification of a 5x concentrated Simulated Body Fluid (SBF) from Kokubo *et al.* [103], without the potassium (K^+) and sulfate (SO_4^{2-}) ions, and also without Tris buffer. The required amount of milliQ water was poured in a beaker while stirring with a magnetic bar and with temperature was set to 37°C. The required amount of NaCl (Sigma-Aldrich, USA), $MgCl_2{\cdot}6H_2O$ (Sigma-Aldrich) and $CaCl_2{\cdot}2H_2O$ (Sigma-Aldrich) were dissolved in milliQ water in this order, obtaining a solution with 684.46 mM NaCl, 7.48 mM $MgCl_2{\cdot}6H_2O$ and 12.53 mM $CaCl_2{\cdot}2H_2O$. Then, CO_2 was diffused in the solution until pH dropped to 4. Afterwards, $Na_2HPO_4{\cdot}2H_2O$ (Sigma-Aldrich) and $NaHCO_3$ (Sigma-Aldrich) were added to the solution while still bubbling with CO_2, obtaining a solution with a concentration of 5 mM $Na_2HPO_4{\cdot}2H_2O$ and 10.47 $NaHCO_3$. The total volume of solution was completed by adding milliQ water. Bubbling with CO_2 was continued until pH dropped below 6.2. Once pH was below 6.2, the solution was added to the samples.

(b) **5xSBF (B)**: This solution is similar to 5xSBF (A), but the concentration of magnesium (Mg^2) and carbonate ions (HCO_3^-) is less, as they are known as crystal growth inhibitors. The required volume of milliQ water was poured in a beaker while stirring and with temperature set to 37°C. By adding the required amount of chemicals, we obtained a solution of 684.46 mM of NaCl, 1.48 mM of $MgCl_2{\cdot}6H_2O$ and 12.53 mM of $CaCl_2{\cdot}2H_2O$. Then, CO_2 was diffused in the solution until pH dropped to 4. Afterwards, the required amounts of $Na_2HPO_4{\cdot}2H_2O$ and $NaHCO_3$ were added to the solution while still bubbling with CO_2, obtaining a concentration of 5 mM $Na_2HPO_4{\cdot}2H_2O$ and 10.47 mM $NaHCO_3$. The total volume of solution was completed by adding milliQ water. Bubbling with CO_2 was continued until pH dropped below 6.2. Once pH was below 6.2, the solution was added to the samples.

The OCP coating is also prepared following a two-step incubation method, where the first incubation is in 2.5x concentrated SBF, yielding a thin amorphous coating, and the second step

in a calcium phosphate saturated (CPS) solution containing only the ions necessary for OCP precipitation. The preparation of solutions is described below:

(c) **2.5x SBF** [102]: This solution was prepared by mixing a Tris buffer solution with two stock solutions of calcium and phosphate ions precursors. First, the Tris buffer solution was prepared (milliQ water with 50 mM of Tris base (Avantor Performance, USA), pH was adjusted at 7.4 by adding 1M HCl (Sigma-Aldrich) at room temperature). A 25 mM $CaCl_2{\cdot}2H_2O$, 1.37 M NaCl and 15 mM $MgCl_2{\cdot}6H_2O$ solution (calcium stock solution) was prepared at room temperature, by dissolving the required amount of chemicals in the Tris buffer. Phosphate stock solution was made of 11.1 mM $Na_2HPO_4{\cdot}2H_2O$ and 42 mM $NaHCO_3$ in Tris buffer. In the last step, Tris buffer was mixed with phosphate and calcium stock solution at a ratio of 2:1:1, in this order.

(d) **CPS**: This solution contained only the ions necessary for octacalcium phosphate (OCP) precipitation. The required amount of chemicals were added into Tris buffer solution (milliQ water with 50 mM of Tris base, pH adjusted at 7.4 by adding 1M HCl at room temperature) in order to obtain a solution with final concentration of 0.14 M NaCl, 2.02 mM $Na_2HPO_4{\cdot}2H_2O$, 4.01 mM $CaCl_2{\cdot}2H_2O$ and 50 mM $NH_2(CH_2OH)_3$. The solution was prepared at room temperature [102].

(e) **PILP solution**: PILP solution was prepared as explained in [20]. Briefly, a Tris-saline buffer was made by dissolving 50 mM Tris-base and 150 mM NaCl in milliQ water. The pH was then adjusted to 7.3 (at room temperature) using 1M HCl. Note that the pH becomes 7.4 at 37°C. This Tris-saline buffer was used to prepare 9 mM $CaCl_2$ and 4.2 mM K_2HPO_4 as a Ca and P precursor solutions, respectively. Poly(L-aspartic acid sodium salt) (pAsp, 27 KDa, Alamanda Polymers, USA) was then added to the 9 mM $CaCl_2$ solution to obtain a concentration of 100 μg/mL in the final volume of PILP solution. Finally, equal volumes of the 9 mM $CaCl_2$ solution (containing the polyaspartic acid) and 4.2 mM K_2HPO_4 were mixed, and solution was added to substrates.

The ionic concentration of each mineralization solution is shown in Table 2.1. Note that all the solutions were filtered with a 0.2 μm filter inside a sterile hood before preparation of the coatings.

Ionic concentration (mM)							
Ions	Blood plasma	SBF	2.5x SBF	Rainbow A	Rainbow B	CPS	PILP
Na^+	142	142	358.55	733.5	733.5	140	150
K^+	5	5	-	-	-	-	8.4
Mg^{2+}	1.5	1.5	3.75	7.5	1.5	-	-
Ca^{2+}	2.5	2.5	6.25	12.5	12.5	4.0	9
Cl^-	103.8	148.4	362.5	721	721	144	178
HPO_3^{2-}	1	1	2.775	5	5	2	-
SO_4^{2-}	0.5	0.5	-	-	-	-	-
HCO_3^-	27	4.2	10.5	21	10	-	-

Table 2.1: Ionic concentration of CaP coating solutions.

2.1.2 Collagen membrane mineralization

In order to verify if the PILP solution was prepared correctly, a mineralization experiment was performed with a commercial collagen membrane, consisting of type-I fibrillar collagen

(MatrixMem, Collagen Matrix, USA). In this experiment, three different concentrations of pAsp were tested: 0, 50 and 100 μg/m. Furthermore, the experiment was divided in two: one with medium refreshment, and the another without medium refreshment. Collagen membrane pieces ($\approx$ 2x3 mm) were weighted, added to a 15 mL of the PILP solution (prepared as explained in previously) and incubated at 37°C for different times. For each pAsp concentration and timepoint, three replicas were prepared. The refreshment experiment was run for 7 days, with refreshment of the PILP solution at day 2 and 5. At day 7, samples were removed from the PILP solution, blotted with filter paper, weighted, freeze-dried for 24h and stored at -25°C. In the case of the no refreshment experiment, samples were incubated for different time-points: 3, 7 and 14 days for 50 and 100 μg/mL of pAsp. Samples without pAsp acid were incubated only for 14 days. After the incubation time, samples were blotted with filter paper, weighted, freeze-dried for 24h and stored at -25°C as in the refreshment experiment. Controls were membrane pieces freeze-dried for 24h without any incubation. Quantification of mineral content in collagen membranes was measured by thermogravimetric analysis (TA Instruments Q500).

2.1.3 Optimization of Collagen coating (for PILP process)

In order to obtain a homogeneous collagen coating, to be mineralized with the PILP solution, a series of experiments were performed. As explained in the Introduction, collagen fibrils with the characteristic 67 nm banding are required to obtain intrafibrillar mineralization, as crystals form in the gaps between collagen molecules.

(a) To obtain the collagen fibres, collagen type I from rat tail (Thermo Fisher Scientific) was dissolved in a fibril formation buffer (FFB), at the concentration of 20, 100 or 500 μg/mL. FFB consists of 10 mM NaH_2PO_4 (Sigma-Aldrich) with different concentrations of NaCl (100, 200 or 400 mM) to test the ionic strength influence on fibre assembly. Each collagen concentration was dissolved with the three different concentrations of NaCl, so in total, 9 different conditions were obtained. Collagen solutions were incubated for 24h at RT to allow fibril formation and an aliquot of each suspension was dispensed on a SEM stub, left for 1h at RT to have collagen fibril deposition and subsequently washed. Samples were sputter coated with iridium (2 nm, Cressington sputter coater 108 auto) before imaging with SEM (Teneo, FEI, USA). From this experiment, the three conditions that gave the best results (100 μg/mL in FFB-200 [1], 100 μg/mL in FFB-400 and 500 μg/mL in FFB-400) were chosen for further optimization.

(b) For each of these three conditions, a coating with different number of layers was prepared, by sequential deposition of the same solution. The three different collagen solutions were prepared and incubated during 24h at RT to allow fibril formation, as done previously. After the incubation time, TCPS pieces of $\approx$1 cm^2 were coated with 3, 6 or 9 layers of each of the three collagen solutions. For each collagen layer, 100 μL of solution were placed on top of a TCPS piece and incubated for 30 min at RT to allow the fibrils to deposit. Afterward, samples were briefly washed with MilliQ water and prepared for SEM. As this attempt did not produce a homogeneous coating, a different approach was followed.

(c) In this case, a two-step collagen coating was performed in TCPS. The first coating deposits a thin, non-fibrillar layer of collagen on the TCPS surface, to ameliorate the adhesion of collagen fibres on the substrate. It was prepared by diluting collagen stock solution (3 mg/mL) to 50, 100 or 500 μg/mL, in 20 mM acetic acid, and covering the substrate for 1h at RT. Solution was gently aspirated before the second incubation. The collagen solutions

[1] From now on, unless indicated the contrary, FFB will be assumed to be composed of 10 mM NaH_2PO_4 and 200 or 400 mM NaCl (FFB-200 or FFB-400 respectively.)

used for the second step were the ones prepared in FFB, as described above. In this case, three different conditions were studied: 100 μg/mL of collagen diluted in FFB-200 (100-FFB-200), 500 μg/mL of collagen diluted in FFB-400 (500-FFB-400) and 2000 μg/mL of collagen diluted in FFB-400 (2000-FFB-400). Collagen solutions were prepared, added to the pre-coated TCPS and incubated for 24h at RT to allow collagen fibril formation and deposition. Furthermore, an extra-condition was studied: 100 μg/mL of collagen diluted in FFB-200 was incubated 24h at RT in a tube and then added to the TCPS for 1h to allow fibril deposition (this sample was called 100-FFB-200-b). Samples were analysed by SEM and immunostaining.

Observation of collagen banding pattern and confirmation of intrafibrillar mineralization of collagen was done by TEM (Tecnai G2 Spirit, FEI, USA).

2.1.4 Preparation of substrates for cell culture

The main aim of this experiment was to study how different CaPs coatings affected osteoclast resorption of CaPs. To evaluate it, a variety of measurements had to be performed: TRAP and actin staining, quantification of TRAP activity and DNA amount, and SEM. Depending on the nature of these measurements, substrates had to be prepared in different way. To assess TRAP and actin staining, or TRAP activity and DNA quantification, 24 and 48-well plates were used, respectively. In the case of samples for SEM, TCPS pieces of $\approx$1 cm^2 were used as substrate. Each TCPS piece was placed in a well of 24-well plate.

Five different substrates were studied:

(a) **TCPS**: polystyrene for cell culture without any modification was used as a control.

(b) **Hydroxyapatite coating**:prepared from 5xSBF (A) and (B) as described in section 2.1.1.

(c) **Collagen coating**: prepared with the two-step method for collagen coating, as described in section 2.1.3 (c). For the first step, consisting of a thin coating, a collagen solution of 100 μg/mL of collagen diluted in 20 mM acetic acid was used. 200 μL/well were added to 24-well plates, and 150 μL/well were added to 48-well plates. For the second step, entailing collagen fibre formation, a collagen solution of 500 μg/mL in FFB-400 was used. 500 μL/well of the solution were used for 24-well plates and 300 μL/well for 48-well plates. This second solution was incubated at 37°C for 48h, with a refreshment at 24h.

(d) **PILP-mineralized collagen**: Before adding the PILP solution, wells were coated with collagen in way described above for collagen coatings on TCPS. Afterwards, PILP solution was added to each well plate (1.3 mL/well in 48-well plates and 2 mL/well in 24-well plates) for 3 days and incubated at 37°C.

(e) **Hydroxyapatite + collagen coating**: this coating was prepared by first coating with hydroxyapatite (section a) followed by coating with collagen (section c).

All samples were rinsed and stored with PBS at 37°C until their use (no more than 3 days).

Surface morphology of the samples was analysed by Scanning Electron Microscopy (XL-30, Philips, Netherlands or Teneo, FEI, USA). Before observation, samples were sputter coated with gold for 30 seconds in argon atmosphere (XL-30), or sputter coated with a 2nm iridium layer (Teneo). Calcium phosphate phases were identified by X-ray diffraction (XRD) with a D2 Phaser diffractometer (Bruker, Netherlands). Data from XRD measurements was analysed with the DIFFRAC.EVA software.

2.2 Cell culture

Murine macrophage cell line RAW 264.7 (ECACC 91062702) was cultured in Dulbecco's Modified Eagle Medium (DMEM) (Gibco, USA) with high glucose, GlutaMAXTM supplement, pyruvate, and supplemented with 10% FBS and 1% penicillin/streptomycin; cells were cultured at 37°C in a humidified atmosphere, with 5% of CO_2. Culture medium was replaced every 2 days unless otherwise indicated. When cells reached 70-80% confluence, they were detached by scraping. In all the experiments described herein, RAW 264.7 were seeded at the maximum density of 20000 cells/cm^2. For differentiation into osteoclasts, RANKL from mouse (Sigma-Aldrich or Peprotech) was used. Cell density, passage and RANKL concentrations are indicated in each particular experiment.

2.2.1 Cell density optimization

This experiment, together with the RANKL optimization experiment, were preliminary studies to find the best conditions (cell density, RANKL concentration and timepoint with highest TRAP activity) for the osteoclast resorption of CaPs experiment. To find the optimal cell density, cells were seeded at 1500, 2500, 4000, 5000, 10000, 15000 and 20000 cells/cm^2 in 24-well plate. Cells were cultured with basic medium and differentiation medium (50 ng/mL of RANKL). Three replicas for each condition were used. Cells were used at passage 9 and cultured for 6 days (for 1500, 2500, 4000 and 5000 cells/cm^2) or used at passage 10 and cultured for 7 days (5000, 10000, 15000 and 20000 cells/cm^2). After that, cells were stained for TRAP enzyme.

2.2.2 RANKL concentration optimization

In parallel with the previous experiment, the effect of RANKL concentration was studied. We were also interested on finding if CaP coatings had any influence in the differentiation process of the cells. To do so, cells were cultured in TCPS and HA coatings with different RANKL concentrations. To optimize all these parameters, three different experiments were performed:

(a) **First trial**: cells were seeded at 20000 cells/cm^2 in 24 and 48-well plate (depending on the characterization technique).Half of the wells of each well plate were HA coated to evaluate the influence of CaPs in the differentiation of the cells. Five different RANKL concentrations were studied: 0, 10, 30, 40 and 50 ng/mL and timepoints were chosen to be 3, 4, 5 and 7 days. At each timepoint, TRAP staining, TRAP activity and DNA quantification were performed. For TRAP staining, 3 replicas per condition were considered, while for TRAP activity and DNA quantification 4 replicas were used. Cells were used at passage 8 and RANKL was from Sigma-Aldrich.

(b) **Second trial**: in this case, 10000 cells/cm^2 were seeded in each well. The rest of the layout of the experiment was very similar to the first, but in order to reduce the size of the experiment, the amount of timepoints (3, 5 and 7 days) was decreased. RANKL was used at the concentration of 0, 30, 50 and 100 ng/mL. The RANKL concentration was increased to 100 ng/mL because at day 4 no differentiation of the cells was observed in the first trial. Differentiation of osteoclast was assessed with TRAP staining, TRAP activity and DNA quantification. In this experiment, cells were used at passage 10 and RANKL was from Sigma-Aldrich.

(c) **Third trial**: as there was no significant differentiation of cells in the first two trials, the RANKL used in this trial was from Prepotech. This company was chosen based on the

bibliography [106] [35]. In this case the concentration of RANKL was 0 , 30, 40, 50 and 100 ng/mL. At day 3, 4, 5 and 7, cells were stained for TRAP enzyme. Cells were used at passage 13 and with a seeding density of 4000 cells/cm^2.

2.2.3 Osteoclast resorption of CaPs

RAW 264.7 (at passage 8) were seeded at the density of 4000 cells/cm^2 in the substrates described in section 2.1.4. After 4h in culture to allow cell attachment to the substrates, medium was refreshed or substituted by differentiation medium. The differentiation medium had 100 ng/mL RANKL. Based on the previous experiments (cell density and RANKL concentration optimization) timepoints were chosen to be 5 and 7 days. After each timepoint, samples were assessed by TRAP and actin staining, resorption (SEM) and quantification of TRAP activity and DNA amount. Depending on the assay performed, the number of samples and the controls chosen were different. In this way, for TRAP and actin staining, two replicates per condition were used and controls were cells cultured in the different substrates without RANKL. For resorption area (SEM), also two replicates per condition were chosen, and controls were samples incubated with medium and no cells, to see if the morphology of the substrates was altered because of the medium. Finally, for quantification of TRAP activity and DNA amount, four replicas per condition were used, with controls consisting of TCPS and HA + collagen incubated in medium without cells. To clarify the experimental layout, a scheme is shown in Figure 2.1.

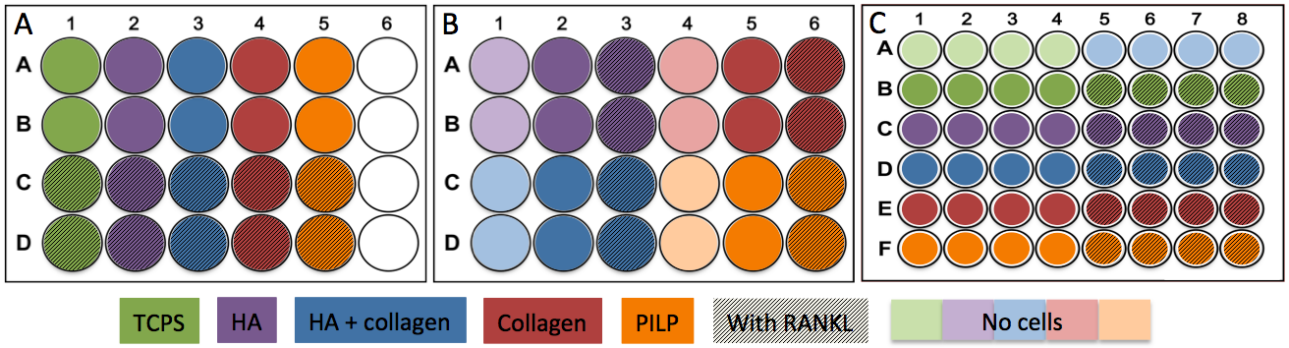

Figure 2.1: Layout of the osteoclast resorption of CaPs experiment. Different colours represent different coatings. The three intensities of these colours represent three different conditions: lighter colours mean that only medium without cells was added to the wells, strong intensity indicates cells were cultured with medium and patterned colours mean that RANKL was added to the medium. White wells were not used. (A) Layout of the 24-well plate for TRAP/actin staining. (B) Layout of the 24-well plate for resorption (SEM). (C) Layout of the 48-well plate for TRAP activity/DNA quantification.

2.3 Cell differentiation and CaPs resorption characterization

2.3.1 Tartrate resistant acid phosphatase (TRAP) staining

For TRAP staining the Leukocite Acid Phosphatase Kit from Sigma was used. After the indicated time-points, cells were fixed with warm 4% paraformaldehyde (PFA) (Sigma-Aldrich) and 0.1% Triton (VWR) in PBS for 10 min and rinsed with PBS. After that, 200 μL of TRAP solution were added to each well (24-well plate) and incubated for 1h at 37°C. TRAP solution was prepared following the protocol from the kit. In brief, for a total of 12 mL of solution, 10.9 mL of milliQ water were added to a 15 mL tube followed by the addition of 0.242 mL of

Diazotized Fast Garnet GBC Solution (formed by mixing equal volumes of Fast Garnet GBC Base Solution and Sodium Nitrite Solution). Then, 0.121 mL of Naphtol AS-Bi Phosphoric acid solution, 0.484 mL of Acetate solution and 0.242 mL of Tartrate solution were also added in this order. Samples were finally washed with PBS and imaged in the microscope.

2.3.2 DAPI/Phalloidin staining

After TRAP staining, samples were rinsed with PBS. Afterward, 200 μL of blocking buffer (5% BSA in PBS) were added to each well and incubated at RT during 30 min. Blocking buffer was removed and 200 μL of Phalloidin (Biotium) (1:200 dilution) were added to each well and incubated at RT for 30 min in a plate shaker (50 rpm). Samples were then washed three times with PBS, followed by the addition of 200 μL of DAPI (Sigma-Aldrich) solution (1 μg/mL diluted in PBS) to each well and incubated at RT for 20 min in a plate shaker (50 rpm). Finally, samples were washed 3 times with PBS and left with PBS and stored at 4°C in the dark until imaging.

2.3.3 Quantification of TRAP activity and DNA amount

Quantification of TRAP activity and DNA amount were assessed following the protocol described by [101]. At each timepoint, cell culture medium was aspirated and wells were washed two times with PBS. After that, PBS was removed and well plates were frozen at -30°C until their use. At the end of the experiment, the well plates of the different timepoints were thawed and cells were lysed in a cell lysis buffer. This lysate was composed of 100 mM sodium acetate (Sigma-Aldrich) and 0.1% of Triton X-100, pH was adjusted to 5.8 with 1M HCl. This buffer was used for both DNA quantification and TRAP activity. 250 μL of cell lysis buffer were added to each well and plates were frozen and thawed twice to break the cell membrane mechanically.

For TRAP activity quantification, TRAP buffer was prepared. This buffer was made of 10 mM sodium tartrate, 100 mM sodium acetate, 150 mM potassium chloride (KCl), 1 mM ascorbic acid, 0.1 mM iron (III) chloride ($FeCl_3$) and 0.1% Triton X-100 (all reagents from Sigma-Alrdich). Solution phosphate precursor, p-nitrophenyl phosphate (pNPP) (Sigma-Aldrich) was added to this buffer, at the concentration of 10 mM. 130 μL of this TRAP buffer + pNPP were pipetted into each well of a 96-well plate. When cell lysis was finished, 20 μL of lysate were added into each well, followed by 1h incubation at 37°C to allow the conversion of pNPP to p-nitrophenol (pNP). A calibration curve of p-nitrophenol (pNP) was also prepared to correlate absorbance with pNP concentration. pNP standards were obtained diluting the pNP in TRAP buffer at 0, 0.05, 0.1, 0.2 and 0.5 mM Afterwards, the reaction was neutralized adding 100 μL of 0.3 M NaOH (VWR) to each well, converting the reaction product to p-nitrophenolate. Finally, absorbance was read at 405 nm by using a microplate reader (CLARIOstar, BMG LabTech). For DNA quantification, CyQuant assay kit from Sigma-Aldrich was used. In brief, 200 μL of cell lysate were pipetted into a glass-bottom black well plate and FR dye reagent was added to the appropriate concentration (1:200 dilution in lysis buffer). A standard curve was also used to correlate DNA amount with fluorescence intensity. In this case, bacteriophage DNA at the concentration of 1.0 μg/mL was diluted to 0, 50, 200, 600 and 1000 ng/mL in GR/lysis buffer. Fluorescence intensity was measured by using a microplate reader with filters for 480 nm excitation and 520 nm emission.

2.3.4 Cell morphology and CaPs resorption

To assess cell morphology and resorption area, samples were imaged with SEM. In the case of cell morphology assessment, after each timepoint, cell medium was removed and cells were

fixed with 4% PFA with 0.1% Triton X-100 during 10 min at RT. For studying resorption, cells were removed from the substrate using a buffer made of 1M NaCl and 0.2% Triton X-100 in dH20. Samples were incubated with this buffer 5 min at RT, followed by a washing with water two times to remove all the salts. After that, all samples were conserved in PBS and dehydrated in a graded ethanol series (from 40 to 100%), incubating the samples 30 min at RT at each ethanol concentration. Samples were finally immersed in hexamethyldisilazane (HMDS) (Sigma-Aldrich) for 30 min and dried overnight. TCPS pieces were then mounted on metal stubs for SEM and gold coated for 30 seconds in argon atmosphere.

Osteoclast size was measured by using imageJ, by measuring the area manually. Cells whose area was higher than 200 μm^2 were considered osteoclasts [35].

2.4 Sample preparation for micropatterning

2.4.1 PDMS moulds

Micropatterned silicon wafers (silicon master templates bearing the desired topographic features) were fabricated using standard photolithography. Polydimethylsiloxane (PDMS) (Sylgard 184 kit, Dow Corning, USA) moulds were obtained by casting the PDMS mixture (10:1 of base to curing agent) on the silicon master. PDMS was poured onto the silicon master and degassed under vacuum at room temperature. The degassed PDMS was then cured at 80°C for 2h and allowed to cool down to room temperature. Afterwards, the PDMS was peeled and cut manually.

2.4.2 Extraction of the oligomers from the PDMS

In order to extract the uncrosslinked PDMS oligomers from the moulds, a protocol described elsewhere [104] was followed. Briefly, moulds were immersed in a sequence of three solvents (triethylamine, ethylacetate, acetone – Sigma-Aldrich), each for 2 hours at room temperature. After the extraction process, samples were dried at 60°C for 4h. PDMS moulds were weighted before and after the extraction process and the weight percent loss was calculated.

2.4.3 Hot-embossing of polystyrene films

Depending on the desired structure to be embossed (micropatterned or flat PS) a micropatterned PDMS mould (parallel channels of 80 μm width and 4.1 μm height), or flat PDMS was placed against a PS film. A glass slide was placed on top and on bottom of the PDMS-PS assembly, with a PTFE piece between PS and glass, and the whole assembly was subjected to pressure by binder clips positioned in the middle. This assembly was introduced in the oven at 130°C for 1h. Samples were then removed from the oven and cooled down at room temperature. When samples were cooled, the structures were disassembled and the desired PS was obtained.

2.4.4 Plasma treatment

When hydrophilic surfaces were necessary, plasma treatment was applied. To do so, PDMS mould was placed against a flat silicon master and plasma treatment with O_2 was done. The plasma exposure time changed depending on the width and height of the channels. For instance, channels from 20 μm up to 80 μm in width were treated for 10 min while channels narrower than 20 μm were treated for 20 min. Surface treatment of PS was done with O_2 too, but only for 2 min. It is important to remark that in order not to lose the activated surfaces due to hydrophobic recovery, treatment was done at most 30 min before the use of the sample.

2.4.5 Microcontact printing (μCP)

Microcontact printing was attempted to obtain a collagen micropattern on a flat PS. A modification of the protocol reported by H. Yu et *al.* [105] was used. In summary, 5% wt. PVA (Sigma-Aldrich) in 20 mL of milliQ water was left at room temperature overnight. Next, the solution was stirred at 90°C for 3h to dissolve PVA particles. The solution was then filtered and poured into a glass Petri dish (80 mm in diameter) and dried at room temperature overnight, in a horizontal laminar-flow cabinet, to allow film formation. Afterwards, PVA was removed from the Petri dish and cut it manually in the desired shape. After PVA film formation, a PDMS mould was immersed in collagen solution (50 μg/mL collagen diluted in PBS) for 1h and blow dried with pressurized purified nitrogen gas. While PDMS was immersed in collagen, PVA film was placed between two flat pieces of PTFE with a 50 g on top of it to ensure that a flat surface was obtained. After 1h incubation, the inked PDMS was placed on the PVA film for 20 min with a 50 g weigh on top, to ensure homogeneous contact. A flat PTFE piece between the PDMS and the 50 g weight was placed to prevent them from sticking together. The patterned side of the PVA film was then placed in conformal contact with the flat PS substrate and incubated for 30 min with a 50 g weight on top. After that, PS-PVA was washed 3 times with PBS (the two first time 5 min and the last one 1h) to dissolve and wash away the PVA film. Samples were kept in PBS (Sigma-Alrdich) until their use. A scheme of the μCP work-flow is shown in Figure 2.2.

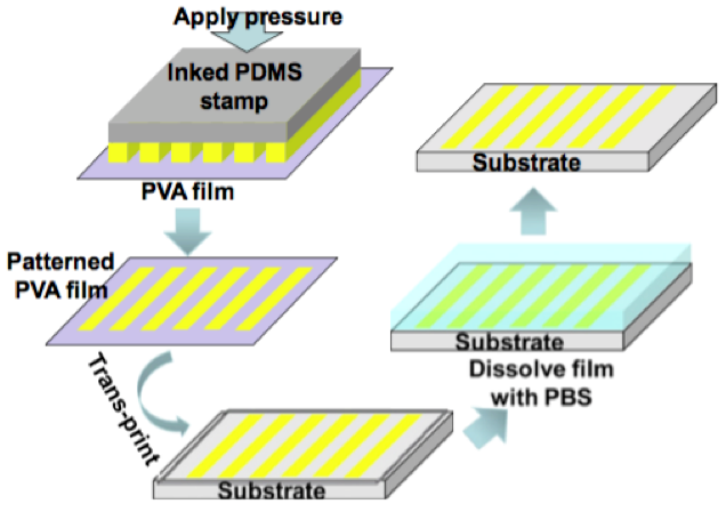

Figure 2.2: Schematic work-flow of μCP [105].

Collagen micropatterning on PS obtained by microcontact printing was evaluated by immunohistochemistry (IHC). First, PBS was removed from the samples, followed by an incubation of the samples with blocking buffer, 5% BSA (VWR, USA) in PBS for 30 min at room temperature. Afterwards, samples were incubated with primary antibody (mouse anti-collagen 1:500 diluted in wash buffer) for 1h at room temperature. Wash buffer was 0.5% BSA in PBS. After one hour incubation, samples were washed three times with wash buffer, followed by incubation with the secondary antibody (anti-mouse AF-568 from Invitrogen 1:500 diluted in wash buffer). Then, samples were rinsed three times with wash buffer, and mounted on a glass slide, with a drop of Mowiol mounting medium. Slides were dried overnight at room temperature. Samples were imaged by Nikon microscope.

In Chapter 3 of the thesis only the results from this technique are shown. However, different techniques, protocols and modifications of them were tried. For further information see Appendix A and B.

Chapter 3: Results and Discussion

3.1 Collagen membrane mineralization

The PILP solution was tested by mineralizating commercial collagen membranes. Two different concentrations of pAsp were used to investigate the effect of it in the mineralization process. Thermogravimetric measurements were performed with a heating rate of 10°C/min, until reach 500°C. Samples were heated at 500°C during 100 min. Afterwards, the mineral content of the samples was measured (Table 3.1).

Sample	Mineral content (wt %)
Control (0d)	6.6 %
No pAsp, 7d	51.9 %
No refresh, 3d, 50 μg/mL pAsp	13.5 %
No refresh, 7d, 50 μg/mL pAsp	8.3 %
No refresh, 14d, 50 μg/mL pAsp	14.1 %
No refresh, 3d, 100 μg/mL pAsp	7.4 %
No refresh, 7d, 100 μg/mL pAsp	1 %
No refresh, 14d, 100 μg/mL pAsp	3.2 %
Refresh, 7d, 50 μg pAsp/mL	6.7 %
Refresh, 7d, 100 μg pAsp/mL	14.1 %

Table 3.1: Mineral content of PILP-mineralized collagen membranes.

Figure 3.1 shows TGA data of collagen membranes mineralized by PILP process without refreshment of the solution, using 50 μg/mL (Figure 3.1 (A)) and 100 μg/mL (Figure 3.1 (B)).

Collagen membranes incubated with 50 μg/mL of pAsp had a final mineral content of 13.5% (day 3), 8.3% (day 7) and 14.1% (day 14). As a consequence, no clear differences where observed between timepoints, indicating that 3 days were enough to mineralize the samples. In the case of the collagen membranes incubated with 100 μg/mL of pAsp, the mineral content after the measurement was 7.4% (day 3), 1% (day 7) and 3.2 % (day 14). In this case, it was not possible to observe differences in mineral content between the timepoints. Interestingly, no big variation in mineral content was observed between samples incubated with 50 μg/mL of pAsp and samples incubated with 100 μg/mL, which may mean that the concentration of pAsp did not influence the mineralization process. Moreover, the sample incubated without pAsp showed a final mineral content of 51.9%, indicating that the pAsp is needed in order to control the mineralization and avoid precipitation of CaPs in the collagen fibers. It can also be observed that the graphs show three drastic weight losses. The fist one is about 100°C, which could correspond to the evaporation of water. Although the samples were freeze-dried, they could absorb some humidity from the atmosphere during the preparation of the samples for the measurement. The second drastic weight loss was found at 500°C, that may be related with the collagen decomposition. Finally, at 500°C another big weight loss was observed. This is

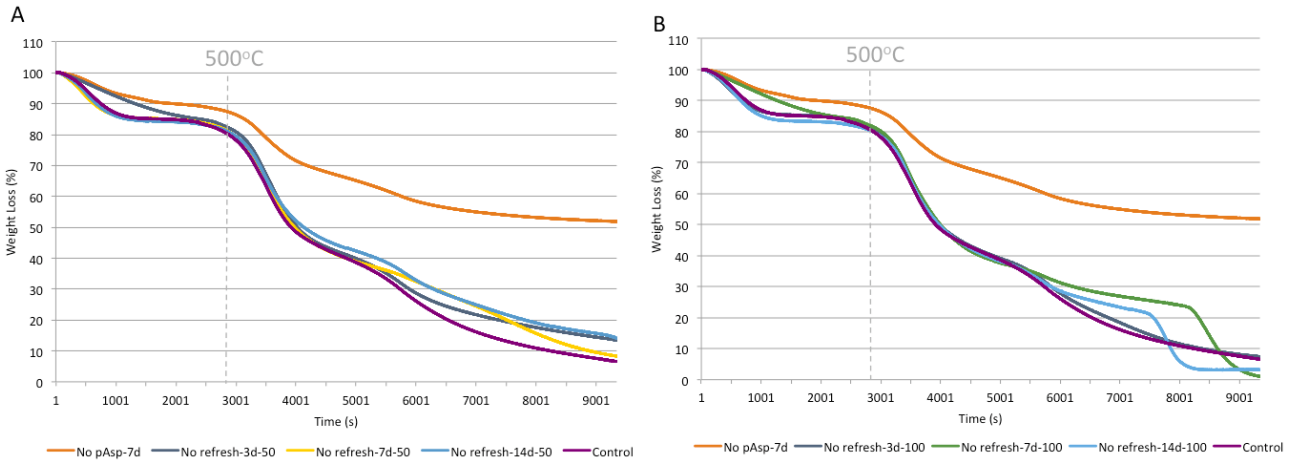

Figure 3.1: TGA of collagen sponges mineralized by the PILP process for 3, 7 and 14 days, without refreshment of the solution, with (A) 50 μg/mL of pAsp and (B) 100 μg/mL of pAsp. Collagen control without mineralization and collagen mineralized with PILP solution without pAsp are included in both graphs.

probably related to the burning of most of the organic components in the sample. Furthermore, in some cases, it is possible to see another drastic weight loss at the end of the measurement. It is suspected that it could be related with the combustion of the pAsp. However, this loss is not shown by all the samples.

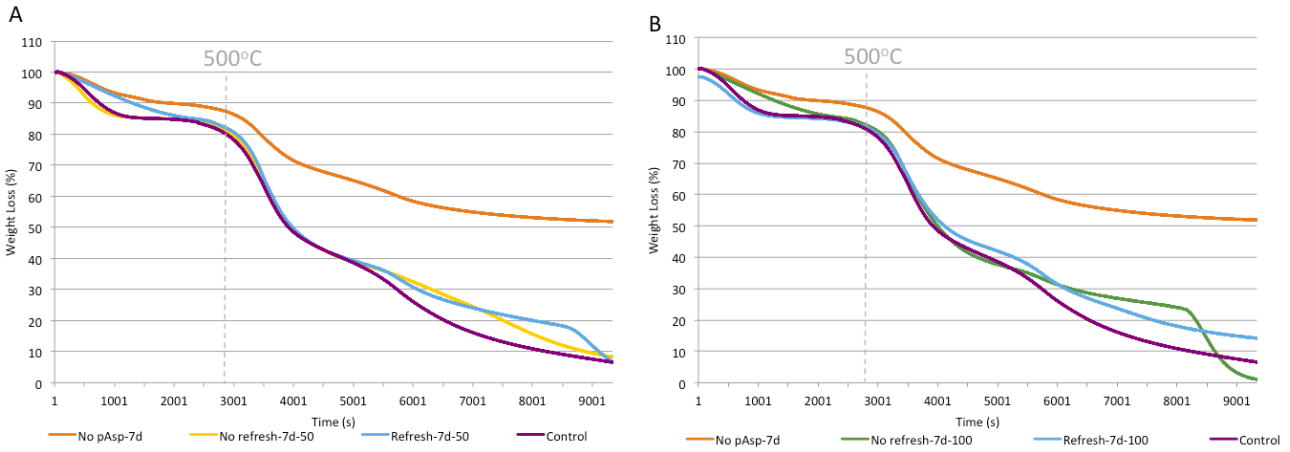

Figure 3.2: TGA of collagen sponges mineralized by the PILP process for 7 days, with and without refreshment of the solution, with (A) 50 μg/mL of pAsp and (B) 100 μg/mL of pAsp. Collagen control without mineralization and collagen mineralized with PILP solution without pAsp are included in both graphs.

Figure 3.2 show the comparison between the experiments with refreshment and without refreshment of the PILP solution. Samples incubated for 7d with 50 μg/mL pAsp had 8.3% (without refreshment) and 6.7% (with refreshment) mineral content. When using 100 μg/mL pAsp, the mineral content after TGA was 1% in the sample without refreshment and 14.1% in the refreshment ones. These results show that no differences in mineral content were observed between samples with and without refreshment, indicating that the PILP solution was no saturated after 7 days. In the samples with refreshment of the PILP solution, the same trend that in the rest of the samples was observed, showing three drastic weight losses around 100°C, 500°C and 500°C, which probably correlates to the evaporation of water and decomposition and combustion of collagen, respectively.

Furthermore, these results were compared with very similar measurements performed by Sang-Soo Jee et *al.* [87]. As expected, they also observed three main drastic weight losses. However, the weight losses of the collagen decomposition and combustion were moved to lower temperatures compare to the results shown here. In particular, they found collagen decomposition around 300°C and collagen combustion around 450°C. It is suspected that this difference was due to the different heating rate used during the measurement, as they applied 5°C/min, while in this experiment a heating rate of 10°C/min was used. Another possible explanation could be the volume of PILP solution used, as they used 500 mL of PILP solution, while in this experiment, 15 mL were used, which is a great difference.

From these results, it is possible to conclude that the concentration of pAsp at 50 and 100 μg/mL performed in the same way, showing that above 50 μg/mL the concentration of pAsp did not influence the ability of the PILP solution for mineralization. However, it was found that this pAsp acid was necessary to control the process. Moreover, no differences were found between samples with refreshment and without it, indicating that at day 7, the PILP solution was not saturated and still had ability to control the mineralization process.

3.2 Optimization of collagen coating

First trial

From the fist trial of collagen coating, the 9 different samples are shown in Figure 3.3. Figure 3.4 shows collagen fibrils at higher magnification.

The main goal of this first trial was to find which collagen-FFB concentrations were able to form fibrils with the characteristic banding pattern. From Figure 3.3, it is possible to observe that collagen solutions with 100 μg/mL of collagen diluted in FFB-100, 500 μg/mL in FFB-100 and 500 μg/mL in FFB-200 did not have sufficient ionic strength to form fibrils. In these conditions, only few fibres were visible but without showing the characteristic banding. In the case of 20 μg/mL collagen in FFB-200 fibril formation was achieved, however, this condition was not chosen because of the low collagen concentration and the only reason to test this condition was to see if with such a low concentration of collagen, fibres were able to form. Regarding the three best conditions (100 μg/mL in FFB-200, 100 μg/mL in FFB-400 and 500 μg/mL in FFB-400), collagen fibrils were perfectly formed and furthermore, in the case of 100 μg/mL in FFB-200 and 500 μg/mL in FFB-400 quite homogeneous coatings were observed. It is important to remark that in the cases where fibres were not seen, it could be probable that some of them were washed away when rinsed with water after the incubation time to avoid salt deposition, as it was observed that collagen did not attached easily to the stub substrates for SEM. It is also suspected that homogeneous coating was probably formed in the condition 100 μg/mL in FFB- 400, as the ionic strength of the solution was enough to allow fibril formation and deposition of these fibrils, but probably most of the fibres were, again, washed away. It is interesting to mention that although all samples were washed in the same way, in some random cases a great amount of collagen was washed away. It can be concluded that even though the washing of the samples was effective as no salt deposition was observed, an optimization of the washing process should be done in the future. Another interesting finding was that as NaCl concentration was increased, collagen fibrils tended to aggregate and form thicker fibres (see Figure 3.3). Nevertheless, that was not a problem, because the characteristic banding of collagen, which is essential for PILP mineralization, was maintained.

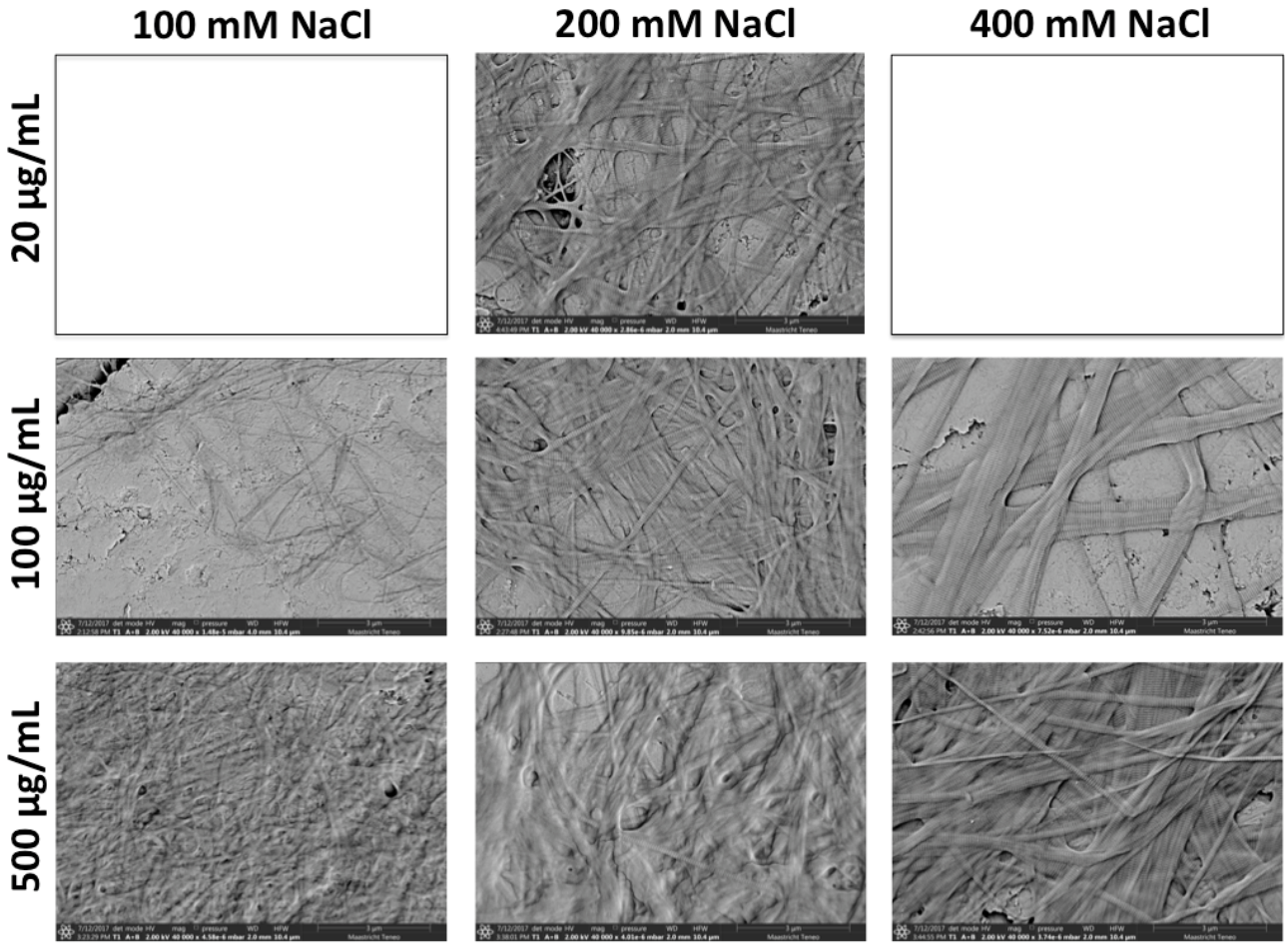

Figure 3.3: Formation of collagen fibrils at different concentrations of collagen (20, 100 and 500 μg/mL) and different concentrations of NaCl (100, 200 and 400 mM) in the fibril formation buffer. Scale bar 3 μm.

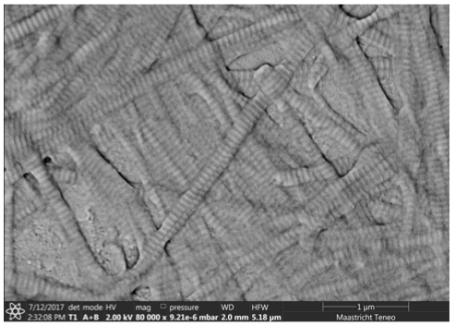

Figure 3.4: Formation of collagen fibrils 100 μg/mL of collagen and 200 mM NaCl at x80000 magnification. Scale bar 1 μm.

Second trial

The main aim of the second study was to test if it was possible to create a homogeneous coating throughout the substrate. The three best conditions of the previous experiment were selected, and a sequential deposition of several layers (3, 6 or 9 collagen layers) was attempted. Figure 3.5 shows an overview in SEM of the different samples.

From this second experiment, it was expected that increasing the number of layers would produce a more homogeneous coating. However, that was not the case and it was observed that collagen fibres had a preference of deposition in places where there were already fibres. As a

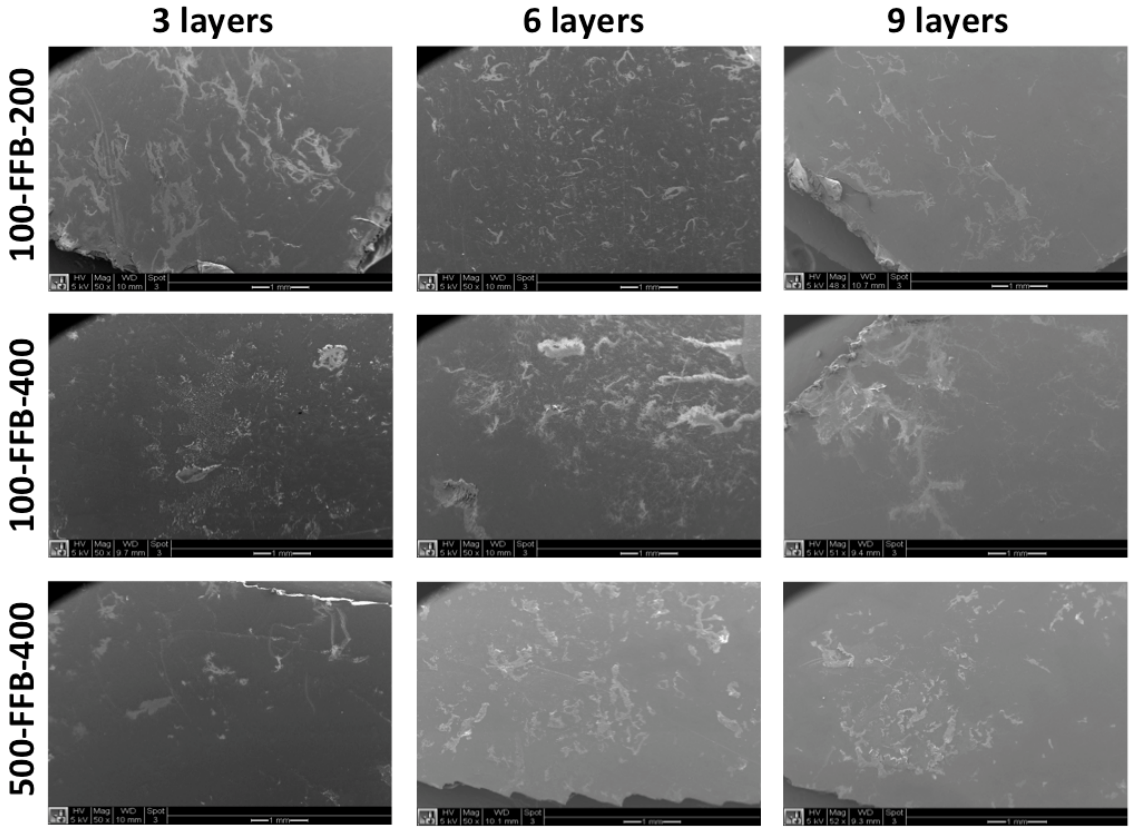

Figure 3.5: Collagen coatings with 3, 6 and 9 layers at different collagen and NaCl concentrations. Magnification at x 50. Scale bar is 1 mm. The nomenclature x-FFB-y refers to "x" concentration of collagen (μg/mL) diluted in FFB with a "y" concentration of NaCl (mM). Images provided by D. Pereira.

consequence, collagen fibrils formed during the first layer deposition, probably acted as nucleation points for the next layers, creating some collagen aggregates rather than new nucleation points, as observed in most of the conditions in Figure 3.5. Moreover, it was also observed that when removing the leftover of solution after 30 min incubation, a lot of fibrils were also removed, which indicates that maybe 30 min were not enough to allow deposition and attachment of the fibrils to the substrate. Another interesting finding was that in the 9 layers condition it seemed that there was less collagen than in 6 or even 3 layers, which was not expected. This fact could be explained by the washing of the samples after the coating, because after 9 layers of collagen deposition, collagen aggregates were bigger and they could be more easily washed away than in the case of, for example, 3 layers, where the collagen aggregates were less abundant. Salt deposition was also observed in some samples, specially in the coating with 9 layers. It has to be remarked that the coatings were done on TCPS pieces placed inside wells of 24-well plate. The amount of collagen solution added on top of the TCPS pieces was enough to form a droplet covering the top part of the substrates. However, in some cases, during the 30 min. incubation, the droplet collapsed and spread all around the well, which lead to a lack of collagen on top of the PS piece, as well as drying of the solution, resulting in salt precipitation between two additions of collagen. As a result, an optimization of this method for depositing collagen is needed. For instance, it may be interesting to add different volumes of collagen solution on top of the TCPS pieces and to have a compromise between the needed droplet volume and the collapse of the droplet during the deposition time. Furthermore, improving the adhesion of the fibrils to the substrate is also needed. This could be achieved by adding a thin non-fibrillar layer of collagen on the TCPS surface before the deposition of the fibrils, as it was done in the third trial.

Third trial

In this case, a two-step collagen coating was performed. First, a non-fibrillar layer of collagen was deposited in order to improve the adhesion of collagen fibrils deposited afterwards. Samples were characterized by immunostaining (Figure 3.6) and SEM (Figure 3.7).

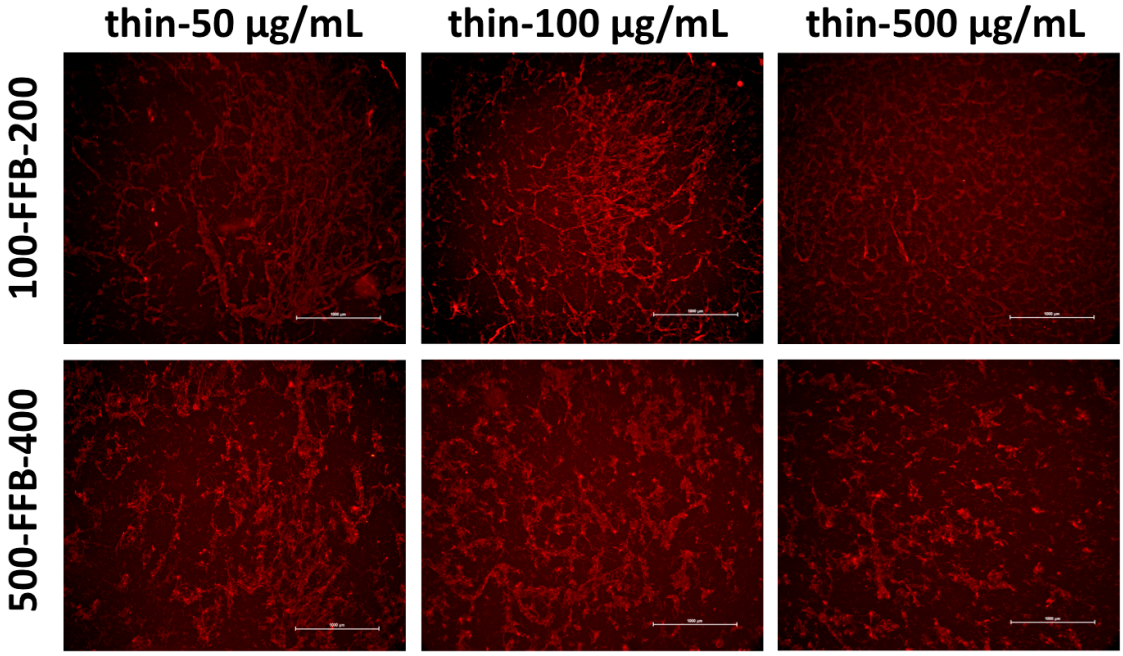

Figure 3.6: Collagen immunostaining. The three columns represent the three different concentrations of the collagen used for the first step of the coating. The rows make reference to the concentration of collagen used in the second step of the coating. The nomenclature x-FFB-y refers to "x" concentration of collagen (μg/mL) diluted in FFB with a "y" concentration of NaCl (mM).

From Figure 3.6, it can be deduced that the concentration of collagen used in the first step of the coating did not affect the amount of collagen fibres deposited in the second step, as a similar amount of collagen was observed in the three conditions. Furthermore, no big differences were found between a collagen concentration of 100 μg/mL and 500 μg/mL for the second step of the coating. Notice that two more conditions (2000-FFB-400 and 100-FFB-200-b) were also studied, which are not shown in Figure 3.6 as non-homogeneous coatings were found. In the case of 2000-FFB-400, it was observed that collagen formed a kind of gel and created and agglomerate in some parts of the TCPS substrate. Regarding 100-FFB-200-b (remember that in this condition, collagen solution was first incubated for 24h in a tube to allow formation of fibrils and then this suspension was added to the substrate for 1h, instead of allowing formation + deposition of fibrils for 24h directly on the TCPS substrates, as in the rest of the conditions), little amounts of collagen fibrils were observed in some parts of the substrate. These findings were corroborated by SEM (see Figure 3.7).

Figure 3.7 (A) and (B) show 100-FFB-200 and 500-FFB-400, respectively. As already seen in Figure 3.6, no differences were observed between both conditions. At higher magnification (Figure 3.7 (C)), it was possible to see the collagen fibrils as well as some salts deposited between them. Figure 3.7 (D) demonstrates that 1h of collagen deposition was not enough to obtain a collagen layer, as only a few fibrils with salt deposition could be observed. Finally, Figure 3.7 (E) and (F), verify that the collagen concentration of 2000 μg/mL was to high to allow fibre formation, creating agglomerates of collagen in some regions of the sample.

It was concluded that the concentration of the first layer of collagen did not affect the amount of collagen fibrils deposited in the second step of the coating. However, this first layer

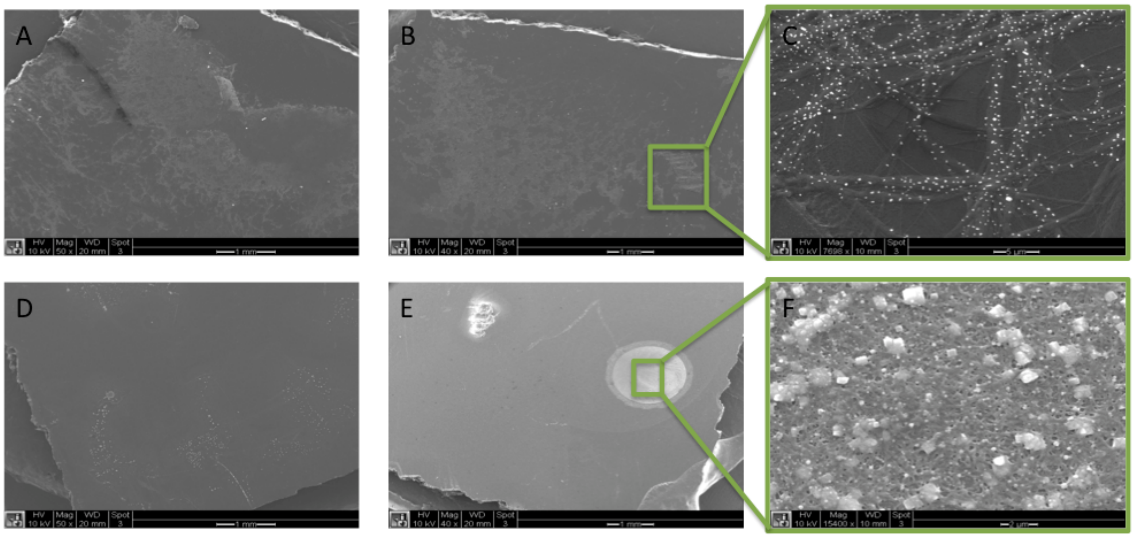

Figure 3.7: Collagen coating with two steps. In all the images the first thin coating was done at the collagen concentration of 500 μg/mL. The second step of the coating was done at the concentration of (A) 100-FFB-200. x50 magnification. Scale bar 1mm. (B) 500-FFB-400. x40 magnification. Scale bar 1mm (C) 500-FFB-400. x7698 magnification. Scale bar 5 μm (D) 100-FFB-200-b x50 magnification. Scale bar 1mm (E) 2000-FFB-400. x40 magnification. Scale bar 1mm (F) 2000-FFB-400. x15400 magnification. Scale bar 2 μm.

was necessary to improve the attachment of the fibrils to the substrate. As a consequence, a collagen concentration of 100 μg/mL was chosen for the thin coating of the samples for the osteoclast resorption experiment. For the second step, 100-FFB-200 and 500-FFB-400 seem to be the best conditions. Nonetheless, although most of the sample was covered by collagen, a completely homogeneous coating was not achieved, as some TCPS regions were uncovered. That could be improved by increasing the deposition time of the collagen. The conditions chosen for the collagen coating of samples for the cell study were the highest concentration of collagen (500-FFB-400), with a deposition time of 48h, and refreshing after 24h.

3.3 Characterization of the coatings

In order to characterize the collagen and CaPs coatings, different measurements were performed. For the identification of the CaPs phases, XRD was used. As this coating was performed in two steps, each step was analysed separately, as well as together. The XRD patterns of the three coatings are shown in Figure 3.8. Note that to obtain this graph, processing and analysis of the raw data was done (see Appendix C for more details).

5xSBF (A) is supposed to give an amorphous coating as the amounts of Mg^{2+} and HCO_3^- are elevated (they are known as inhibitors of crystal growth). However, a sharp peak at 31.7° was observed, which could correspond to one of the characteristics peaks of HA (211). Furthermore, a small peak at 45.4° was also found. This peak perfectly matches with the NaCl spectra. Interestingly, the sharp peak at 31.7° also matches with the NaCl spectra. The presence of NaCl may be explained by the fact that 5xSBF (A) solution is mainly composed of NaCl, which could precipitate and be deposited into the substrate during the coating process. However, this is not probable, as the solution is not saturated with respect to NaCl. The presence of NaCl could also have its origin in the drying process of the coating, if the washing did not remove all ions.

5xSBF (B) solution contains the required amounts of ions to obtain an HA phase. In this coating, peaks were found at 4.6°, 9.3°, 9.6°, 16°, 26°, 27.3°, 31.5°, 31.6° and 45.4°. All these

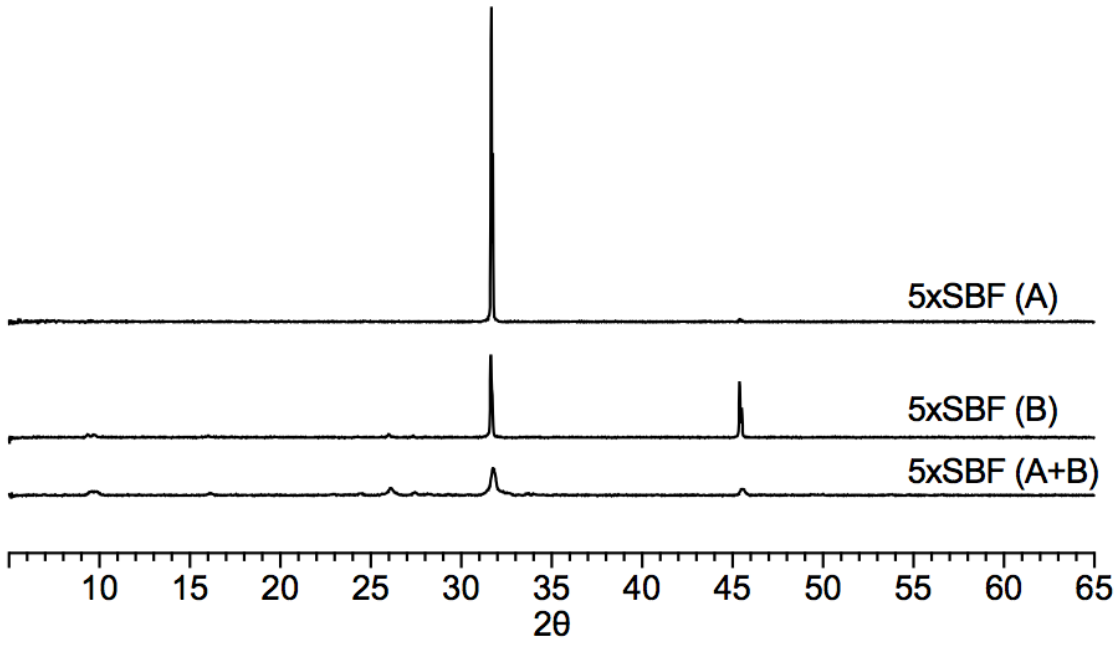

Figure 3.8: XRD patterns of 5xSBF (A), 5xSBF (B) and 5xSBF (A + B).

peaks match the pattern of $Ca_8H_12O_29P_6$ (OCP). In particular, the characteristic peak of OCP at 4.6° (100) is remarkable (see Appendix D to better see this peak). The peaks at 27.3°, 31.6° and 45.4° could also correspond to the precipitation of NaCl.

In 5xSBF (A) + 5xSBF (B) coating, peaks were found at 9.3°, 9.6°, 16.1°, 24.4°, 26.1°, 27.5°, 31.8°, 32.6°, 33.7° and 45.6°. As expected, the pattern of A + B was practically the same than the 5xSBF (B).

The identification of the peaks with the OCP pattern was not expected, and might indicate a mistake in the preparation of the solution for obtaining the coatings. Nonetheless, it seems improbable, as similar XRD patterns were found in the 5xSBF (B) and the HA coating, which were prepared separately. Moreover, the 5xSBF (B) solution was prepared at 37°C, while in the original protocol [66] temperature was set at 50°C. As a consequence, that could be one of the reasons why the peaks were identified with OCP instead of HA. It is also important to take into account that the coatings measured in XRD where not washed with water between the drying step and the measurement, because the coating could wash away from the flat Si sample holder for XRD, which could explain the presence of NaCl. Furthermore, each time that this kind of coatings are prepared, the conditions are never exactly the same (variations in temperature, pH or weight of the salts are found). Nevertheless, if these variations are small, they should not account for different phases.

Substrates for cell culture were also imaged in SEM, to verify if there was any visible degradation or alteration to the morphology of the different substrates. Figure 3.9 shows representative areas on the four different coatings used for the osteoclast resorption, previous to the experiment and after, ageing for 7 days in culture medium.

No changes in morphology were observed, for all substrates. Interestingly, the HA coatings show the typical morphology of HA (Figure 3.9 (A)) rather than the typical morphology of OCP [102], where tiny crystals can be observed around the CaPs spheres. As added characterization on the CaP coating, it would be interesting to measure the thickness of this coatings, as well as surface roughness.

Regarding the HA + collagen coating, most of the sample had an aspect similar to the one shown in Figure 3.9 (B), although in some regions was not possible to find a complete

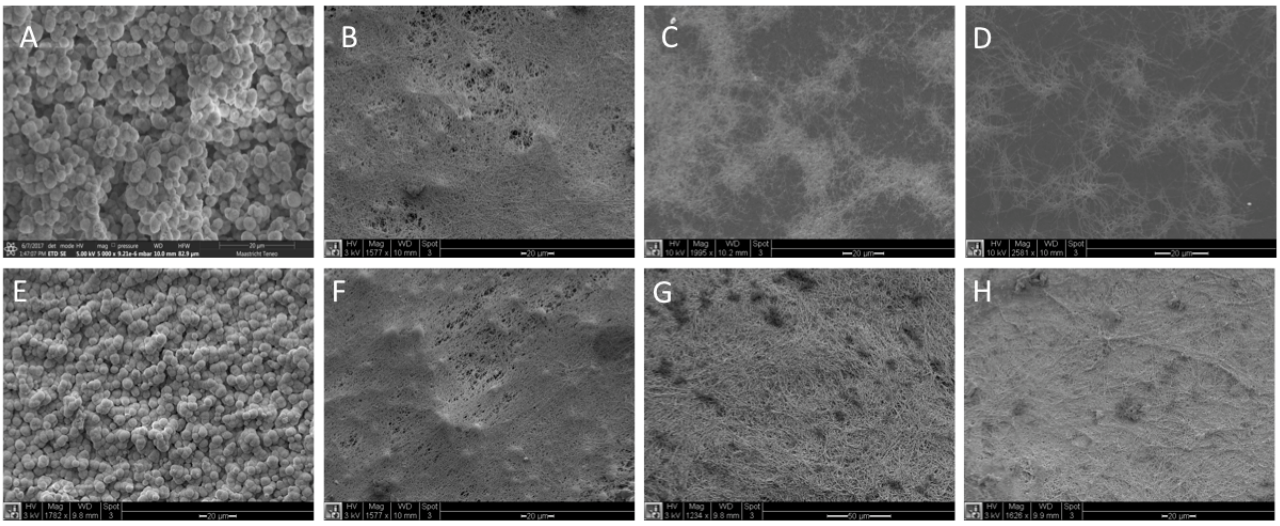

Figure 3.9: SEM images of the different substrates before (A, B, C and D) and after 7 days incubated in culture medium (E, F, G, H). (A) HA coating before the experiment at x5000 magnification. Scale bar 20 μm. (B) HA + collagen coating before the experiment at x1577 magnification. Scale bar 20 μm. (C) Collagen coatring before the experiment at x1995 magnification. Scale bar 20 μm. (D) PILP coating before the experiment at x2581 magnification. Scale bar 20 μm. (E) HA coating at x1782 magnification. Scale bat 20μm. (F) HA + collagen coating at x1577. Scale bar 20 μm. (G) Collagen coating at x1234 magnification. Scale bar 50 μm. (H) PILP coating at x1626 magnification. Scale bar 20 μm.

layer of collagen on top of the HA. The same fact was observed in the Collagen and PILP coatings: a completely homogeneous layer of collagen was not achieved. Nevertheless, the homogeneity of the coatings was increased compared to the samples coated with collagen for 24h in the "Optimization of collagen coating" (see Figure 3.9 (B, C and D) and Figure 3.7 (B and C), indicating the efficiency of incubating the samples during 48h to allow fibril deposition. Moreover, salt deposition was found in some samples, although is probably due to the sample preparation for SEM (washing and drying). It was concluded that although further optimization of the coating could be done, most of the substrates were successfully coated, in particular the central area.

Finally, to verify the intrafibrillar mineralization of the collagen by the PILP process, samples were imaged by TEM (Figure 3.10).

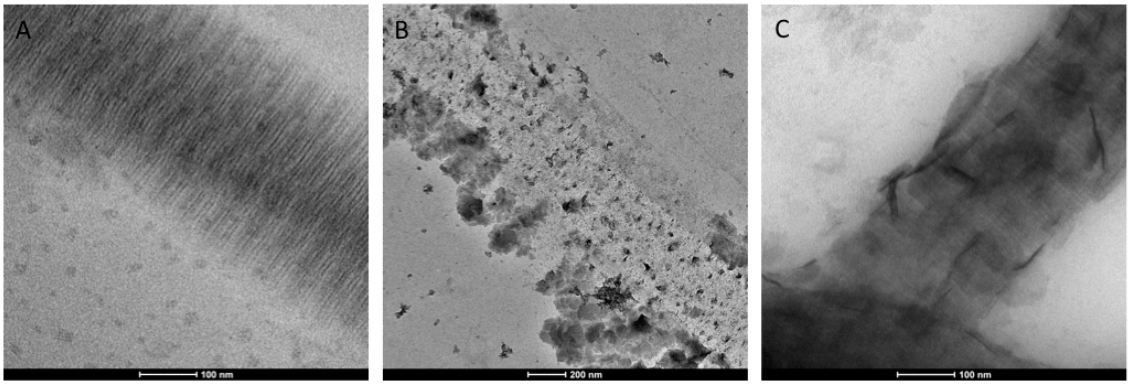

Figure 3.10: TEM micrographs of collagen fibrils before and after mineralization with PILP solution. (A) Non-mineralized collagen fibril. Scale bat 100 nm. (B) PILP mineralized collagen fibril without pAsp. Scale bar 200 nm. (C) PILP-mineralized collagen fibril with 100 μg/mL pAsp. Scale bar 100 nm. Images provided by Daniel P.

From TEM analysis, it was possible to confirm the characteristic banding of the collagen fibrils (Figure 3.10 (A)). Moreover, collagen fibrils mineralized with PILP solution but with no pAsp were also observed ((Figure 3.10 (B)), as well as fibrils incubated with PILP solution ((Figure 3.10 (C)). It was found that the pAsp was essential to orchestrate the mineralization process of the collagen fibrils, because when no pAsp was used, agglomeration of calcium phosphate was found all around the fibril. Interestingly, when pAsp was used, HA crystals were observed between the bandings of the fibril as well as around it. To confirm intrafibrillar mineralization, diffraction was tried. However, it was not possible to confirm the presence of HA crystals.

3.4 Cell density optimization

The purpose of this experiment was to find which was the optimal cell density at seeding to have RAW 264.7 cells in culture for 7 days without reaching confluence, and whether or not it played a role in differentiation to osteoclasts. Cell densities at day 6 or 7 are shown in Figure 3.11.

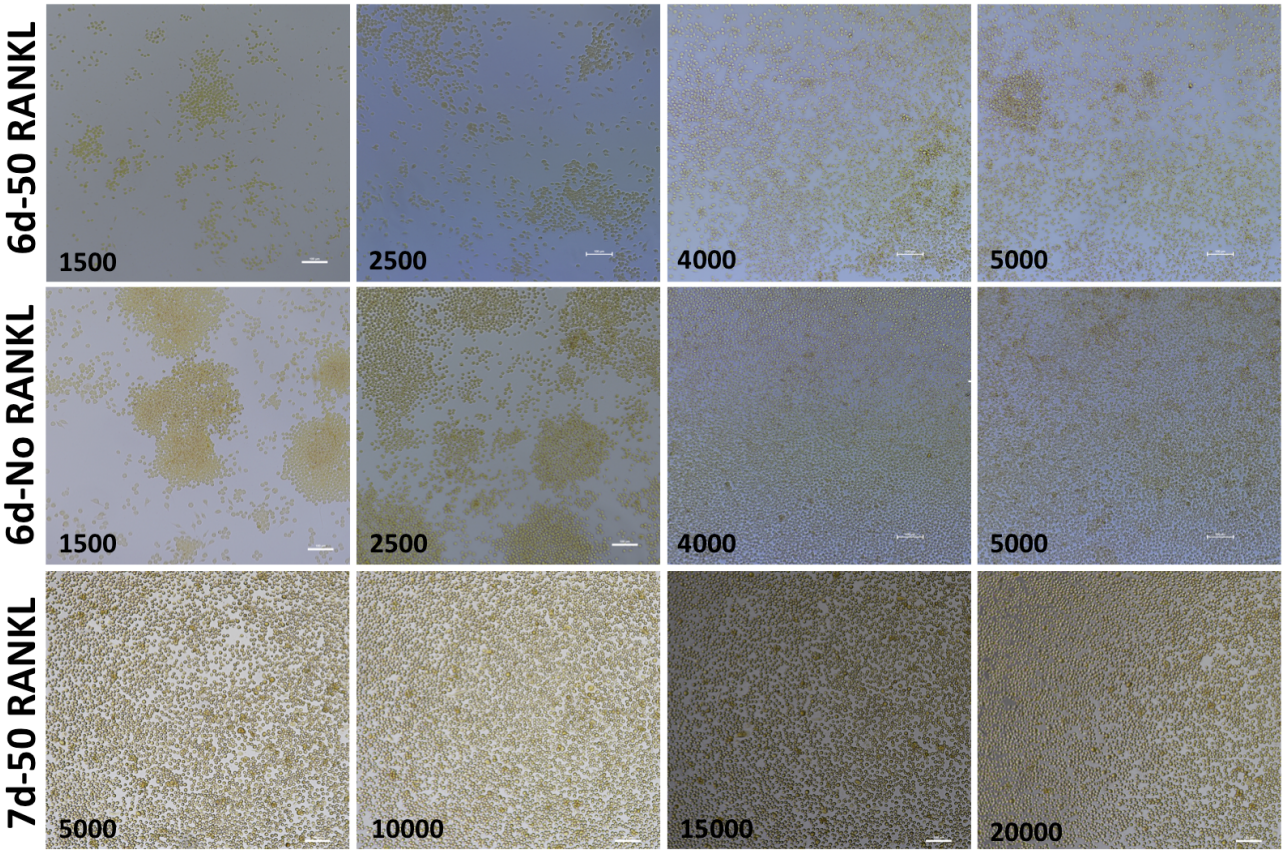

Figure 3.11: Comparison of cell densities at the end of the experiment (day 6 or 7 depending on the condition) at x10 magnification. Pictures of low seeding densities with and without RANKL are shown in the first and second row, respectively. Pictures of high seeding densities are only shown with RANKL condition in the third row. Numbers in each image represent the seeding cell density (cell/cm^2). Scale bar is 100 μm.

The first interesting fact from this experiment is that at day 7, wells seeded with more than 5000 cells/cm^2 reached confluence as can be observed in the images of the last row in Figure 3.11. However, this over-confluence does not seem to affect the ability of macrophages to differentiate into osteoclast as some of these cells can be observed in the images (bigger cells).

Another interesting finding was that the presence of RANKL affected cell growth. First and second row of Figure 3.11 show cell density at day 6 for the different seeding densities (values in each image) with and without the presence of RANKL. Interestingly, the presence of RANKL decreased cell growth and at day 6 it is possible to observe less cell density in the wells that contained RANKL. This could be explained by the fact that when differentiation medium was added to the cells, macrophages were forced to differentiate into osteoclast, preventing cells to enter in the mitotic phase. Furthermore, by using 50 ng/mL of RANKL, not more than 20% of the cells differentiated into osteoclasts, which was contradictory to the indications of the company (the expected ED50 for osteoclast differentiation was $\leq$10 ng/mL, Sigma-Aldrich). As a result, it was thought that culture medium may also influence the differentiation of the cells. Actually, although the European Collection of Authenticated Cell Cultures (ECACC) recommended culture medium for RAW 264.7 is DMEM, most of the differentiation experiments in the literature done with this type of cells used α-MEM instead [106] [35] [101].

Based on this, a small experiment was performed, where RAW 264.7 were cultured with DMEM and α-MEM Gln (+) with and without added RANKL. After 7 days in culture, cells were TRAP stained and imaged. However, no significant differences were found between different culture mediums (images not shown because of the lack of added value). H. Hotokezaka and colleagues also studied optimal seeding density of RAW 264.7. They observed that the cell density and growth played an important role for the differentiation of RAW 264.7 into osteoclasts [106]. They also found an optimal seeding density of 2000 cells/well when cultured in α-MEM Gln (+). However, when the cells were cultured in α-MEM Gln (-), the optimal seeding density was found at 8000 cells/well. This experiment was performed in 96-well plate (A_{well}=0.32 cm^2), which means that when cells were cultured with α-MEM Gln (+), the optimal cell density was $\approx$ 6000 cells/cm^2, obtaining similar results that the ones presented here.

It is also remarkable that the images at higher seeding density ($>$ 5000 cells/cm^2) do not actually show over-confluence. This can be explained by the fact that these RAW 264.7 cells are considered semi-adherent cells. As a consequence, when the culture medium was removed for TRAP staining, a large quantity of cells was also removed with the medium, particularly the cells that were not well attached to the substrate. Moreover, over-confluence causes cells aggregates to detach, although they are not really in suspension.

Finally, and based on these results, cell density for the osteoclast resorption experiment was chosen to be 4000 cells/cm^2 as it was shown that after 6 days in culture a confluence of about 80% was reached without differentiation medium added to the culture.

3.5 RANKL optimization

Several experiments were performed for optimization of RANKL concentration. For the two first trials, cells were seeded at 10.000 and 20.000 cells/cm^2 and kept in culture for 7 days. At given timepoints, cells were stained for TRAP, and TRAP activity and DNA amount were quantified. The results obtained from TRAP activity were normalized to the amount of DNA.

Although TRAP activity and DNA quantification were measured at day 3, 4, 5 and 7 for the first trial, data from TRAP activity for the two first time-points (day 3 and 4) could not be used, because of a mistake in the amount of $FeCl_3$ added to the TRAP buffer. As a consequence, TRAP/DNA were only analyzed for day 5 and 7. Figure 3.12 shows these results.

Interestingly, TRAP/DNA between day 5 and 7 in HA substrates increased under the influence of RANKL, except for 10 ng/mL, indicating that this concentration was not enough to differentiate the cells. Nevertheless, no increase under the influence of RANKL was observed

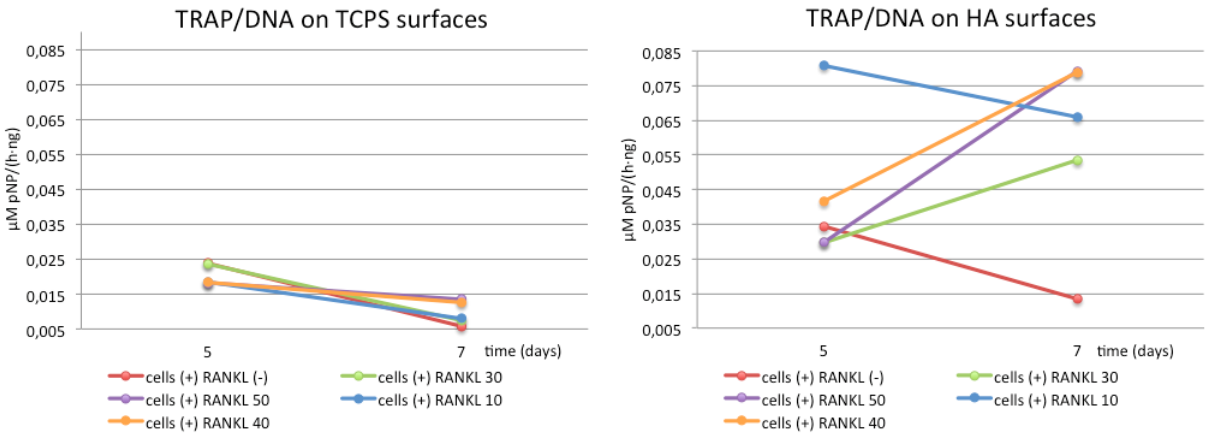

Figure 3.12: TRAP activity/DNA amount in TCPS and HA substrates for the first trial of RANKL optimization.

on the TCPS substrates, where actually TRAP/DNA decreased between day 5 and 7. Furthermore, the increment of TRAP/DNA observed in HA was larger at higher concentrations of RANKL. Similarly, the decrease of TRAP/DNA in TCPS between day 5 and 7 was less for higher RANKL concentrations. From these results, it is suspected that HA substrates under the effect of 40-50 ng/mL RANKL improved the ability of RAW 264.7 to produce TRAP enzyme. It was noted as well that the DNA amount increased from day 3 to 5, while decreased between day 5 and 7 (see Figure 3.13).

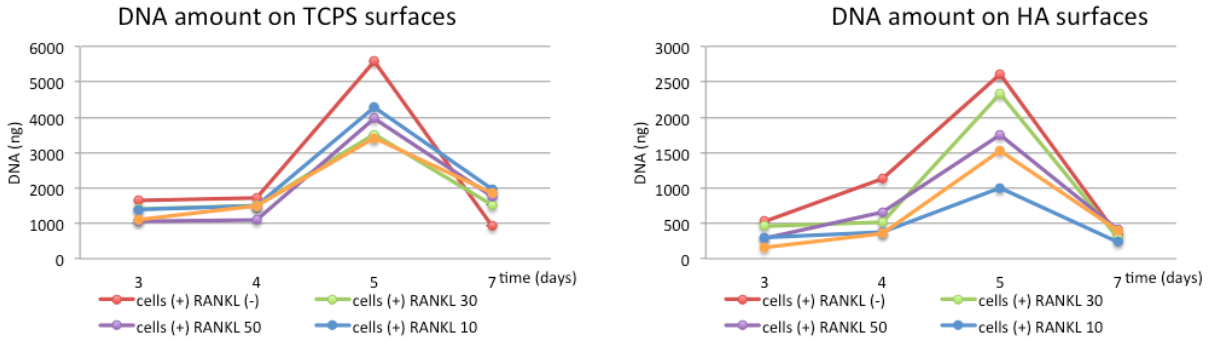

Figure 3.13: DNA amount in TCPS and HA substrates for the first trial of RANKL optimization.

As previously explained, this fact could be due to the removal of a lot of cells when the medium was aspirated at day 7. This correlates with what was found in the "Cell density optimization" experiment (less cell density at day 7 than 5).

In order to verify if TRAP activity was correlated to the amount of osteoclast, TRAP staining was performed. Cell nuclei were also stained by DAPI. Figure 3.14 shows TRAP/DAPI staining for 4, 5 and 7 days. Cells positively stained for TRAP and containing three or more nuclei were considered osteoclasts.

In Figure 3.14 it is possible to observe how the cell density increased between day 4 and 5, while between day 5 and 7, it decreased. However, previous to the staining, cells were checked with bright-field light microscope and over-confluence was observed at day 5, 6 and 7. Again, this fact supports the hypothesis that mentioned previously: a great amount of cells was removed with the aspiration of the medium to prepare samples for TRAP staining and TRAP activity.

Regarding differentiation of the cells, some osteoclasts were found from day 4 onwards at the higher concentration of RANKL (40 and 50 ng/mL), and an increase of osteoclasts was

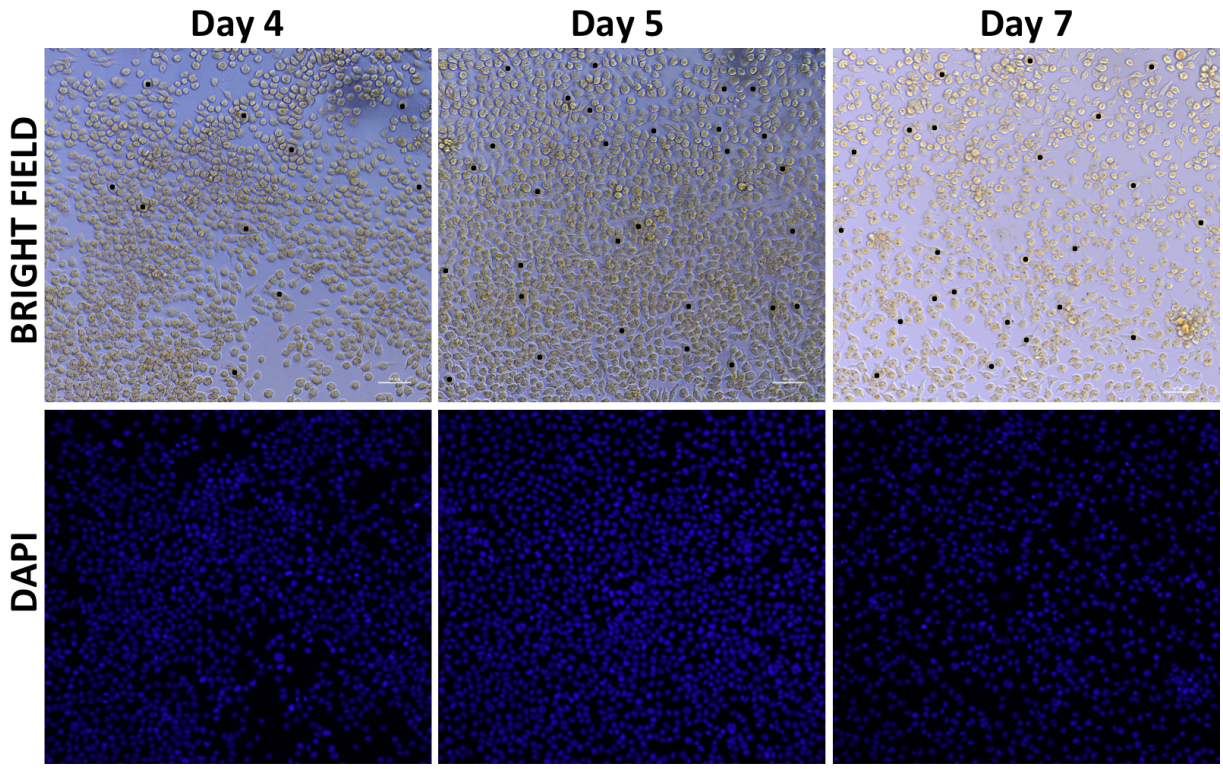

Figure 3.14: TRAP/DAPI staining in TCPS substrates for the first trial of RANKL (50 ng/mL) optimization at day 4, 5 and 7. x20 magnification. Scale bar is 50 μm.

observed between day 4 and 5 and a similar number of osteoclast was observed between day 5 and 7 (Figure 3.14). Nonetheless, the cell density at day 7 is lower than at day 5, due to the aspiration of non-adherent cells in over-confluence. However, a great amount of osteoclast is still observed at day 7, indicating the good adhesion of these cells to the substrate. Although osteoclasts were found in the samples, they were in less amount and smaller than what was reported in literature. In order to verify the efficacy of the RANKL, RANKL from another supplier was used in the third trial (as explained in the next section).

Unfortunately, the imaging of TRAP staining in HA substrates was not possible due to the thickness of the coatings, which made it translucent, and cells were indistinguishable from background. Although the nuclei could be observed due to the DAPI staining, it was not possible to identify osteoclasts, especially at higher cell densities. As a result, it was not possible to verify that HA influenced the differentiation of the cells, as concluded from the TRAP activity results.

The TRAP/DNA results (Figure 3.15) from the second trial, where cells were seeded at 10000 cells/cm2, confirm the findings of the first trial.

In this second trial, measurements were also performed at day 3. It is interesting to observe how TRAP/DNA increased between day 3 and 5 in both TCPS and HA surfaces. Furthermore, the same trend was observed in the first trial, between day 5 and 7: an increase of TRAP/DNA under the influence of RANKL for the HA coatings, but not for the TCPS substrates. However, no differences were found between different concentrations of RANKL, which could be an indication that the RANKL was not effective in differentiating the cells. Another indication of that is that the negative control for RANKL has more TRAP activity than the differentiation conditions, at day 5 in both types of substrates. Nevertheless, TRAP/DNA in the condition without RANKL decreased between day 5 and 7 in both TCPS and HA substrates, which could also be another indication that no differentiation was taking place.

It was also observed that DNA amount at day 7 was lower in samples with RANKL compare

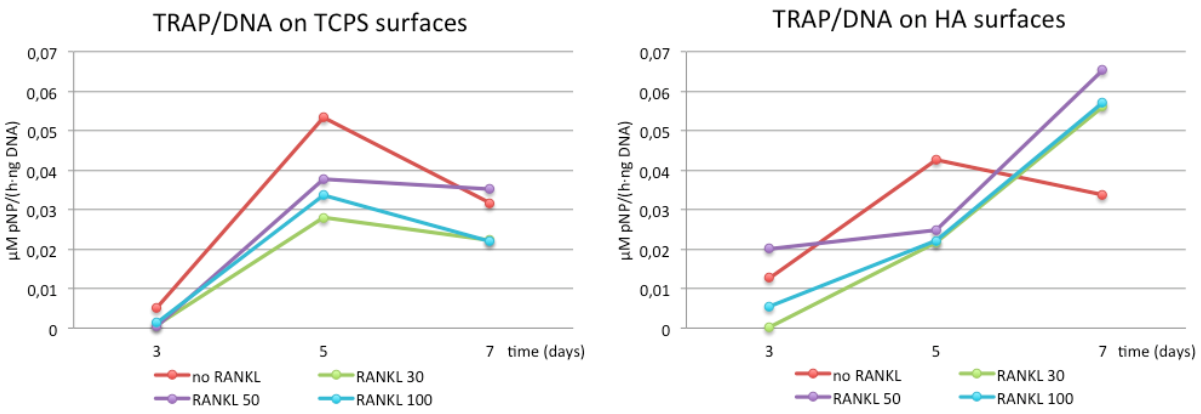

Figure 3.15: TRAP activity/DNA amount in TCPS and HA substrates for the second trial of RANKL optimization.

to the controls, corroborating that RANKL decreased the growth speed of the cells, as found in the previous experiment.

TRAP staining was also performed, and Figure 3.16 shows TRAP staining for the last time-point (7 days) for a RANKL concentration of 50 and 100 ng/mL.

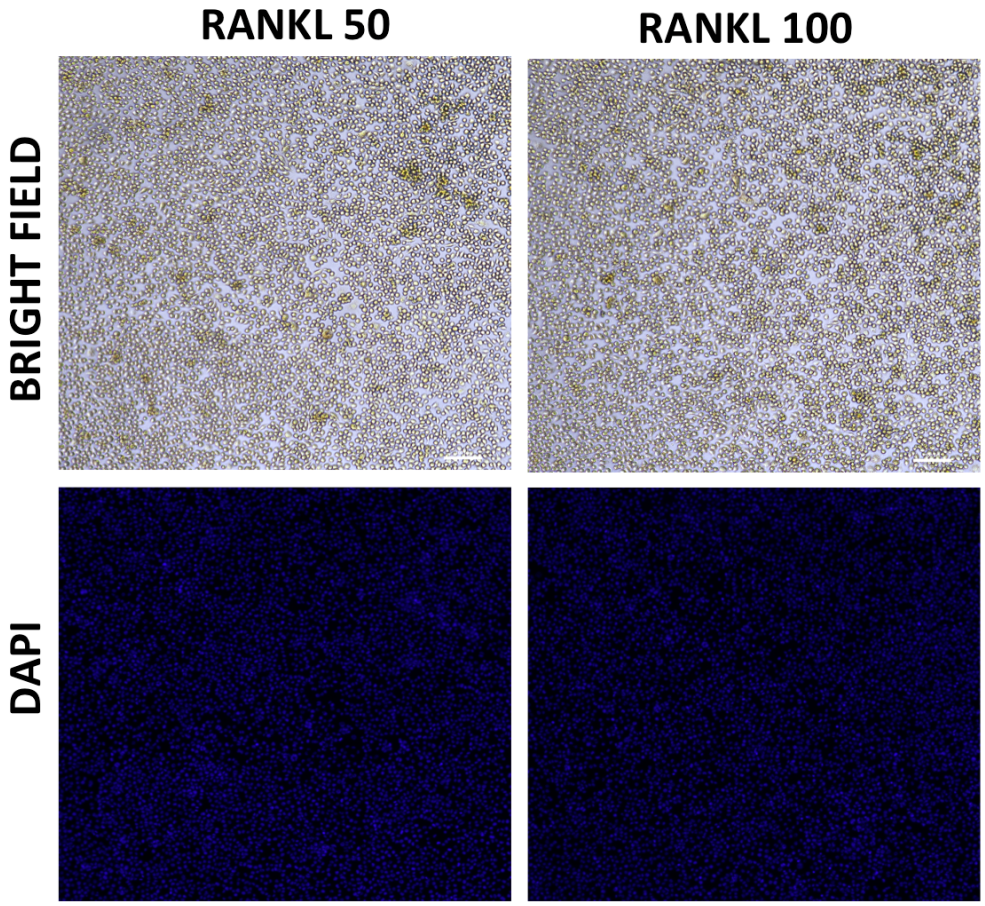

Figure 3.16: TRAP/DAPI staining in TCPS substrates for the second trial of RANKL optimization at day 7. x10 magnification. Scale bar is 100 μm.

As already suspected from TRAP/DNA results, the increment of RANKL from 50 to 100 ng/mL did not have a big influence in the differentiation of the RAW 264.7 into osteoclasts. Moreover, as already confirmed in the cell density optimization experiment, the use of 50 or even 100 ng/mL of RANKL was not enough to differentiate more than 20% of the cells. Based

on these results, a last trial was performed using RANKL from another company (Peprotech).

A seeding density of 4000 cells/cm^2 was used, and TRAP staining was performed at days 3, 4, 5 and 7. At day 3 and 4, some differentiation (less than 10%) was observed in 30 and 40 ng/mL of RANKL. Similarly, the condition without RANKL showed differentiation in the same range of the conditions with 30 and 40 ng/mL of RANKL. In this experiment cells were used at passage 13, which could also affect the behaviour of the cells. However, cells were maintained in culture until passage 19 and no big differences were observed from those at low passages. Furthermore, although the ratio of cells that were differentiating into osteoclasts was still low, a small increase was observed when using 50 ng/mL of RANKL and even a higher increment was observed at 100 ng/mL RANKL. At day 5, the conditions at 30, 40 and 50 ng/mL had the same trend: no many differences were observed between day 4 and 5 at these conditions. The same occurred in the conditions without differentiation medium. However, a large increase of osteoclast numbers compared to the control condition was observed at 100 ng/mL of RANKL (Figure 3.17).

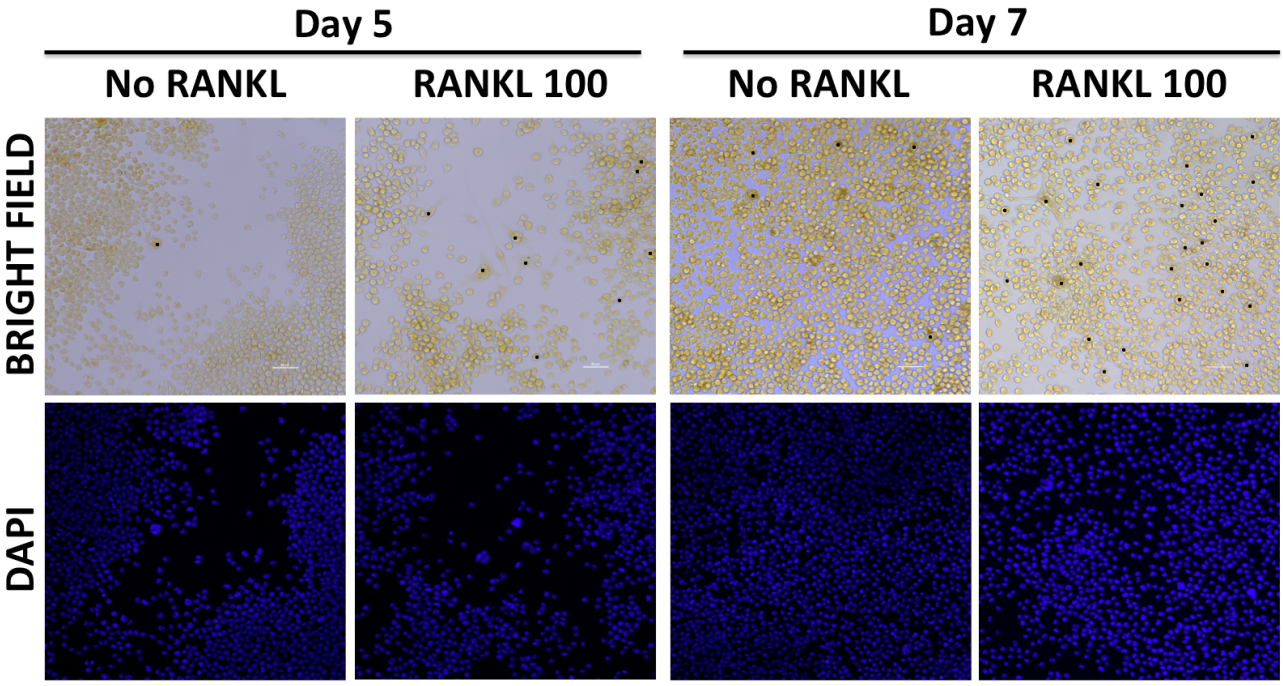

Figure 3.17: TRAP/DAPI staining in TCPS substrates for the third trial of RANKL optimization at day 5 and 7, without and 100 ng/mL of RANKL. Black dots in the images designate osteoclasts. x20 magnification. Scale bar is 50 μm.

At day 7, a similar increase in osteoclast number was observed at 30, 40 and 50 ng/mL, indicating that this difference of concentration did not affect the differentiation of RAW 264.7 into osteoclasts. Nonetheless, at the condition of 100 ng/mL of RANKL, a significant increment of osteoclasts was observed (Figure 3.17). When comparing these results to similar studies, like the one performed by Noel L. *et al.*, some differences were found. By using the same type of cells and RANKL, but with less concentration (40 ng/mL), they could see osteoclast-like cells at day 3 on TCP surfaces. A possible explanation to this difference in RANKL concentration giving differentiated osteoclasts could be the influence of the TCP substrates that they used. Furthermore, they cultured the cells with α-MEM, while here, DMEM was used, which could also be another factor influencing the differentiation.

Note also from Figure 3.17 the lower cell density under the presence of RANKL compare to the No RANKL condition. It has to be mentioned that the analysis of this last trial was done only qualitatively (TRAP staining), and osteoclast were counted manually. All the above

observations can be further verified by more quantitative analysis.

It was finally concluded that the concentration of 100 ng/mL RANKL was the best one to differentiate RAW 264.7 cells into osteoclasts. As a consequence, this concentration was chosen for the study of osteoclast resorption of CaPs.

3.6 Osteoclast resorption of CaPs

From the two previous experiments, a seeding density of 4000 cells/cm^2 and a concentration of 100 ng/mL of RANKL were chosen for studying the osteoclast resorption of different CaPs. Also from the above experiments, time-points were considered at day 5 and 7, as we previously saw that before day 5, a low differentiation rate of RAW 264.7 into osteoclasts was obtained. At each time-point, quantification of TRAP activity and DNA, TRAP/DAPI staining and SEM were performed. Figure 3.18 shows the TRAP/DNA results.

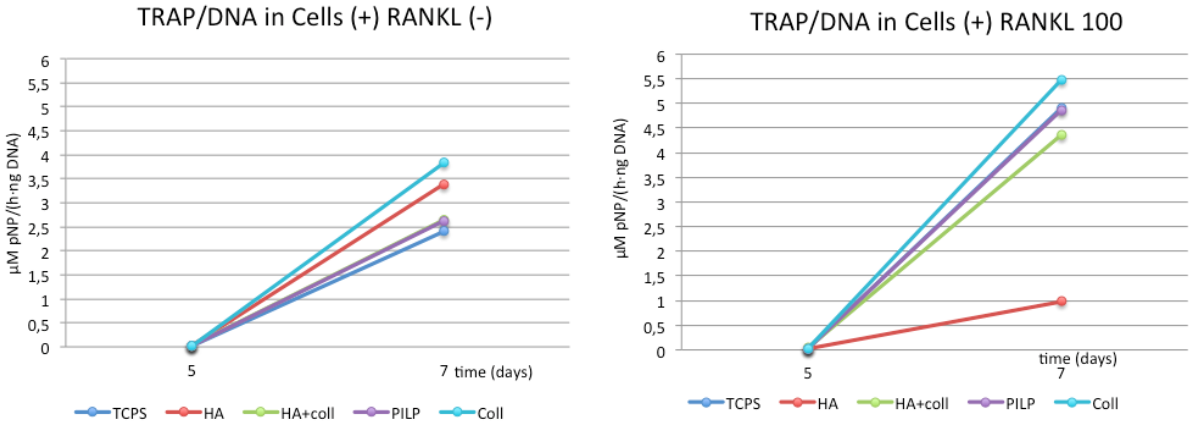

Figure 3.18: TRAP activity/DNA amount for the different substrates under (A) no influence and (B) influence of RANKL. Note that it is difficult to distinguish the curve of HA + collagen in the condition without RANKL, this is due to the fact that it is overlapped with the PILP condition. Similarly, the TCPS curve under the influence of RANKL is overlapped with the PILP condition as well.

It can be observed that the TRAP/DNA increased between day 5 and 7, independently of the influence of RANKL. The average standard deviation at day 7 (not shown in the graph for clarity) is ± 1.5 for the measurements without RANKL and ± 3.1 under the influence of RANKL. As a consequence, the observed differences are likely not significant, except for the case of HA with RANKL, where the TRAP/DNA was very low compared to the rest of the substrates. In Figure 3.18 is also difficult to distinguish the curve of HA + collagen in the condition without RANKL, this is due to the fact that it is overlapped with the PILP condition. Similarly, the TCPS curve under the influence of RANKL is overlapped with the PILP condition as well.

From this data it follows that the nature of the substrates did not greatly affect the differentiation of macrophages into osteoclasts. This is controversial to what was observed in the previous experiments, where TCPS substrates showed a decrease in TRAP/DNA between day 5 and 7 (compare Figure 3.18 with Figure 3.12 and 3.15). Furthermore, the magnitude of TRAP/DNA was much higher in this experiment than in the previous ones. This could be explained by the fact that the DNA amount found at day 7 was almost null in all the samples (Figure 3.19). This finding was unexpected and it is thought that mistakes occurred during sample preparation.

In the case of the HA substrate, TRAP activity was lower on the RANKL positive condition than in the control, suggesting mistakes during sample preparation as well. Actually, when

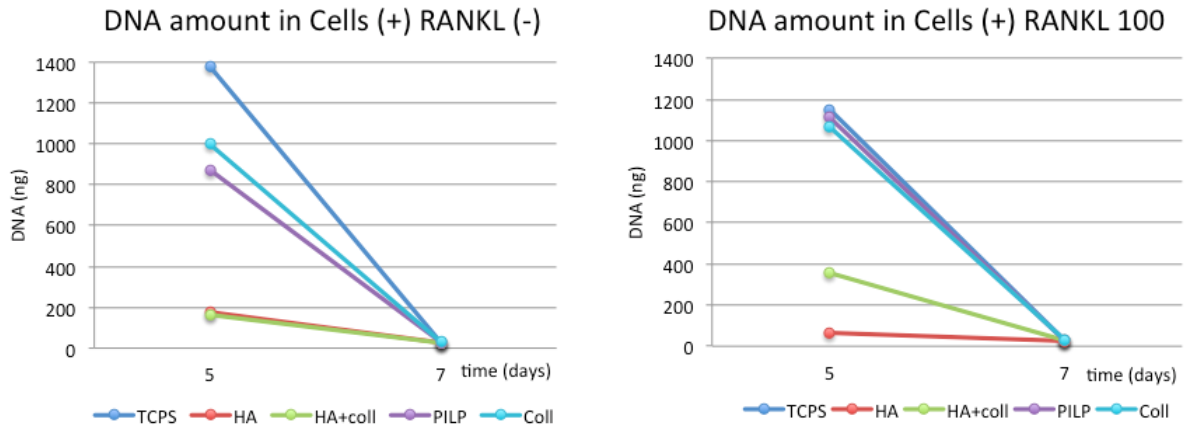

Figure 3.19: DNA amount for the different substrates under no influence and influence of RANKL.

looked at raw data, it was observed that wells under the effect of RANKL showed less TRAP activity than the wells without RANKL, which is very strange. However, that could be due to an effect of the number of cells in each plate, which is why, TRAP activity was normalized to DNA amount. One possible explanation to the fact that no differences were observed between different substrates may be that the collagen layer on the substrates was not completely homogeneous, allowing the cells to be in direct contact with the TCPS in some parts of the substrate.

Two main conclusions were made from these results: first, that the nature of the coating did not influence the TRAP activity and second, that the PILP coating did not perform better than the rest of the coatings when differentiating RAW 264.7 into osteoclasts, which was our initial hypothesis.

Figure 3.20 shows TRAP/DAPI staining at day 7.

In TRAP staining, it was observed that the PILP-mineralized collagen presented more osteoclasts than the rest of the substrates (TCPS and collagen). However, this difference was not very pronounced (Figure 3.20). Although in general, more osteoclasts were found in the PILP substrates at day 7, it is important to remark that this was a qualitative measurement, where the number of osteoclast was evaluated visually, considering osteoclasts cells positively stained for TRAP enzyme with three or more nuclei.

Finally, at each time-point, the different substrates were also imaged by SEM. For each condition, there was one sample with cells (to observe osteoclast number and morphology) and one sample where the cells were removed from to see if resorption was taking place. At day 5, almost no cells were found in the HA and HA + collagen substrates, which is suspected to from cells falling to the bottom of the well instead of staying in the TCPS piece during seeding. Furthermore, at day 5 few osteoclasts were found in all the conditions (also in the ones without RANKL, confirming the findings of TRAP staining in this and the previous experiments). In concordance with what was shown in TRAP staining, at day 7, the number of osteoclasts in collagen and PILP substrates increased (no conclusions could be taken about the HA and HA + collagen substrates due to the problem of seeding density). Interestingly, PILP substrates under the effect of RANKL showed much more osteoclasts in comparison with the rest of the substrates, confirming the TRAP staining. Figure 3.21 shows SEM images for all the substrates at day 7.

Unfortunately, the HA + collagen coating in this sample was not very homogeneous and moreover, and it was very hard to distinguish between the cells and HA particles at the same magnification as the rest of the samples (Figure 3.21 (B)). Agglomerations of mononuclear cells were observed in some regions, for all coatings, and in particular, on coatings containing

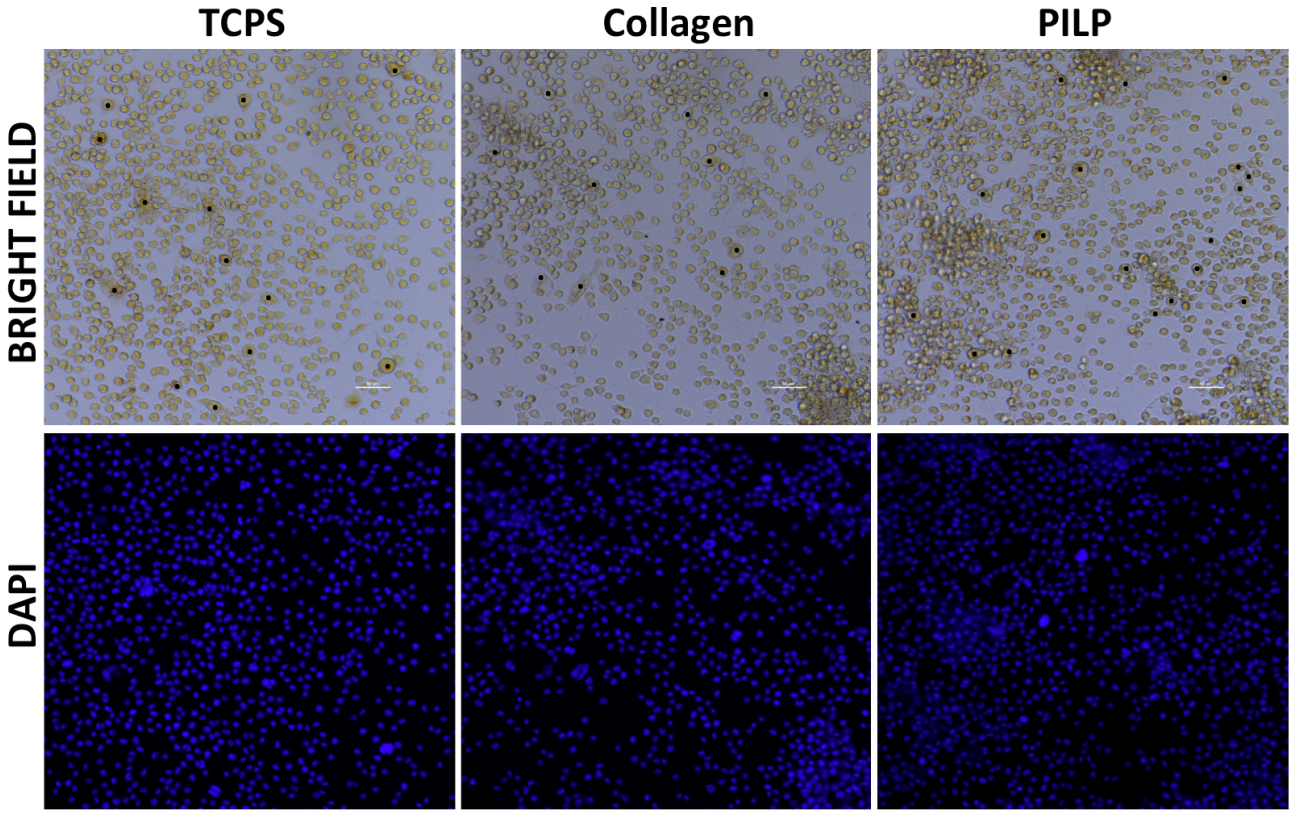

Figure 3.20: TRAP/DAPI staining in TCPS, Collagen and PILP substrates at day 7 under the influence of 100 ng/mL of RANKL. Black dots in the images designate osteoclasts. x20 magnification. Scale bar is 50 μm.

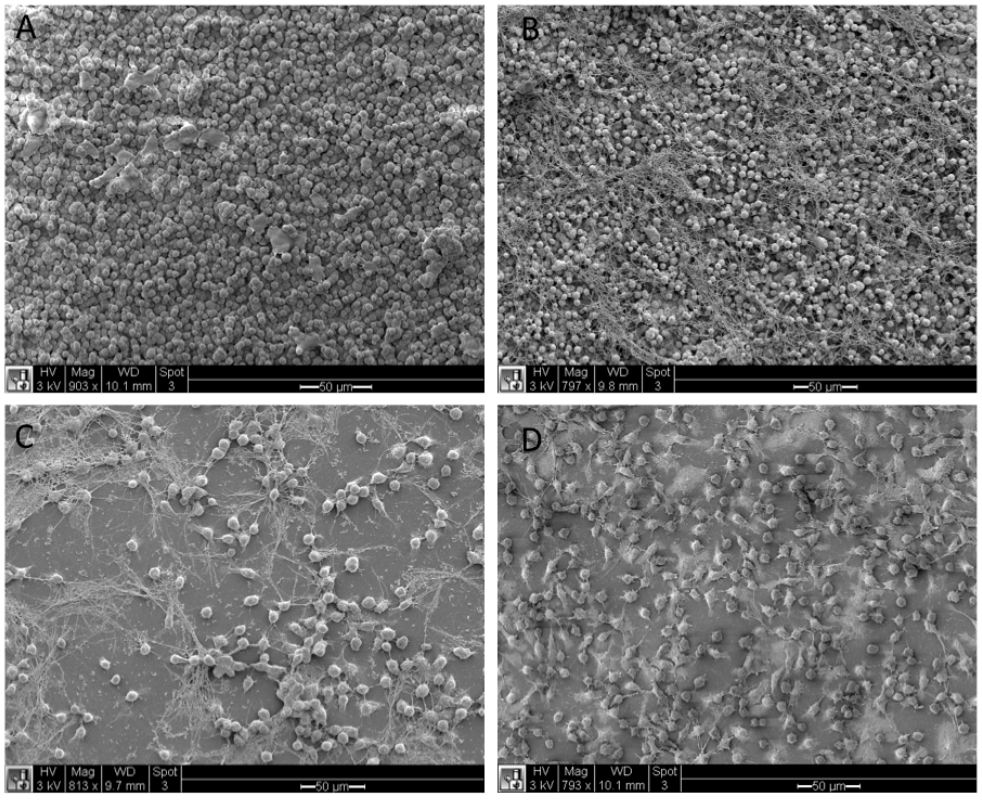

Figure 3.21: SEM images of cells under the effect of RANKL on (A) HA coating, (B) HA + collagen coating, (C) Collagen coating and (D) PILP coating. Scale bar: A, C, D = 50 μm; B = 20 μm.

collagen, some cells were entrapped within the collagen fibrils. When cells were in contact with HA, they showed more roundish morphology than in contact with collagen. Furthermore, fewer cells were present in coatings containing HA than in coatings containing collagen. This could be explained by the fact that if cells had more roundish morphology in coatings containing HA, they were weaker attached to the substrate than on the collagen and PILP coatings. As a consequence, when culture medium was aspirated at day 7 and under over-confluence conditions, much more cells were aspirated with the medium in HA coatings. Moreover, from TRAP activity results, less cells were present in HA coatings, which correlates with this findings. On PILP coatings, cells were more spread and in particular, osteoclasts were larger and with a flatter morphology than in the rest of the substrates. This fact can be observed in Figure 3.21 (D), where most of the whitish areas represent osteoclasts. A comparison of the osteoclasts morphology between the different substrates is also shown in Figure 3.22. Moreover, some osteoclasts exhibit the characteristic ruffled border, especially in the HA and HA + collagen substrates (see Figure 3.22 (A) and (B)).

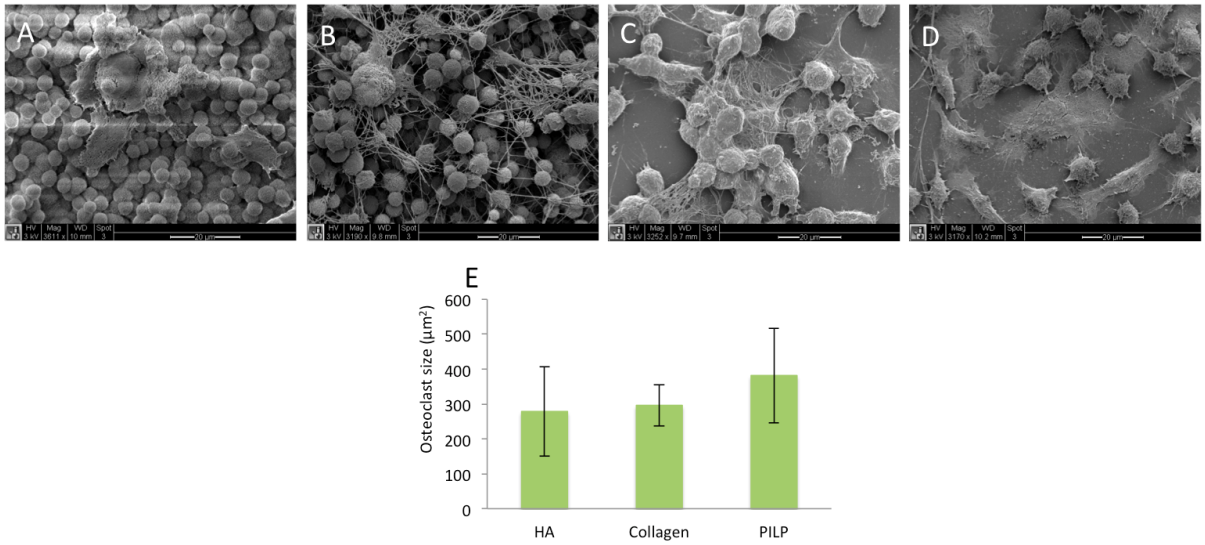

Figure 3.22: SEM images of osteoclasts at day 7 on (A) HA coating, (B) HA + collagen coating, (C) Collagen coating and (D) PILP coating. Scale bar is 20 μm. (E) Osteoclast size after 7 days in culture.

Cells were counted and the ones with area larger than 200 μm^2 were considered osteoclasts (Figure 3.22 (E)). As expected from SEM, osteoclasts on PILP coating were larger than in the rest of the coatings. Furthermore, only a few osteoclasts ($<$ 10 osteoclast/cm^2) were present in the HA and collagen coatings, while in the PILP substrate this range incremented to $\approx$ 30 osteoclast/cm^2.

To study osteoclast resorption of CaPs, cells were removed from the substrate. No resorption pits were observed in any of the substrates and the coatings that did not contain collagen appeared identical to the controls. It is suspected that 7 days in culture was not enough time to allow resorption of calcium phosphates. It has been observed that in some CaPs, the time needed for resorption is higher. For instance, S. Patntirapong *et al.* only observed resorption of CaPs after 9 days in culture [102]. Moreover, N. L. Davison and colleagues, found resorption of TCP with small grains (average grain diameter of 0.95 μm) after 25 days in culture, while with the same conditions, no resorption pits were found in TCP with big grains (grain diameter of 3.66 μm) [101], confirming that the architecture of CaPs influences osteoclast resorption. Nevertheless, in samples containing collagen (HA + collagen, collagen and PILP), degradation was observed at day 7. An example is shown in Figure 3.23, where (A) shows a footprint of a cell in HA + collagen coating. This footprint can only be from an osteoclast, as this area is $>$500 μm^2. Figure 3.23 (B) shows an alteration of the PILP structure regarding to the control

(compare Figure 3.23 (B) with 3.9 (D)). It is thought that this alteration could be due to degradation of collagen by osteoclasts as well. In the same image, it is possible to identify regions of collagen similar to what is found in the control, while in other regions (centre of sample), collagen seems to have been degraded.

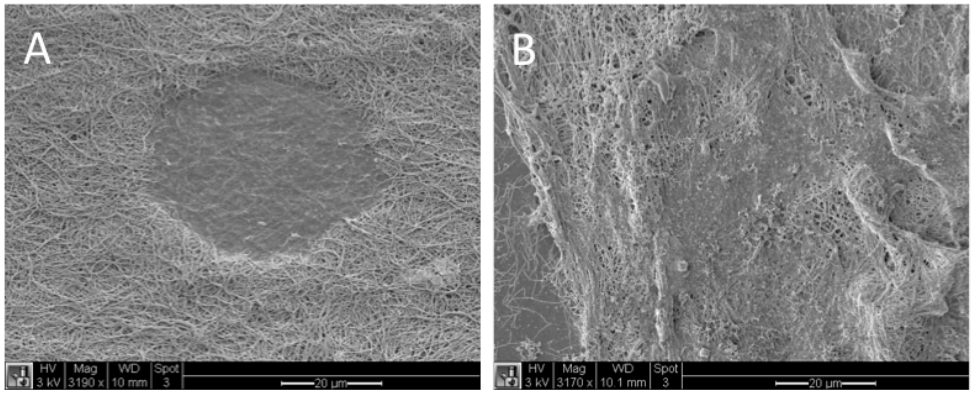

Figure 3.23: SEM images of (A) HA + collagen (x3190 magnification) and (B) PILP (x3170 magnification) coatings, after 7 days in culture and removal of the cells to study osteoclast resorption of CaPs. Scale bar is 20 μm.

This might indicate the start of osteoclast resorption. However, there is not enough evidence to ensure that resorption was being produced. As a consequence, longer experiments and further characterization would be needed to confirm it.

It is possible to conclude that TRAP staining and SEM results shown a higher amount of osteoclasts on the PILP coatings than in the rest of the conditions, supporting our hypothesis of increased resorption potential of this coating due to closer structure to native bone. Nevertheless, this was not upheld by the TRAP activity and DNA quantification results, in which no relevant differences were found between substrates. As a consequence, more characterization is needed to actually confirm that PILP-mineralized collagen coatings perform better than the rest.

3.7 Micropatterning

The PDMS moulds used in the micropatterning techniques were first treated to remove the oligomers that did not crosslink during the curing process. The removal of these oligomers was assessed by weighting the samples before and after the extraction procedure. Table 3.2 shows the percentage reduction in weight of the samples when oligomers were extracted.

From these data, it is possible to obtain the average reduction and the standard deviation: 4.33 ± 0.15. No big differences were observed in the weight reduction between channels of different width.

In order to verify that the μCP technique with PVA worked properly, samples were immunostained for collagen. Results are shown in Figure 3.24. In this figure it is possible to clearly see the collagen micropatterning in the PS substrate, confirming that the μCP with the intermediate PVA step was successful.

The PDMS used for transferring the collagen to the PVA was also imaged and no rest of collagen was found around the sample, indicating that the collagen transfer was completed.

It is important to remark that the collagen solution used in this technique was made of PBS, and consequently, the collagen was non-fibrillar. As a result, further PILP-mineralization would not be possible, because as previously explained, this method is based on the fact that mineralization starts in the characteristic bandings of collagen fibrils. Then, a modification

Channel width (μm)	Initial weight (mg)	Final weight (mg)	Reduction (%)
5	159.8	152.5	4.38
5	119.3	113.9	4.53
5	130.5	124.8	4.37
5	151.7	144.8	4.55
5	154.4	147.4	4.53
5	147.6	141.2	4.34
10	128.4	122.8	4.36
10	149.4	143.3	4.08
10	138.9	133.0	4.25
80	108.8	103.9	4.50
80	119.2	114.2	4.19
80	95.7	91.7	4.18
80	143.7	137.6	4.24
80	102.4	98.2	4.10

Table 3.2: PDMS weight reduction after removing oligomers.

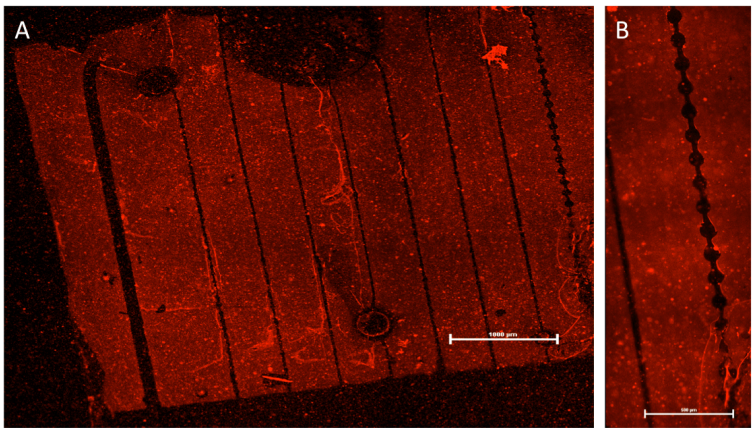

Figure 3.24: Fluorescent microscopy of μCP samples.

and optimization of this μCP technique using the FFB solution is required. The use of this solution may have the potential to obtain fibrillar-micropatterned collagen, allowing to apply the PILP method to mineralize it. This was the original idea of this experiment. However, due to the limitation of time, it was not possible to perform it, leaving an open window to further investigation of this kind of micropatterning. It is aimed that these collagen/CaPs microppatterned coatings may have a promising application in hip implants, directing osteoclast resorption and potentially guiding osseointegration.

Chapter 4: Conclusions and future perspectives

Coatings obtained by PILP-mineralized collagen method have been successful in mimicking the intrafibrillar mineralization of collagen, and as a consequence, a coating was obtained that more closely resembles the native bone, in composition and structure. Its biological performance was tested by studying the osteoclast resorption of these coatings and comparing it to collagen and hydroxyapatite coatings.

In order to PILP-mineralize the collagen coatings, an optimization of collagen fibril formation and deposition on substrates was first done. After different trials, the most homogeneous coatings were obtained by doing a two-step collagen coating: initially, a thin non-fibrillar layer of collagen was performed. It was found that the thin collagen layer was essential to improve the adhesion of the collagen fibrils to the TCPS substrates. In the second step, collagen fibrils were formed and deposited on the thin coating. It was observed that 1h of deposition was not enough to obtain a homogeneous coating. Increasing the deposition time, the coatings became more homogeneous and after 48h of incubation, refreshing the collagen solution at 24h, quite homogeneous coatings were obtained. However, further effort is needed to optimize the coating, to improve the collagen adhesion to the substrate as well as to have a better control of the deposition process. Possible alternative techniques to improve collagen homogeneity and adhesion may be to use sedimentation by centrifuging the collagen in the wells or to use electrospinning.

Further characterization is also needed in the CaPs and collagen coatings and supplementary techniques to XRD, such as Inductively coupled plasma mass spectrometry (ICP-MS) or Energy-dispersive X-ray spectroscopy (EDX) could be used in order to detect the elements present in the coatings and their chemical composition.

Murine RAW 264.7 macrophages were cultured and differentiated into osteoclasts by using RANKL. It was found that the optimal seeding density to culture this cells under the influence of RANKL and have a $\approx 100\%$ confluence after 7 days in culture was 4000 cells/cm^2. Moreover, it was also observed that RANKL at ≥ 50 ng/mL affected the growth of the cells, decreasing it in comparison to culture them in basic medium. No significant differences were observed in morphology when these cells were culture in DMEM or α-MEM.

Further improvement of the imaging of the coatings containing CaPs is required as well, as it was not possible to image the cells on top of the CaPs coatings with an inverted microscope. The use of a stereomicroscope with high resolution may solve this problem. Another possible improvement is the seeding of the cells in the TCPS pieces, as the volume of the cell suspension used for the seeding was in excess, collapsing and spreading all around the well, which decreased the number of cells seeded in the TCPS pieces.

TRAP activity and DNA quantification results from the RANKL optimization experiment showed that CaPs coatings improved the differentiation of the cells into osteoclasts under the RANKL condition. However, these findings were not observed in the results of TRAP activity and DNA quantification of the osteoclast resorption experiment. Although it is suspected that something went wrong in the DNA quantification of this last experiment (very low values of DNA were obtained for day 7), which could explain those differences in the osteoclasts experiment, no clear conclusions can be made. Interestingly, TRAP staining and SEM results showed a higher amount of osteoclasts in the PILP-mineralized collagen coating compare to the rest of the substrates, and osteoclast were also bigger as well as flatter in these coatings than in the rest of the conditions, supporting our initial hypothesis that PILP-mineralized collagen coatings performed better than the rest. Although clear resorption was not observed in any of the substrates, the coatings containing collagen showed some degradation where osteoclasts were adhered. However, longer experiments should be perform to actually confirm resorption.

The coating obtained by PILP-mineralized collagen method may be promising in substituting the biomimetic coatings of some prosthesis, such as the hip implants, that are already used in the clinic.

The μCP technique used to obtain collagen micropatterning was very successful. Nonetheless, the collagen solution used for this experiment was in PBS, which did not have the buffer capacity to form collagen fibrils, without which, the PILP mineralization cannot happen. However, this opens many possibilities of research. The same micropatterning method used with FFB solution may lead to fibrillar-micropatterned collagen, allowing then the use of PILP solution to mineralize the collagen. Further studies with cells would be also interesting to study the biological performance of these micropatterns compared to CaPs and collagen only.

Finally, achieving a collagen/CaP coating micropatterned by using the PILP-mineralization method, may have a potential for controlling cell morphology, growth or differentiation, and more interesting even, the ability to direct osteoclastic resorption and guide osseointegration of an implant.

Bibliography

[1] Josh E. Schroeder, Rami Mosheiff, *Tissue engineering approaches for bone repair: Concepts and evidence*. Injury, Int. J. Care Injured 2011, 42, 609–613.

[2] Ami R. Amini, Cato T. Laurencin, and Syam P. Nukavarapu, *Bone Tissue Engineering: Recent Advances and Challenges*. Crit. Rev. Biomed. Eng. 2012, 40 (5), 363–408.

[3] Kanis JA (2007) WHO Technical Report, University of Sheffield, UK: 66.

[4] M. H. Atkinson, *Osteoarthrosis*. Can. Fam. Physician 1984, 30, 1503–1507.

[5] P. Habibovic, K. de Groot, *Osteoinductive biomaterials-properties and relevance in bone repair*. Journal of tissue engineering and regenerative medicine 2007, 1, 25–32.

[6] Molly M. Stevens, *Biomaterials for bone tissue engineering*. Biomaterials Today 2008, 11, 18-25.

[7] Yuchun Liu, Jing Lim, Swee-Hin Teoh, *Development of clinically relevant scaffolds for vascularised bone tissue engineering*. Biotechnology Advances 2013, 31, 688–705.

[8] Fergal J.O'Brien, *Biomaterials scaffolds for tissue engineering*. Materials Today 2011, 14 (3), 88-95.

[9] L.A. Cyster, D.M. Grant, S.M. Howdle, F.R.A.J. Rose, D.J. Irvine, D. Freeman, C.A. Scotchford, K.M. Shakesheff, *The influence of dispersant concentration on the pore morphology of hydroxyapatite ceramics for bone tissue engineering*. Biomaterials 2005, 26, 697–702.

[10] Taco J. Blokhuis, Marco F. Termaat, Frank C. den Boer, Peter Patka, Fred C. Bakker, and Henk J. Th. M. Haarman, *Properties of calcium phosphate ceramics in relation to their in vivo behavior*. The Journal of Trauma: Injury, Infection, and Critical Care 2000, 48, 179-186.

[11] Maria A.Woodruffa, Claudia Langeb, Johannes Reichertc, Arne Bernerd, Fulen Chene, Peter Fratzlb, Jan-Thorsten Schantzf, and Dietmar W. Hutmachera, *Bone tissue engineering: from bench to bedside*. Advanced Materials 2012, 24 (11), 1445-50.

[12] Monika Saini, Yashpal Singh, Pooja Arora, Vipin Arora, Krati Jain, *Implant biomaterials: A comprehensive review*. World Journal of Clinical Cases 2015, 3 (1), 52-57.

[13] Karen J.L. Burg, Scott Porter, James F. Kellam *Biomaterial developments for bone tissue engineering*. Biomaterials 2000, 21, 2347-2359.

[14] Valerio Sansone, Davide Pagani, Marco Melato, *The effects on bone cells of metal ions released from orthopaedic implants. A review*. Clinical Cases in Mineral and Bone Metabolism 2013, 10, 34-40.

[15] Bergmann Carlos P., Stumpf Aisha, *Dental Ceramics. Microstructure, Properties and Degradation. Ch. 2: Biomaterials*. 2013, ISBN 978-3-642-38224-6.

[16] M. Navarro, A. Michiardi, O. Castaño, and J.A Planell, *Biomaterials in orthopaedics*. J. R. Soc. Interface. 2008, 5 (27), 1137–1158.

[17] Josh E. Schroeder, Rami Mosheiff, *Tissue engineering approaches for bone repair: Concepts and evidence*. Injury, Int. J. Care Injured 2011, 42, 609–613.

[18] Carlos Oldani, Alejandro Dominguez, *Recent Advances in Arthroplasty. Ch. 9: Titanium as a Biomaterial for Implants*. Edited by Dr. Samo Fokter, 2012. ISBN 978-953-307-990-5.

[19] John D. Currey, *Bones: structures and mechanics*. 2002, ISBN 0-691-09096-3.

[20] Matthew J. Olszta, Xingguo Cheng, Sang Soo Jee, Rajendra Kumar, Yi-Yeoun Kim, Michael J. Kaufman, Elliot P. Douglas, Laurie B. Gower, *Bone structure and formation: A new perspective*. Materials Science and Engineering R. 2007, 58, 77–116.

[21] Dimitrios J. Hadjidakis and Ioannis I. Androulakis, *Bone remodeling*. New York Academy of Sciences 2006, 1092, 385–396.

[22] Tamara A. Franz-Odendaal, Brian K. Hall, P. Eckhard Witten, *Buried alive: How osteoblasts become osteocytes*. Developmental Dynamics 2006, 235 (1), 176-190.

[23] Adele L. Boskey, *Bone composition: relationship to bone fragility and antiosteoporotic drug effects*. BoneKEy Reports 2013, 2, 447.

[24] Hamid Shegarfi, Olav Reikeras, *Review article: Bone transplantation and immune response*. Journal of Orthopaedic Surgery 2009, 17(2), 206-11.

[25] Compton, J.T., Lee, F.Y., *A review of osteocyte function and the emerging importance of sclerostin*. J. Bone Joint Surg. Am. 2014, 96 (1), 1659–1668.

[26] Zhao, S., et al., *MLO-Y4 osteocyte-like cells support osteoclast formation and activation*. J. Bone Miner. Res. 2002a, 17 (11), 2068–2079.

[27] Jeffrey O. Hollinger, Thomas A. Einhorn, Bruce A. Doll and Charles Sfeir, *Bone Tissue Engineering*. CRC Press 2004, ISBN 0-8493-1621-9.

[28] Donald L. Bartel, Dwight T. Davy, Tory M. Keaveny, *Orthopaedic biomechanics: Mechanics and Design in Musculoskeletal system*. Person Prentice Hall Bioengineering, 2013, ISBN 978-0130089090.

[29] Farbod, K., et al., *Interactions between inorganic and organic phases in bone tissue as a source of inspiration for design of novel nanocomposites*. Tissue Eng. Part B Rev. 2014, 20 (2), 173–188.

[30] S. Su, K. Sun, F. Z. Cui, W. J. Landis, *Organization of apatite crystals in human woven bone*. Bone 2003, 32 (2), 150-162.

[31] Gulati G. L., Ashton J.K., Hyun B.H., *Structure and function of the bone marrow and hematopoiesis*. Hematol. Oncol. Clin. North Am. 1988, 2 (4), 495-511.

[32] Je-Young Rho, Liisa Kuhn-Spearing and Peter Zioupos, *Mechanical properties and the hierarchical structure of bone*. Medical Engineering Physics 1998, 20, 92–102.

[33] I. Manjubala, M. Sivakumar, R. V. Sureshkumar, T. P. Sastry, *Bioactivity and Osseointegration Study of Calcium Phosphate Ceramic of Different Chemical Composition*. J. Biomed. Mater. Res. 2002, 63 (2), 200-208.

[34] Fwu-Hsing Liu, *Synthesis of bioceramic scaffolds for bone tissue engineering by rapid prototyping technique*. Journal Sol-Gel Science Technology 2012, 64, 704–710.

[35] N. Davison, X.Luo, T. Schoenmaker, V. Everts, H. Yuan, F. Barrère-de Groot, J. D. de Bruijn, *Submicron-scale surface architecture of tricalcium phosphate directs osteogenesis in vitro and in vivo*. European Cells Materials 2014, 27, 281-297.

[36] Satyavrata Samavedi, Abby R. Whittington, Aaron S. Goldstein, *Calcium phosphate ceramics in bone tissue engineering: A review of properties and their influence on cell behavior*. Acta Biomaterialia 2013, 9, 8037–8045.

[37] Donglu Shi, *Introduction to Biomaterials*. Tsinghua University Press, 2006.

[38] Hongjian Zhou, Jaebeom Lee, *Nanoscale hydroxyapatite particles for bone tissue engineering*. Acta Biomaterialia 2011, 7, 2769–2781.

[39] Sergey V. Dorozhkin, *Calcium orthophosphate-based biocomposites and hybrid biomaterials*. Journal of Materials Science, 2009, 44 (9), 2343–2387.

[40] Leming J. E., Cornell C.N. and Muschler G.F., *Bone cells and matrices in otrhopaedic tissue engineering*. Orthop. Clin. 2000, 31, 357.

[41] Gérard Eddy Poinern, Ravi Krishna Brundavanam, Nicholas Mondinos, Zhong-Tao Jiang,*Synthesis and characterisation of nanohydroxyapatite using an ultrasound assisted method*. Ultrasonics Sonochemistry 2009, 16, 469–474.

[42] Yokozeki H., Hayashi T., Nakagawa T., Kurosawa H., Shibuya K., Ioku, K., *Influence of Surface Microstructure on the Reaction of the Active Ceramics in vivo*, J. Mater. Sci.: Mater. Med. 1998, 9, 381–384.

[43] Chengde Gao, Youwen Deng, Pei Feng, Zhongzheng Mao, Pengjian Li, Bo Yang, Junjie Deng, Yiyuan Cao, Cijun Shuai and Shuping Peng, *Current Progress in Bioactive Ceramic Scaffolds for Bone Repair and Regeneration*. Int. J. Mol. Sci. 2014, 15, 4714-4732.

[44] R. Z. Legeros, S. Lin, R. Rohanizadeh, D. Mijares, J. P. Legeros, *Biphasic calcium phosphate bioceramics: preparation, properties and applications*. Journal of Materials Science: Materials in Medicine 2003, Volume 14, Issue 3, pp 201–209

[45] Florence Barrère, Clemens A van Blitterswijk, Klaas de Groot, *Bone regeneration: molecular and cellular interactions with calcium phosphate ceramics*. International Journal of Nanomedicine 2006, 1 (3), 317–332.

[46] Samar J. Kalita, Abhilasha Bhardwaj, Himesh A. Bhatt, *Nanocrystalline calcium phosphate ceramics in biomedical engineering*. Materials Science and Engineering C 2007, 27, 441–449.

[47] J.C. Elliott, *Structure and Chemistry of the Apatites and Other Calcium Orthophosphates. Ch.1: General chemistry of the calcium orthophosphates*. 1994, ISBN 0-444-81582-1.

[48] Brown, W. E., *Octacalcium phosphate and hydroxyapatite*. Nature 1962, 196, 1048– 1055.

[49] O. Suzuki, *Octacalcium phosphate: Osteoconductivity and crystal chemistry.*Acta Biomaterialia 2010, 6, 3379–3387.

[50] Osamu Suzuki, *Octacalcium phosphate (OCP)-based bone substitute materials.* Japanese Dental Science Review 2013, 49 (2), 58-71.

[51] Tisdel C.L., Goldberg V.M., Parr J.A., Bensusan J.S., Staikoff L.S., Stevenson S., *The influence of a hydroxyapatite and tricalcium-phosphate coating on bone growth into titanium fiber-metal implants.* J. Bone Joint Surg. Am. 1994, 76(2), 159-71.

[52] Ritwik A., Dr. Saju K. K., *A Review on Different Coating Methods of Hydroxyapatite on Titanium Implants.* International Journal of Innovative Research in Science, Engineering and Technology, 2017, 6 (4), 103-106.

[53] León Betty, Jansen John, *Thin Calcium Phosphate Coatings for Medical Implants. Ch. 1: Introduction.* Ed. León Betty, Jansen John. Springer 2009, ISBN: 978-0-387-77718-4.

[54] K. de Groot, R. Geesink, C. P. A. T. Klein, P. Serekian, *Plasma sprayed coatings of hydroxylapatite.* Journal of Biomedical Materials Research 1987, 21, 1375-1381.

[55] Oerlikon, Merko.*Atmospheric Plasma Spray Solutions.* 2017,6.

[56] Florence Barrère, *Biomimetic Calcium Phospahte Coatings. Physicochemistry and Biological Activity. Ch. 1: General Introduction.* 2002, ISBN: 90-365-1733-8.

[57] Tanya J. Levingstone, Malika Ardhaoui, Khaled Benyounis, Lisa Looney, Joseph T. Stokes, *Plasma sprayed hydroxyapatite coatings: Understanding process relationships using design of experiment analysis.* Surface Coatings Technology 2015, 283, 29–36.

[58] P. Habibovic, C.M. Van der Valk, C. A. Van Blitterswijk, K. de Groot, *Influence of octacalcium phosphate coating on osteoinductive properties of biomaterials.* J. of Mat. Science: Materials in Medicine, 2004, 15, 373-380.

[59] Limin Sun, Christopher C. Berndt, Karlis A. Gross, Ahmet Kucuk, *Material Fundamentals and Clinical Performance of Plasma-Sprayed Hydroxyapatite Coatings: A Review.* J. Biomed. Mater. Res. 2001, 58 (5), 570-592.

[60] Oguchi H., Ishikawa K., Ojima S., Hirayama Y., Seto K., Eguchi G., *Evaluation of a high-velocity flame-spraying technique for hydroxyapatite.* Biomaterials 1992, 13 (7), 471-477.

[61] C. S. Chai, B. Ben-Nissan, *Bioactive nanocrystalline sol-gel hydroxyapatite coatings.* J. of Mater. Science: Materials in Medicine 1999, 10, 465-469.

[62] Dr. Catherine M. Cotell, Douglas B. Chrisey, Kenneth S. Grabowski, James A. Sprague, Charles R. Gossett, *Pulsed laser deposition of hydroxylapatite thin films on Ti-6Al-4V.* Journal of Applied Biomaterials 1992, 3 (2), 87-93.

[63] Y. Abe, T. Kokubo, T. Yamamuro, *Apatite coating on ceramics, metals and polymers utilizing a biological process.* J. of Materials Science: Materials in Medicine, 1990, 1, 233-238.

[64] Tadashi Kokubo, *Bioactiveglass ceramics:properties and applications.* Biomaterials 1991, 12, 155-163.

[65] Tadashi Kokubo , Hiroaki Takadama, *How useful is SBF in predicting in vivo bone bioactivity?.* Biomaterials 2006, 27, 2907–2915.

[66] Pamela Habibovic, Florence Barrère, Clemens A. van Blitterswijk, Klaas de Groot, Pierre Layrolle, *Biomimetic Hydroxyapatite Coating on Metal Implants*. J. Am. Ceram. Soc. 2002, 85 (3), 517–22.

[67] K. Madhumathi, K.T. Shalumon, V.V. Divya Rani, H. Tamura, T. Furuike, N. Selvamurugan, S.V. Nair and R. Jayakumar, *Wet chemical synthesis of chitosan hydrogel–hydroxyapatite composite membranes for tissue engineering applications*. International Journal of Biological Macromolecules 2009, 45, 12–15.

[68] Allison A. Campbell, *Bioceramics for implant coatings*. Materials Today 2003, 6 (11), 26-30.

[69] Byers P. H., Pyott S. M., *Recessively inherited forms of osteogenesis imperfecta*. Annu. Rev. Genet. 2012, 46, 475-497.

[70] Hoang Q.Q., Sicheri F., Howard A.J., Yang D.S., *Bone recognition mechanism of porcine osteocalcin from crystal structure*. Nature 2003, 425 (6961), 977-80.

[71] J. An, S. Leeuwenburgh, J. Wolke, J. Jansen, *Biomineralization and Biomaterials. Fundamentals and Applications. Ch. 4: Mineralization processes in hard tissue: Bone*. Edited by Conrado Aparicio and Maria-Pau Ginebra, Woodheat Publishing, Elsevier, 2016. ISBN: 978-1-78242-338-6.

[72] F. Nudelman, K. Pieterse, A. George, P. H. H. Bomans, H. Friedrich, L. J. Brylka, P. A. J. Hilbers, G. de With and N. A. J. M. Sommerdijk, *The role of collagen in bone apatite formation in the presence of hydroxyapatite nucleation inhibitors*. Nat. Mater. 2010, 9 (12), 1004–1009.

[73] Lajos Kalmar, Daniel Homola, Gabor Varga, Peter Tompa, *Structural disorder in proteins brings order to crystal growth in biomineralization*. Bone 2012, 51, 528–534.

[74] L.B. Gower, *Biomineralization and Biomaterials. Fundamentals and Applications. Ch. 6: Biomimetic mineralization of collagen*. Edited by Conrado Aparicio and Maria-Pau Ginebra, Woodheat Publishing, Elsevier, 2016. ISBN: 978-1-78242-338-6.

[75] Katherine A Staines, Vicky E MacRae and Colin Farquharson,

[76] . Journal of Endocrinology 2012, 214, 241–255.

[77] Jeffrey Paul Gorski, *Biomineralization of bone: a fresh view of the roles of non-collagenous proteins*. Front Biosci (Landmark Ed). 2014, 16, 2598–2621.

[78] Roach H.I., *Why does bone matrix contain non-collagenous proteins? The possible roles of osteocalcin, osteonectin, osteopontin and bone sialoprotein in bone mineralisation and resorption*. Cell Biol Int. 1994, 18 (6), 617-28.

[79] Curtin, Paul; McHugh, Kevin P.; Zhou, Hia-Yan; Flückiger, Rudolf; Goldhaber, Paul; Oppenheim, Frank G.; Salih, Erdjan. Modulation of bone resorption by phosphorylation state of bone sialoprotein. Biochemistry. 2009; 48:6876–6886

[80] Gordon JA, Tye CE, Sampaio AV, Underhill TM, Hunter GK, Goldberg HA, *Bone sialoprotein expression enhances osteoblast differentiation and matrix mineralization in vitro*. Bone 2007, 41 462–473.

[81] F. Nudelman, A. J. Lausch, N. A.J.M. Sommerdijk, E. D. Sone, *In vitro models of collagen biomineralization*. Journal of Structural Biology 2013, 183, 258–269.

[82] Ulrike G. K. Wegst, Hao Bai, Eduardo Saiz, Antoni P. Tomsia and Robert O. Ritchie, *Bioinspired structural materials*. Nature Materials 2015, 14, 23-36.

[83] W. F. Zambuzzi, D. D.P. Campos, T. L. Ogeda,C. V. Ferreira, C. A. Bertran and S. Bertazzo, *Hydroxyapatite surface solubility and effect on cell adhesion*. Colloids and Surfaces B: Biointerfaces 2010, 78, 177–184.

[84] A. S. Deshpande and E. Beniash, *Bio-inspired Synthesis of Mineralized Collagen Fibrils*. Cryst. Growth Des. 2008, 8(8), 3084–3090.

[85] K. Jiao, L. Niu, C. Ma, X. Huang, D. Pei, T. Luo, Q. Huang, J. Chen and F.R. Tay, *Complementary and Uncertainty in Intrafibrillar Mineralization of Collagen*. Adv. Funct. Mater. 2016, 26, 6858-6875.

[86] Sang Soo Jee, Lauren Culver, Yuping Li, Elliot P. Douglas, Laurie B. Gower, *Biomimetic mineralization of collagen via an enzyme-aided PILP process*. Journal of Crystal Growth 2010, 312, 1249–1256.

[87] Sang-Soo Jee, Taili T. Thula, Laurie B. Gower, *Development of bone-like composites via the polymer-induced liquid-precursor (PILP) process. Part 1: Influence of polymer molecular weight*. Acta Biomaterialia 2010, 6, 3676–3686.

[88] Yuping Li, Taili T. Thula, Sangsoo Jee, Sasha L. Perkins, Conrado Aparicio, Elliot P. Douglas, and Laurie B. Gower, *Biomimetic Mineralization of Woven Bone-Like Nanocomposites: Role of Collagen Cross-Links*. Biomacromolecules 2012, 13, 49−59.

[89] Taili T. Thula, Felicia Svedlund, Douglas E. Rodriguez, Jacob Podschun, Laura Pendi, Laurie B. Gower, *Mimicking the Nanostructure of Bone: Comparison of Polymeric Process-Directing Agents*. Polymers (Basel) 2011, 3 (1), 10–35.

[90] Katrin Bleek, Andreas Taubert, *New developments in polymer-controlled, bioinspired calcium phosphate mineralization from aqueous solution*. Acta Biomaterialia 2013, 9, 6283–6321.

[91] Yuping Li, Xi Chen, Alex Fok, Jose Carlos Rodriguez-Cabello, Conrado Aparicio, *Biomimetic Mineralization of Recombinamer-Based Hydrogels toward Controlled Morphologies and High Mineral Density.*ACS Appl. Mater. Interfaces 2015, 7, 25784−25792.

[92] Noel Davison, *Cell and Tissue Response to osteoinductive Calcium Phosphate Architecture. Ch. 1: General Introduction*. 2014, ISBN: 978-90-365-3773-5.

[93] Sin-Hua Liu, Alexander Kirschenbaum, Shen Yao, Alice C. Levine, *Interactive Effect of Interleukin-6 and Prostaglandin E_2 on Osteoclastogenesis via the OPG/RANKL/RANK System*. Ann. N.Y. Acad. Sci. 2006, 1068, 225–233.

[94] Racquel Zapanta LeGeros, *Properties of Osteoconductive Biomaterials: Calcium Phosphates*. Clinical Orthopaedis and related research 2002, 395, 81–98.

[95] Barrère F., van der Valk C. M , Dalmeijer R.A., Meijer G., van Blitterswijk C.A., de Groot K., Layrolle P., *Osteogenecity of octacalcium phosphate coatings applied on porous metal implants*. J. Biomed. Mater. Res. A. 2003, 66 (4), 779-788.

[96] Yukari Shiwaku, Lynn Neff, Kenichi Nagano, Ken-Ichi Takeyama, Joost de Bruijn, Michel Dard, Francesca Gori, Roland Baron, *The Crosstalk between Osteoclasts and Osteoblasts is dependent upon the cmposition and structure of Biphasic Calcium Phosphates*. PLoS One. 2015, 10 (7).

[97] N. Kondoa, A. Ogose, K. Tokunaga, H. Umezu, K. Arai, N. Kudo, M. Hoshino, H. Inoue, H. Irie, K. Kuroda, H. Mera, N. Endo, *Osteoinduction with highly purified β-tricalcium phosphate in dog dorsal muscles and the proliferation of osteoclasts before heterotopic bone formation.*Biomaterials 2006, 27, 4419–4427.

[98] Norihiro Akiyama, Mitsuru Takemoto, Shunsuke Fujibayashi, Masashi Neo, Masahiro Hirano, Takashi Nakamura, *Difference between dogs and rats with regard to osteoclast-like cells in calcium-deficient hydroxyapatite-induced osteoinduction.* Journal of Biomedical Materials Reserach 2011, 96 (2), 402-412.

[99] Julia F. Charles and Antonios O. Aliprantis, *Osteoclasts: more than 'bone eaters'.* Trends Mol Med. 2014, 20(8), 449–459.

[100] S. Yamada, D. Heymann, J.M. Bouler, G. Daculsi, Osteoclastic resorption of calcium phosphate ceramicss with different hydroxyapatite/β-tricalcium phosphate ratios. Biomaterials 1997, 18, 1037-1041.

[101] Noel L. Davison, Bas ten Harkel, Ton Schoenmaker, Xiaoman Luo, Huipin Yuan, Vincent Everts, Florence Barrère-de Groot, Joost D. de Bruijn, *Osteoclast resorption of beta-tricalcium phosphate controlled by surface architecture*, Biomaterials 2014, 35 (26), 7441-7451.

[102] S. Patntirapong, P. Habibovic and P.V. Hauschka, *Effects of soluble cobalt and cobalt incorporated into calcium phosphate layers on osteoclasst differentiation and activation.* Biomaterials 2009, 30, 548-555.

[103] T. Kokubo, H. Kushitani, S. Sakka, T. Kitsugi, and T. Yamamuro, *Solutions able to reproduce in vivo surface-structure changes in bioactive glass-ceramics A-W*[3], *J.Biomed.Mater.Res.*, 1990, 24, 721˘734.

[104] Zeyad Almutairi, Carolyn L. Ren, Leonardo Simon, *Evaluation of polydimethylsiloxane (PDMS) surface modification approaches for microfluidic applications*. Colloids and Surfaces A: Physicochem. Eng. Aspects 2012, 415, 406–412.

[105] Haiyang Yu, Sijing Xiong, Chor Yong Tay, Wen Shing Leong, Lay Poh Tan, *A novel and simple microcontact printing technique for tacky, soft substrates and/or complex surfaces in soft tissue engineering.* Acta Biomaterialia, 2012, 8, 1267–1272.

[106] H. Hotokezada, E. Sakai, K. Kanaoka, K. Saito, K. Matsuo, H. Kitaura, N. Yoshida, K. Nakayama, *U0126 and PD98059, Speficific Inhibitors of MEK, Accelarete Differentiation of RAW264.7 Cells into Osteoclast-like Cells.* The Journal of Biological Chemistry 2002, 277 (6), 47366-47372.

[107] C. Dennison, *A Simple and Universal Method for Making up Buffer Solutions*. Biochemical Education, 1988, 16 (4), 210-211.

[108] Yang Liu and D J Williams, *Processing of collagen gels to create in vitro cell growth matrix without damage to the collagen native structure.* Proc. IMechE Part B: J. Engineering Manufacture, 2006, 220, 787-791.

[109] Y. K. Zhu, T. Umino, X. D. Liu, H. J. Wang, D. J. Romberger, J. R. Spurzem, S. I. Rennard, *Contraction of fibroblast-containing collagen gels: initial collagen concentration regulates the degree of contraction and cell survival.* In Vitro Cell. Dev. Biol. Animal 2001, 37, 10-16.

Appendix A: Micropatterning techniques

Although only μCP with intermediate PVA worked successfully for obtaining collagen micropatterning, diverse techniques and methods were used. In this appendix, all the attempted micropatterning techniques are summarized.

A.1 MIMIC

PDMS moulds with 80 μm channels width and 4.1 μm in height were placed on top of Si wafers and plasma treatment (O_2) was applied for 10 min. Afterwards, collagen was diluted with FFB-I at the concentration of 100, 200 and 500 μg/mL. Then, 10 μL of collagen solution were infiltrated in different PDMS/Si assemblies. Infiltration was allowed during 5 min at room temperature and afterwards, samples were placed in the incubator at 37°C, 5% CO_2 during 2h in order to allow collagen fibril formation. After incubation period, PDMS was peeled off from the Si wafer.

A.2 μCP

Different protocols of microcontact printing were developed:

(a) **First protocol**: flat PS and PDMS moulds (previously treated to get rid of PDMS oligomers) with 5, 10 and 80 μm width and 4.1 μm height were treated with plasma (O_2) for 2 minutes, followed by a FOTS treatment to obtain a very hydrophobic surface. To do the FOTS treatment, the bottom and the top part of a glass Pettri dish as well as PDMS moulds were heated up to 120°C. After that, a drop of FOTS was applied on a glass coverslip and place it in the Petri dish with the samples. The Petri dish was then sealed and incubated at 120°C for 2h. After 2h incubation, the Petri dish was removed from the oven and allowed it to cool down to room temperature. Finally, samples were taken out from the Petri dish. Once the samples were ready, a 100 μL droplet of collagen diluted in FFB (200 μg/mL) was placed on top of the PDMS mould and incubated during 5h to allow collagen fibril formation and deposition. Afterwards, samples (except the PDMS mould of 10 μm width) were gently washed with milliQ water and dried. PDMS moulds were then placed in conformal contact with the flat PS during 10 min to allow collagen transferring.

(b) **Second protocol**: a modification of the first protocol was developed. The preparation of the flat PS and PDMS mould was the same. However, two different collagen solutions were prepared: one diluted with FFB (100 μg/mL) and another diluted with PBS (50 μg/mL), this one based on [105]. A droplet (100 μL) of each collagen solution was placed on top of two PDMS moulds and collagen deposition was allowed for 1h. Samples were then washed very gently with milliQ water and dried overnight in a laminar-flow hood. For microcontact printing, the inked PDMS moulds were placed in conformal contact with

the flat PS for 20 min with a 50g weight on top of the samples to ensure homogeneous pressure. Afterwards, the PDMS mould was gently peeled off and PS substrate was washed with milliQ water.

(c) **Third protocol**: in this trial, a flat PDMS without any treatment was used to transfer the collagen to a PS mould treated with plasma (O_2) for 2 min. The PS mould was prepared as explained in Chapter 2. Collagen was diluted with PBS at the concentration of 50, 100 and 200 μg/mL. A droplet (100 μL) of each solution was deposited on three different flat PDMS and collagen deposition was allowed for 1h. After that, flat PDMS were gently rinsed with water and dried overnight. Once samples were dried, the flat PDMS inked with collagen were placed in conformal contact with the PS mould for 20 min with a 50g on top. Finally, PDMS were peeled off from PS, washed with milliQ water and allow them to dry.

A.3 Embossing

For obtaining collagen micropatterning, an embossing technique was also used. In this case, a drop of 20 μL of collagen gel was added on a flat substrate (PS or Si wafer) followed by the placement of the PDMS mould in conformal contact with the flat substrate. Some weight ($\approx$15 g) was put on top of the PDMS mould and pressure by hand was applied. Samples were then introduced in an incubator for 4h at 37°C to allow gel formation. Afterwards, the PDMS mould was gently peeled off from the flat substrate and the patterned substrate was washed with milliQ water to get rid of the salts. For this approach three different combinations of mould/substrates were used:

(a) **First approach**: in this case, PDMS mould was treated with FOTS and flat PS treated with plasma (O_2) for 2 min as a substrate. As the PDMS mould was very hydrophobic due to FOTS treatment, with this approach it was expected to obtain micropatterning in the flat PS.

(b) **Second approach**: PDMS with 80 μm width channels was used as a mould. The channels were treated with plasma (O_2) for 10 min. The substrate used was a Si wafer treated with FOTS. Contrarily to the first approach, in this one it was expected to obtain micropatterning in the channels of the PDMS mould.

(c) **Third approach**: this last approach was a modification of the first one. Same mould and substrates were used, but in this case, the PS was not treated with plasma.

A summary of all the attempted trials with the different materials, collagen solutions and conditions is shown in Table A.1. Appendix B shows the SEM results of all these techniques.

Technique	Mould (patterned)	Substrate (flat)	Collagen solution and incubation conditions
MIMIC	PDMS (plasma)	Si	Gel: 2 mg/mL, 2h incubation, 37°C FFB: 100, 200 and 500 μg/mL, 2h incubation, 37°C
μCP	PDMS (FOTS)	PS (plasma)	FFB 200 μg/mL, 5-6h incubation, RT FFB: 100 μg/mL, 1h incubation, RT PBS: 50 g/mL, 1h incubation, RT
	PS (plasma)	PDMS	PBS: 50, 100 and 200 μg/mL, 1h incubation, RT
Embossing	PMDS (FOTS)	PS (plasma)	Gel: 2 mg/mL, 4h incubation, 37°C
	PDMS (plasma)	Si (FOTS)	Gel: 2 mg/mL, 4h incubation 37°C
	PDMS (FOTS)	PS	Gel: 2 mg/mL, 4h incubation 37°C

Table A.1: Summary of attempted micropatterning techniques.

Appendix B: Results and discussion of the failed attempted micropatternings

B.1 MIMIC

Two trials of MIMIC infiltration were performed. In the first one, infiltration only occurred next to the edges (a few μm in the channels) of the PDMS/Si assembly, where the collagen solution was introduced. After this observation, two hypothesis to explain why infiltration did not work were considered. The first one was based on the fact that collagen solution was gelifying while infiltration, which did not allow further infiltration. However, it is improbable this to happen as the collagen solution was kept on ice until its use. Another possibility could be that the effect of plasma treatment in the PDMS mould would have decreased, as 2h passed between the treatment and the infiltration. Taking this last consideration into account, in a second trial, plasma treatment was performed just before the infiltration and consequently, complete infiltration occurred in less than 5 min. After 2h incubation and preparation of the samples, the PDMS mould and the Si substrate were observed in stereomicroscope and SEM.

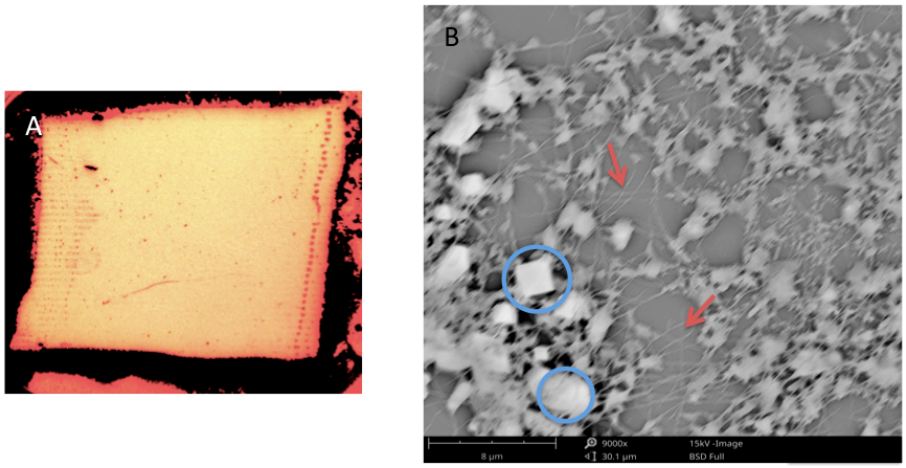

Figure B.1: Si wafer after infiltration. (A) is an overview of the Si wafer. (B) shows a zoom in one of the channels in SEM, at 9000x magnification. Blue circles show salt deposition and red arrows collagen fibers. Scale bar is 8 μm.

The purpose of Figure B.1 (A) is to show that it was possible to see some micropatterning in the Si wafer, especially in the extremities of the substrate, confirming that total collagen infiltration occurred in the assembly of flat Si/PDMS mould. Although Figure B.1 (B) is a little bit blurry, it is still possible to distinguish between some crystal deposition and collagen fibers between these crystals. However, only tinny amounts of collagen were deposited, while most of the deposition were salt crystals, probably coming from the the buffered solutions

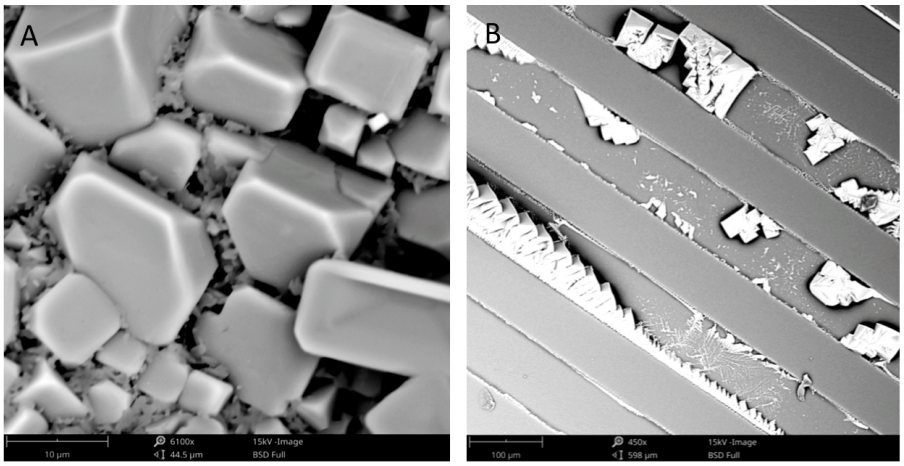

Figure B.2: SEM images of MIMIC method with infiltration of collagen diluted in FFB (100 μg/mL). (A) Salt deposition near the edges in Si wafer used in collagen infiltration, photographed at 6100x magnification. Scale bar is 10 μm. (B) PDMS mould after infiltration, photographed at 450x magnification. Scale bar is 100 μm.

used in the FFB approach, as samples were not rinsed with water before their preparation to SEM. Salt formation was also observed in the PDMS mould, but only around the edges of the mould. In Figure B.2 (A), salt crystals in the Si wafer are shown. It is also possible to observe what it seems collagen between different crystals. However, collagen fibers could not be observed and further analysis is necessary to confirm that actually this is collagen formation. Figure B.2 (B) verifies the infiltration of collagen. However, only salt formation is observed, without finding any evidence of collagen. From this figure it is also possible to conclude that the micropatterning was not completed, because after peeling off the PDMS mould, some deposition was still observed in the channels. As a consequence, this technique has to be optimized.

B.2 μCP

SEM results of the different protocols used to obtain collagen micropatterning by microcontact printing are shown in this section.

(a) **First protocol**: After 5h incubation to allow collagen fibril formation and deposition, 5 μm and 80 μm moulds were washed before the μCP, while the one of 10 μm was directly put in conformal contact with the flat PS without washing in order to see if there were some differences of the samples when they were washed or not. The first interesting finding was that 5h of incubation was too much time, as a lot of collagen deposition was observed all around the PDMS mould, covering completely the surface without being possible to differentiate between the channels and the flat parts of the PDMS. Furthermore, a lot of salts were also found in the PDMS mould. When the mould was not washed (10 μm width), the amount of salt formation increased (see SEM images in Figure B.3). Nevertheless, collagen fibers where clearly observed and homogeneously distributed, which confirms that is possible to obtain homogeneous collagen coatings.

Regarding the PS substrate, it was not possible to find any signal to confirm the transfer of collagen from the PDMS mould to the PS. We only observed what seems collagen fibrils between salt crystals. From this results it was possible to conclude that first, the incubation time had to be reduced in order to decrease the amount of collagen deposition and be able to distinguish the channels in the PDMS mould and second, that the amount

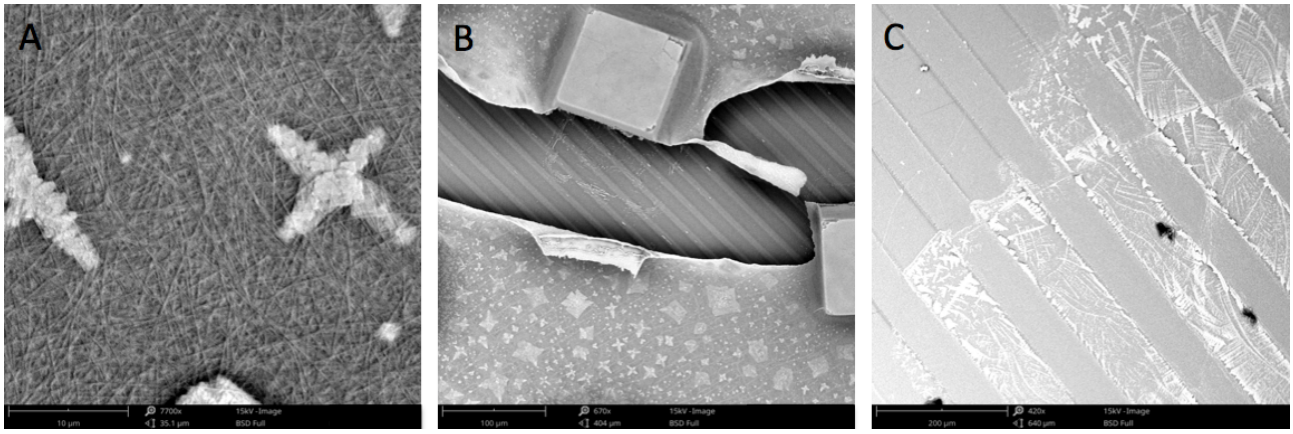

Figure B.3: SEM images of the PDMS mould in the first attempt of μCP. (A) Washed PDMS mould with 80 μm width channels after μCP, photographed at 7700x magnification. Scale bar is 10 μm. (B) Not washed PDMS mould with 10 μm width channels after μCP, photographed photographed at 670x magnification. Scale bar is 100 μm. (C) Washed PDMS mould with 5 μm width channels after μCP, photographed at x420 magnification. Scale bar is 200 μm.

of salt deposition had to be decreased as well. Then, the second protocol was tried (see Appendix A for the protocol).

(b) **Second protocol**: Reducing the collagen deposition for 1h was successful for obtaining an homogeneous layer of collagen and distinguish between the channels and the top part of the PDMS mould (this layer can be observed in Figure B.4 (A). When the collagen layer was looked it into more detail, there were observed kind of tinny collagen agglomerations with elongated shape (Figure B.4 (B)). In this Figure it is also possible to observe a huge particle, which probably corresponds to some dust deposition while preparing the sample for SEM. What is also interesting is that no differences in morphology were observed between the collagen dissolved with PBS (images not shown) and with FFB and collagen fibrils were not observed in any case. Furthermore, the amount of salt deposition was less in comparison with the first trial. Regarding the flat PS, it was observed that collagen was transferred from the PDMS mould. Nevertheless, micropatterning was not achieved and most of the transferring took place in the scratches of the PS film (Figure B.4 (C) and (D)). In order to remove those scratches from the PS, it was treated as explained in Chapter 2.

(c) **Third protocol**: In a last trial of μCP, collagen was transferred from a flat PDMS to a PS mould. The first finding of this experiments was that no collagen clue was found on the flat PDMS after the transferring. It could be that all the collagen was transferred to the PS, although having a complete transferring is quite difficult, so probably, the SEM used for characterization could not rich enough magnification to detect this remaining collagen. As a consequence, more characterization would be needed. With respect to PS mould, results are shown in Figure B.5. From this figure it is possible to observe that micropatterning was achieved. Collagen only was observed on top surfaces, but not inside any channel (Figure B.5 (A)), indicating that micropatterning was working. In Figure B.5 (B) a magnification of the transferred collagen is observed. The collagen shows similarities to the one observed in Figure B.4 (A), where a collagen layer is formed. However, this layer was not homogeneous and could not be seen all around the surface and collagen fibers were not observed at any concentration of collagen. Moreover, no significant differences were found on the transferring with different collagen concentrations, a part of more collagen was found at higher concentrations. Although samples were washed with water,

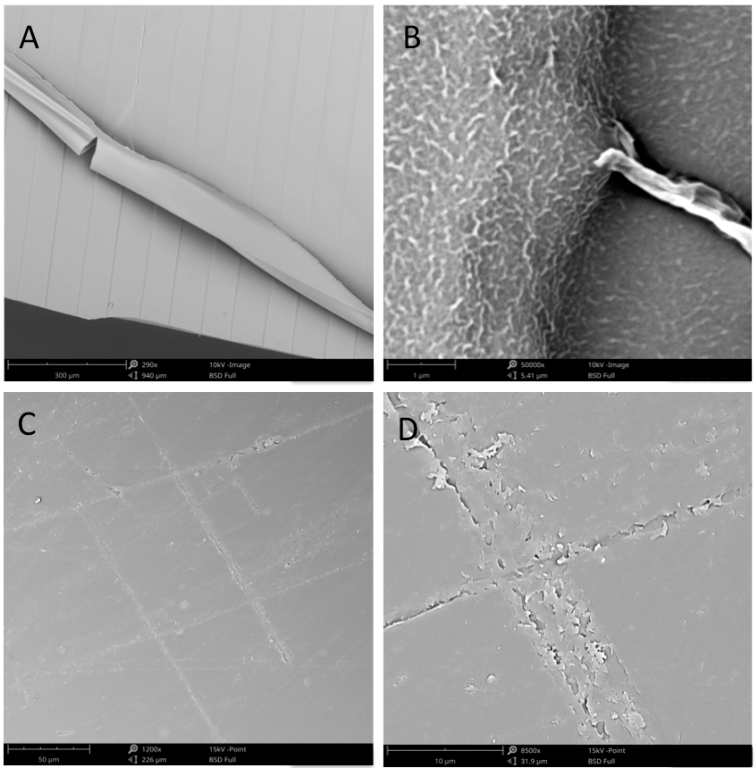

Figure B.4: SEM images of the second attempt of μCP, (A) PDMS mould after μCP (100 μg/mL collagen diluted in FFB), photographed at 290x magnification. Scale bar is 300 μm. (B) PDMS mould after μCP (100 μg/mL collagen diluted in FFB), photographed photographed at 27500x magnification. Scale bar is 3 μm. (C) Flat PS after μCP, photographed at 1200x magnification. Scale bar is 50 μm. (D) Flat PS after μCP, photographed at 8500x magnification. Scale bar is 10 μm.

salt deposition was still found in some regions of the PS mould (Figure B.5 (C)), but this salt deposition was not very common. It can be concluded that this last approach is the best one regarding μCP, because transferring occurred in a controllable way. On the other hand, an optimization of the technique is needed: an homogeneous collagen layer showing fibrils with the characteristic banding of collagen is required and the washing method should also be improved to get totally rid of the salt formation.

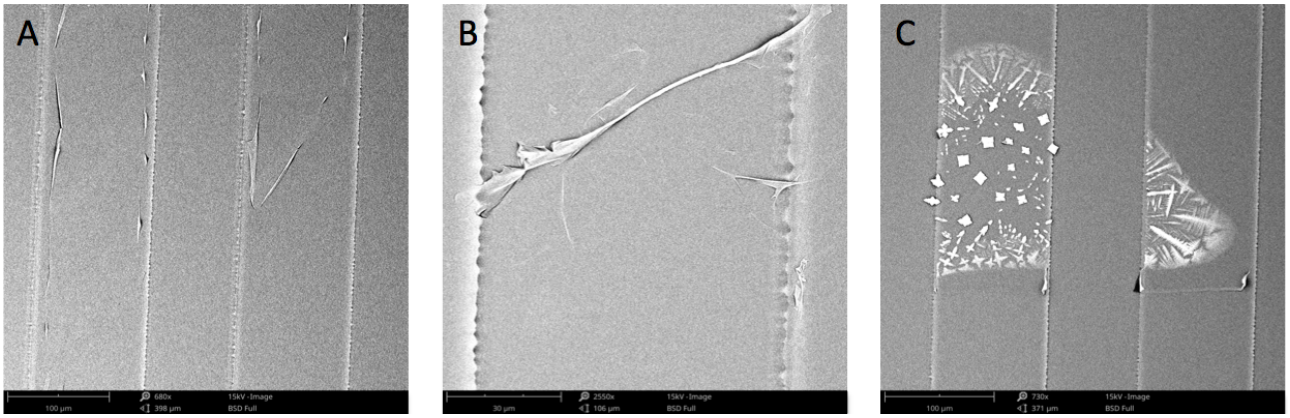

Figure B.5: SEM images of the third attempt of μCP, (A) PS mould after μCP 200 μg/mL, photographed at 680x magnification. Scale bar is 100 μm. (B) PS mould after μCP 50 μg/mL, photographed photographed at 2550x magnification. Scale bar is 30 μm. (C) PS mould after μCP 50 μg/mL, photographed at 730x magnification. Scale bar is 100 μm.

B.3 Embossing

(a) **First approach**: from this first approach, it was expected to obtain collagen micropatterning in the flat PS as it was treated with plasma (hydrophilic surface), while the PDMS mould was FOTS treated (obtaining a hydrophobic surface). The first comment to remark is that when the collagen solution was added on top of the flat PS, the collagen solution was spread all around the substrate and when the PDMS was put in conformal contact with the PS, surface was very slippery, making the PDMS/PS assembly very unstable. This occurred due to high hydrophilicity of the PS surface, which made the PS to have very high affinity with the collagen solution.

After the incubation time and peeled off the PDMS, some collagen and salt deposition were observed inside the channels of the mould (Figure B.6 (A)), although they were located in some specific regions and not in high amounts, showing that the FOTS treatment was effective. Salt deposition around the PS was also observed. Moreover, some blackish areas were found randomly around the PS (Figure B.6 (B)), which could be collagen fibers, without any characteristic pattern.

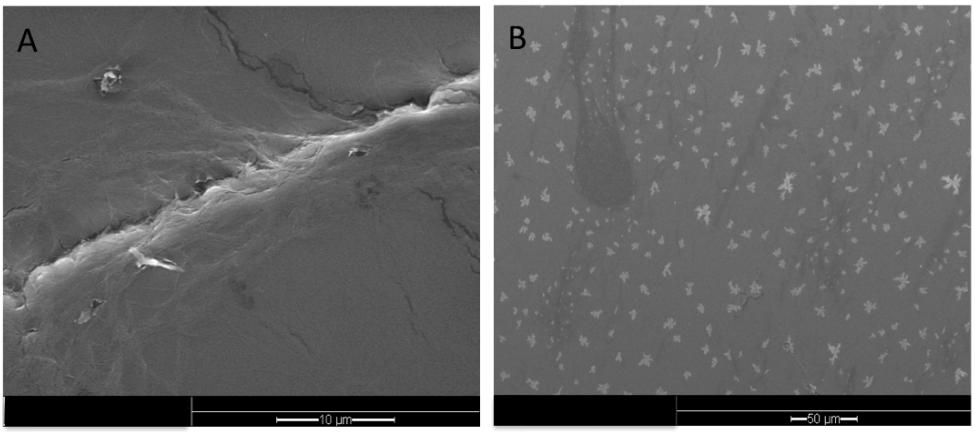

Figure B.6: SEM images of (A) PDMS mould (scale bar is 10 μm) and (B) PS substrate (scale bar is 50 μm) for the first embossing approach.

(b) **Second approach**: Trying to obtain collagen inside the PDMS moulds, this second trial was performed. Figure B.7 shows the PDMS mould and the Si substrate used in this trial. In this case, collagen was observed not only inside the channels but also on the top surface of the mould, which was not expected, as only the channels were plasma treated. This indicates that when applying pressure on top of the PDMS/PS assembly, this pressure was not enough to allow collagen solution to escape from the PDMS in contact with the PS, and collagen was entrapped between these two surfaces. At this point, it is important to notice that the initial pressure was applied by hand, which means that there was not a real control of the pressure applied and it was more a personal feeling. As a consequence, this should be improved and a more automatic technique to apply pressure should be used. Some salt formation was also observed all around the PDMS mould.

(c) **Third approach**: trying to improve the first approach, this third experiment was performed. When the PS was not plasma treated, collagen was not overspread all around the PS substrate and the slippery surface was also avoided, obtaining a very stable assembly. This led to a better conformal contact between the PDMS mould and the flat PS. Indeed, when PS was imaged in SEM after peeling of the PDMS mould, micropatterning was observed (Figure B.8). However, when analyzing this pattern in more detail, it was

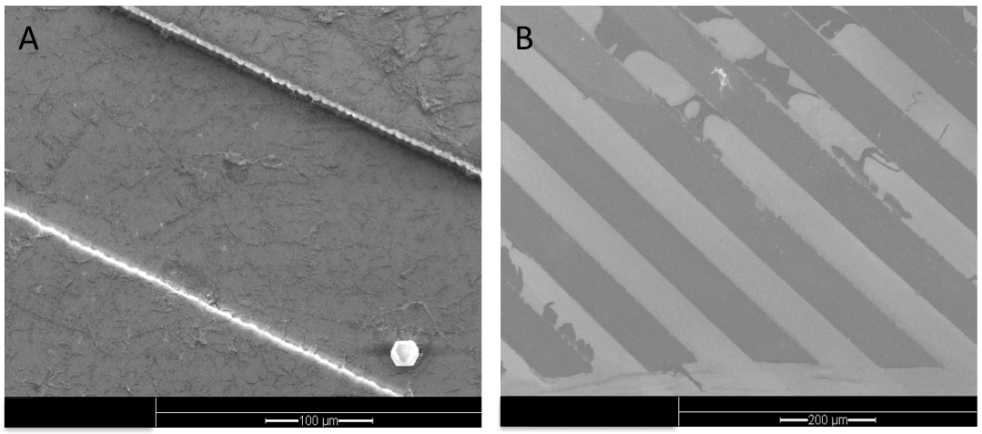

Figure B.7: SEM images of (A) PDMS mould (scale bar is 100 μm) and (B) Si substrate (scale bar is 100 μm) for the second embossing approach.

found that most of the material was salt deposition and only some collagen was observed between the salts (Figure B.8 (B)). This huge amount of salts come from the collagen gel formation, as after the μCP, samples were not washed, otherwise micropatterning went away with the washing. From all the attempted techniques, this is the most promising one, showing clear patterning. Nevertheless, a lot of work is still needed to improve the technique: other kinds of collagen solutions should be tried to avoid the high amounts of salt formation.

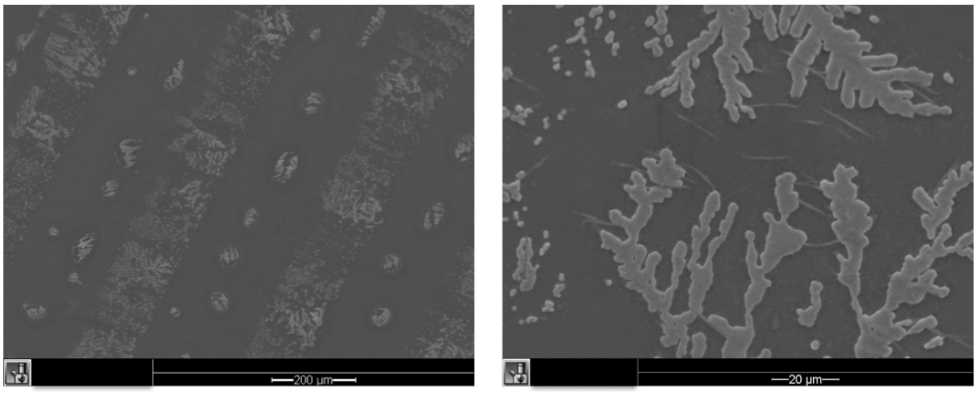

Figure B.8: SEM images of flat PS after the third embossing approach, (A) Scale bar is 200 μm. (B) Scale bar is 20 μm.

Appendix C: Analysis of XRD from raw data

XRD measurements were performed in the range of 5 to 65°C, measured in steps of 0.02°C. For each angle the time measurement was set to 0.05 s/step. After the measurement, processing and analysis of the XRD patterns was performed using the software DIFRACC.EVA.

First, the raw measurement was exported to the analysis software and the background of the measurement was subtracted. Then, Kα2 contributions were checked to verify if there were peaks due to the Kα2 radiation. Afterwards, a peak search was performed, editing manually the list of peaks. From the obtained peaks, a search/match was done using the database. For matching, the possible candidates were limited by selecting the chemicals that were known to be present in the sample. Different phases of CaPs were added for matching until all the peaks had a phase attributed. Figure C.1 shows the analysis of the HA coating.

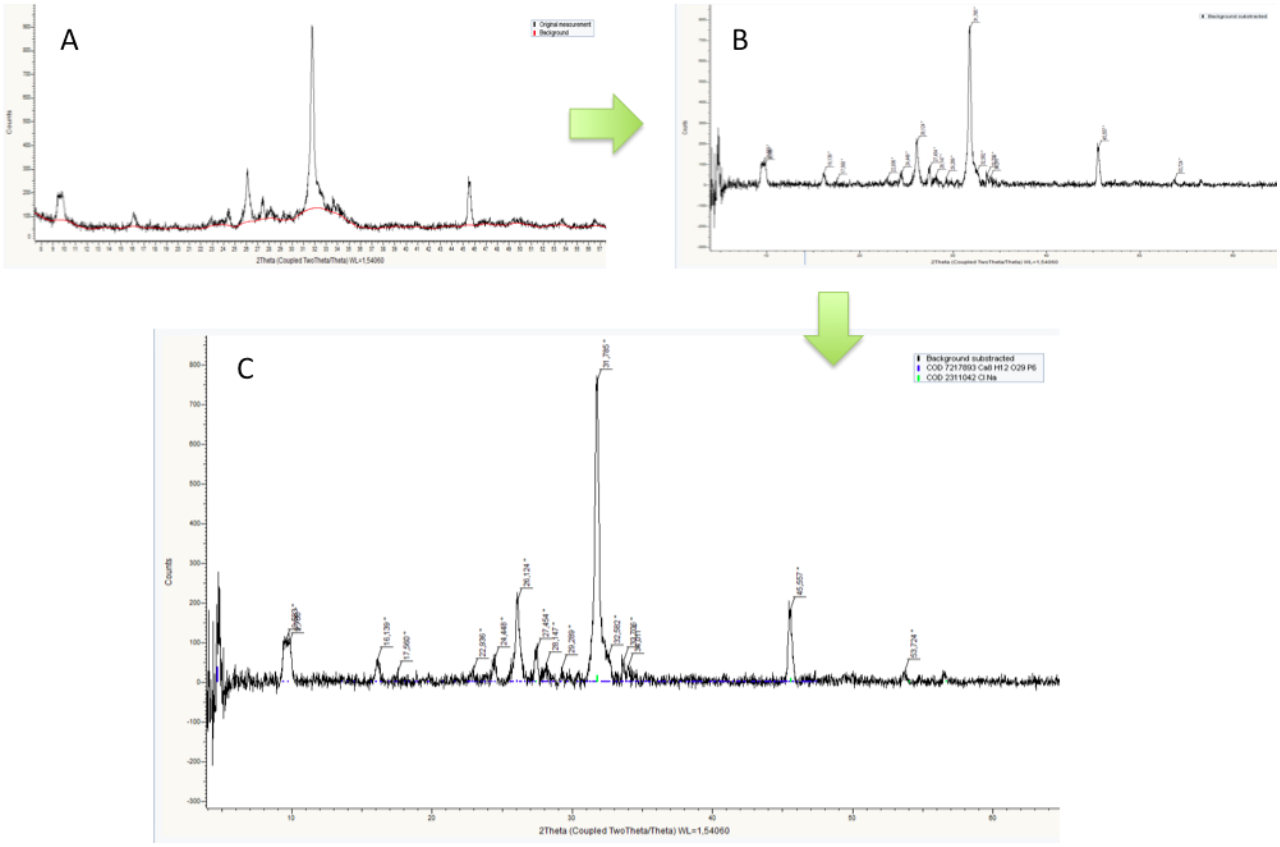

Figure C.1: Workflow of XRD analysis for HA coating. (A) Original measurement in black and background in red. (B) Measurement with background subtracted and with the main peaks. (C) Matching of the main peaks with possible CaPs phases: in blue, peaks matching with $Ca_8H_12O_29P_6$ and in green, peaks matching with NaCl.

The same method was applied for analyzing 5xSBF (A), 5xSBF (B), 2.5xSBF, CPS and

2.5xSBF + CPS.